GEOLOGY OF THE LOWER CRETACEOUS TRAVIS PEAK FORMATION, EAST TEXAS: CHARACTERIZATION OF A TIGHT GAS SANDSTONE

TOPICAL REPORT

(November 1982 - February 1990)

Prepared by

Shirley P. Dutton, Stephen E. Laubach, Robert S. Tye,
and Robert W. Baumgardner, Jr.

Bureau of Economic Geology
W. L. Fisher, Director
The University of Texas at Austin
Austin, Texas 78713-7508

Prepared for

THE GAS RESEARCH INSTITUTE
Contract No. 5082-211-0708
Robert Arner, GRI Project Manager

March 1990

DISCLAIMER

LEGAL NOTICE This report was prepared by the Bureau of Economic Geology as an account of work sponsored by the Gas Research Institute (GRI). Neither GRI, members of GRI, nor any person acting on behalf of either:

a. Makes any warranty or representation, expressed or implied, with respect to the accuracy, completeness, or usefulness of the information contained in this report, or that the use of any apparatus, method, or process disclosed in this report may not infringe privately owned rights; or

b. Assumes any liability with respect to the use of, or for damages resulting from the use of, any information, apparatus, method, or process disclosed in this report.

RESEARCH SUMMARY

Title	Geology of the Lower Cretaceous Travis Peak Formation, East Texas: characterization of a tight gas sandstone
Contractor	Bureau of Economic Geology, The University of Texas at Austin, GRI Contract No. 5082-211-0708, entitled "Geologic Analysis of Primary and Secondary Tight Gas Sand Objectives."
Principal Investigator	S. P. Dutton
Report Period	November 1982 - February 1990 Topical Report
Objectives	To summarize the results of the geologic studies of the Travis Peak Formation in East Texas, to document the geologic parameters that influence reservoir behavior in the Travis Peak, and to provide a methodology for geologic characterization of a tight gas sandstone.
Technical Perspective	Since 1982 the Gas Research Institute (GRI) Tight Gas Sands Project has supported geological investigations designed to develop knowledge necessary to efficiently produce low-permeability, gas-bearing sandstones. As part of that program, the Bureau of Economic Geology has conducted research on low-permeability sandstone in the Lower Cretaceous Travis Peak (Hosston) Formation in East Texas. The first phase of the study, which lasted from 1983 until 1986, involved extensive collection of core and production data in seven cooperative wells. Information gained from the cooperative wells, combined with geologic characterization of the Travis Peak throughout the study area, led to the drilling by GRI of three Staged Field Experiment (SFE) wells between 1986 and 1988. The SFE wells were drilled and completed by GRI specifically for the purpose of research on low-permeability gas reservoirs. This report summarizes the results of the geologic studies of the Travis Peak Formation, and it focuses on the contribution of geology to evaluation and completion of tight gas sandstone wells.
Results	Geologic characterization of the Travis Peak Formation focused on three major areas: (1) stratigraphy and depositional systems; (2) diagenesis of reservoir sandstones; and (3) analyses of the structural history and current structural setting. Depositional systems in this region of the East Texas Basin include: (1) a braided- to meandering-fluvial system that forms the majority of the Travis Peak section; (2) deltaic deposits that are interbedded with and

encase the distal portion of the fluvial section; (3) paralic deposits that overlie and interfinger with the deltaic and fluvial deposits near the top of the Travis Peak; and (4) shelf deposits that are present at the downdip extent of the Travis Peak. Geometry and reservoir quality vary with respect to the original depositional processes that controlled sediment lithology, texture, and bedding, in addition to the degree of diagenesis. Sandstones at the top of the formation that were deposited in paralic and meandering-fluvial environments are thin and separated by mudstones. In most of the middle and lower portions of the Travis Peak, sandstones are dominantly braided-fluvial. Best-quality reservoir sandstone exists in wide bands oriented parallel to depositional dip. Sandstone quality decreases at channel margins (levees), channel tops (abandoned channel deposits), and in interchannel areas where sediments are poorly sorted (siltstones and mudstones).

Petrographic studies indicate that the Travis Peak Formation contains mainly fine- to very fine grained sandstone, muddy sandstone, silty sandstone, and sandy mudstone. True claystones that could provide stress barriers to contain hydraulic fracture growth are rare. The sandstones are mineralogically mature, consisting of quartzarenites and subarkoses. Well-sorted sandstones had high porosity and permeability at the time of deposition, but their reservoir quality has been reduced by compaction and cementation. Cementation by quartz, dolomite, ankerite, illite, and chlorite and introduction of reservoir bitumen by deasphalting have reduced porosity to less than 8 percent and permeability to less than 0.1 md throughout most of the formation. Diagenetic studies indicate that structurally deeper Travis Peak sandstones are more intensely quartz cemented than are shallower sandstones. This variability in cementation results in differences in mechanical properties, porosity, and permeability between upper and lower parts of the Travis Peak. Furthermore, differences in diagenetic history between fluvial and paralic sandstones have resulted in fluvial sandstones having an order of magnitude higher permeability than paralic sandstones at all depths.

Because of the correspondence between extensive quartz cementation and fracture occurrence, abundant, open natural fractures should be expected in highly cemented sandstones. Natural fractures may contribute to production in lower Travis Peak sandstones that have very low matrix permeability. Predicting the propagation direction of hydraulically induced fractures is a key part of completion strategy, and geologic studies of core showed that borehole breakouts and drilling-induced fractures in core can be used as inexpensive and reliable methods of predicting horizontal stress directions and the direction of hydraulic fracture propagation. Hydraulic fractures propagate in directions subparallel to the east-northeast strike of the natural fracture; thus, hydraulically induced fractures may not intersect many natural fractures. Among the effects that natural fractures can have on well treatments are increased leakoff, fracture branching, and curvature. Branching could cause high treatment pressures and detrimentally affect

treatment results if not accounted for in treatment design. Geologic models indicate that natural fractures are not likely to be common in the upper Travis Peak sandstones and that special precautions for treating naturally fractured rock are not required in the upper zone, but in the lower Travis Peak, natural fractures are common and locally are extensively developed.

Technical Approach

Stratigraphy of the Travis Peak Formation was studied using 300 geophysical logs from wells in 12 counties in East Texas and 5 parishes in West Louisiana. Regionally correlative resistivity markers divide the Travis Peak into lithostratigraphic units. Cores recovered throughout the stratigraphic section from 26 wells (3,680 ft) distributed across the study area provided lithologic and sedimentologic data that were essential for well log calibrations and interpretations of depositional processes and environments. Composition of sandstones and mudstones was determined by standard thin-section petrography, cathodoluminescent petrography, scanning electron microscopy (SEM) with energy dispersive X-ray spectrometer (EDX), electron microprobe analyses, X-ray analysis, and isotopic analyses. Organic geochemical methods include measurement of total organic carbon content and vitrinite reflectance, pyrolysis, elemental analysis, and chromatography. Porosity and permeability were measured by routine core analysis and by special techniques designed to simulate in situ conditions. Fractures were examined in core and were oriented by standard and digital multishot and paleomagnetic techniques and by Borehole Televiewer and Formation Microscanner logs. Petrographic and scanning electron microscopes were used for fracture characterization and mineral identification. Borehole ellipticity and borehole televiewer logs were used to define borehole ellipticity patterns.

CONTENTS

Figures

Tables

INTRODUCTION

Since 1982 the Gas Research Institute (GRI) has supported geological investigations designed to develop knowledge necessary to efficiently produce low-permeability, gas-bearing sandstones. As part of that program, the Bureau of Economic Geology has been conducting research on low-permeability sandstone in the Lower Cretaceous Travis Peak (Hosston) Formation in East Texas. This effort is part of a broader program designed to increase the understanding and ultimate utilization of gas resources in low-permeability formations through integration of geology, formation evaluation, and reservoir engineering.

Geologic analysis of tight gas sandstones by the Bureau of Economic Geology began in 1982 with a national assessment of low-permeability reservoirs potentially suitable for an extensive research program (Finley, 1984). As a result of that analysis, the Travis Peak Formation in East Texas was chosen for comprehensive geologic, engineering, and petrophysical assessment beginning in 1983. The first phase of study of the Travis Peak, which lasted from 1983 until 1986, involved extensive collection of core and production data in seven cooperative wells; these were gas wells in which operating companies allowed GRI contractors access to collect the data necessary for complete formation and fracture evaluation. Information gained from the cooperative wells, combined with detailed geologic characterization of two fairways within the East Texas study area, led to the drilling by GRI of three Staged Field Experiment (SFE) wells between 1986 and 1988. The SFE wells were drilled and completed by GRI specifically for the purpose of research on low-permeability gas reservoirs.

This report summarizes the results of the geologic studies of the Travis Peak Formation in East Texas by the Bureau of Economic Geology. It focuses on the contributions of geology to evaluation and completion of tight gas sandstone wells. The goals of the geologic studies were to (1) apply geologic techniques to characterize the stratigraphic, petrographic, and structural attributes of the Travis Peak Formation; (2) understand the distribution of gas-bearing, low-

permeability sandstones within the formation; and (3) determine the geologic parameters influencing reservoir behavior. Once the physical and geological processes that controlled reservoir behavior were understood, then reservoir engineering and fracturing mechanics principles could be applied to more accurately predict well performance.

TECHNICAL APPROACH

In addition to reaching specific conclusions about the Travis Peak Formation, this study also provides a methodology for future geologic studies of other low-permeability, gas-bearing sandstones. Geologic goals were achieved through research in three major areas: (1) stratigraphy and depositional systems; (2) diagenesis of reservoir sandstones; and (3) analyses of the structural history and current structural setting. Investigations in each of these three areas are necessary for complete geologic characterization of a tight formation.

Depositional Systems and the Reservoir Framework

Stratigraphic studies provide an understanding of the physical framework in which the tight gas resource exists. Because the physical framework is a major factor in determining the distribution and reservoir behavior of the tight gas resource, it is necessary to understand this framework in order to test and apply new technologies for gas extraction. The stratigraphic studies conducted for this project are based on the concept that sand bodies are products of physical processes operating within major environments or depositional systems that are active during infilling of a basin. Typically, these systems include several major environments of sand deposition (i.e., fluvial, paralic, deltaic); resultant sand bodies are the genetic facies such as meanderbelt, tidal flat, or distributary channel. Each of these facies has consistent physical attributes within an individual system where processes and available sediment types were relatively uniform. Consequently, interpretive description and mapping of the depositional

systems and their component facies are basic steps in the geologic characterization of a tight gas sandstone.

Factors such as initial porosity and permeability, proximity to source or sealing lithologies, and interconnection with other permeable units are inherent attributes of genetic facies that control or affect migration and distribution of hydrocarbons. Thus, facies analysis can identify preferred reservoir types and provide the basis for improved resource estimation and geographic extrapolation or prediction of tight gas trends.

Delineation of the depositional framework has greatest application in providing the basis of characterization of tight gas reservoirs, both on a regional and local basis. Delineation of depositional systems outlines the principal building blocks of the basin fill that may produce gas. Within the depositional systems, sandstone bodies of component facies will have similar dimensions, orientation, interconnectedness, and internal permeability variations or compartmentalization. Extrapolation of detailed studies of sandstone beds based on limited areas of dense data is guided by the regional interpretation.

Diagenesis and Reservoir Quality

Production characteristics of tight gas reservoirs are in part controlled by diagenetic modifications to the reservoirs; extensive cementation is commonly the reason for the low permeability. An understanding of the diagenetic history can aid in predicting where the formation will be tight and in determining appropriate production methods. The microscopic-scale characteristics of tight gas reservoirs are investigated by petrographic studies that summarize detrital and authigenic mineral composition, pore type, grain size, and texture. By combining this information with core-analysis data, it can be determined how each parameter affects porosity and permeability. Petrographic studies also reveal the nature, extent, and distribution of diagenetic reactions. On the basis of these results, geochemical analyses are conducted to determine the chemical conditions and timing of diagenetic alteration. The

resulting integrated diagenetic history for the reservoir provides a method for predicting reservoir quality throughout the formation.

Petrographic studies of core samples provide compositional data necessary to calibrate the geophysical log response of the reservoir and adjacent nonreservoir rocks in the formation. Composition of detrital minerals and authigenic cements, as well as the type of pores and size of pore throats, is correlated to log response and petrophysical properties such as permeability, porosity, pore-throat diameter, and water saturation. The effect of diagenetic changes on log responses is thereby identified.

Structural Geology Analysis

Structural geological studies are particularly important to understanding tight gas resources because extracting gas from low-permeability formations requires hydraulic fracture treatment to achieve economic flow rates. Structural studies provide improved prediction of induced hydraulic fracture propagation direction and fracture containment through determination of present stress state in reservoir rocks and adjacent strata. The structural setting of the reservoir rock is a significant influence on the producibility of tight gas sandstones because this controls the state of stress and the abundance and pattern of natural fractures. Where fractures are sufficiently interconnected, large, or closely spaced, their effects on fluid flow in the reservoir will contribute to gas production. Rock anisotropy due to natural fractures may affect the orientation and shape of the hydraulic fracture envelope in the horizontal plane. It also controls which natural fractures will be reactivated as shear fractures or extension fractures during subsequent artificial deformation of the rock by hydraulic fracturing. Natural fractures may need to be taken into account in fracture-treatment design because of their contribution to leakoff. Models for predicting fracture shape are highly dependent on the stress history of viscoelastic rocks, such as shale, and to a lesser extent on the behavior of more elastic rocks

such as sandstone. The overall structural history, including uplift or subsidence, of a basin may influence present pressure gradients and state of stress.

GEOLOGIC SETTING

The East Texas Basin (fig. 1) formed initially during Late Triassic rifting (Buffler and others, 1980). Crustal extension produced thinning and heating of the lithosphere. Subsequent cooling and subsidence formed a basin in which a thick sequence of Mesozoic and Cenozoic sediments accumulated (fig. 2). Carbonates dominated the early phases of deposition in the East Texas Basin (Moore, 1983). The earliest progradation of terrigenous clastics in the basin is recorded by the Upper Jurassic-Lower Cretaceous Cotton Valley Group (fig. 2). The Travis Peak Formation represents a second period of fluvial-deltaic progradation; it is equivalent to the Hosston Formation of Louisiana, Arkansas, and Mississippi. In updip portions of the basin, the Travis Peak unconformably overlies the Cotton Valley Group. Downdip, the Travis Peak is separated from the Cotton Valley Group by a thin, transgressive-marine deposit, the Knowles Limestone. The Travis Peak Formation is gradationally overlain by micritic and oolitic limestones of the Cretaceous Sligo Formation forming a time-transgressive boundary (Bebout and others, 1981).

Structural features in the study area include the north-trending Sabine Arch, the East Texas Basin, the northeast- and east-trending Mexia-Talco fault zone, the east-trending Elkhart-Mount Enterprise fault zone, and east-trending Angelina-Caldwell flexure (fig. 1), and various structures caused by diapiric movement of salt. The largest structure in the study area is the Sabine Arch, a basement-cored, low-amplitude anticline centered near the Texas-Louisiana state line (Granata, 1963). A Jurassic structural high, the arch had no topographic expression by Early Cretaceous time. Uplift in the early Late Cretaceous (Granata, 1963; Halbouty and Halbouty, 1982; Jackson and Laubach, 1988) removed as much as 1,825 ft (556 m) of deposits in the study area. A second period of uplift and erosion in the early Tertiary may have removed as much as 1,500 ft (457 m) of strata (Dutton, 1986; Jackson and Laubach, 1988). Movement may be the

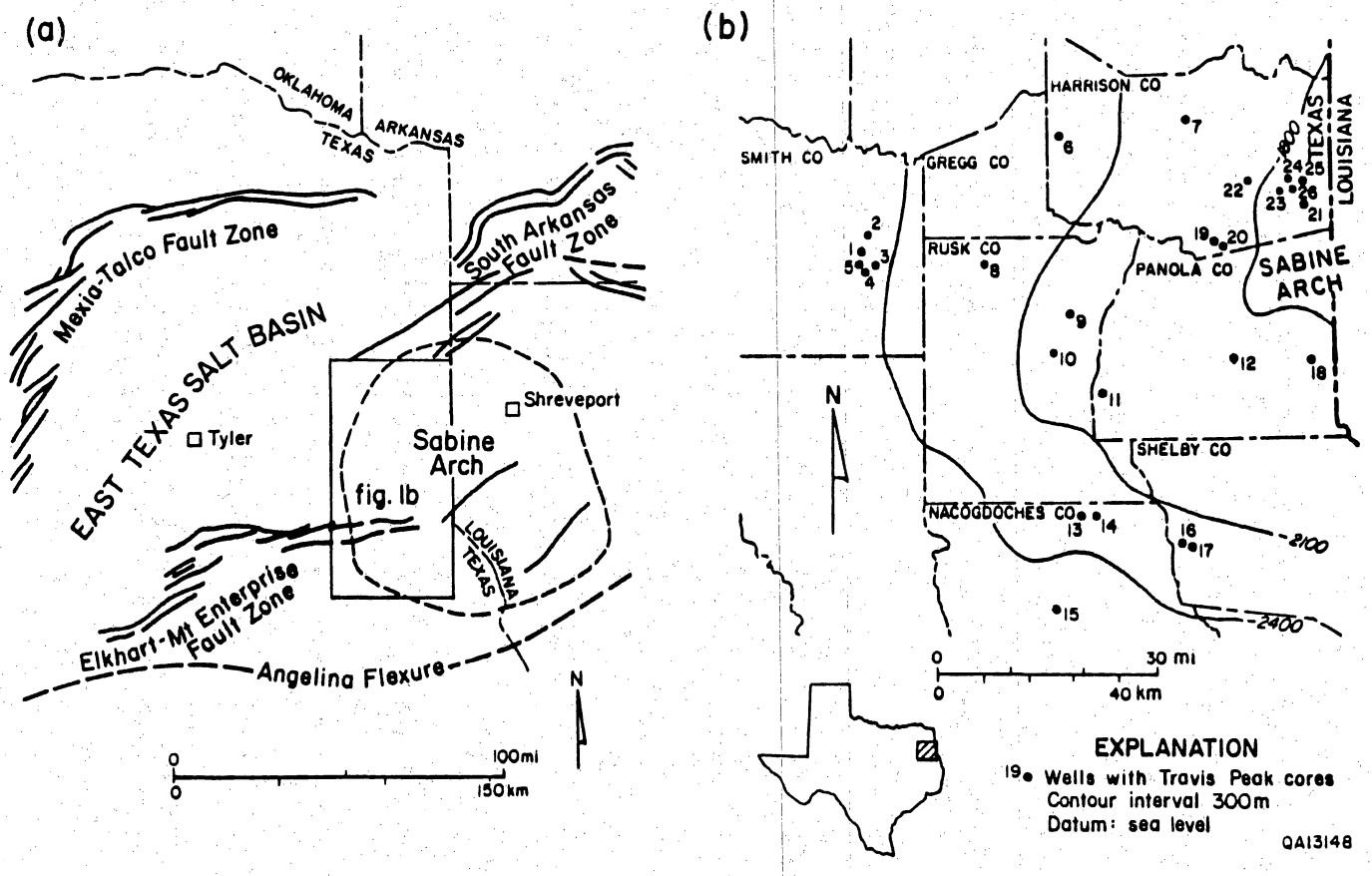

Figure 1. Location of study area and wells. (a) Structural setting of the Travis Peak Formation, East Texas. (b) Location of wells for which Travis Peak cores are available and structure on the top of the Travis Peak. See table 1 for well names.

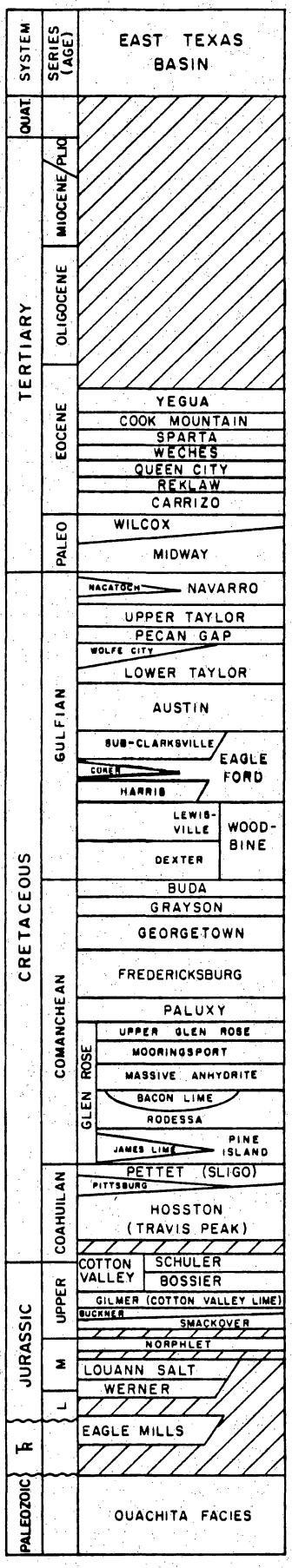

Figure 2. Stratigraphic nomenclature, East Texas Basin (modified from Galloway and others, 1984).

result of Cretaceous and Tertiary episodes of mild northeast-directed compression of the Gulf of Mexico Basin, deep-seated Cretaceous plutonism, or reactivation of preexisting basement blocks (Jackson and Laubach, 1988; Laubach and Jackson, in press).

A group of smaller domal and low-amplitude anticlinal structures is located on the western flank of the Sabine Arch. Deep wells in most of these structures have penetrated salt. Saucier and others (1985) have interpreted these structures to be salt-cored, low-amplitude anticlines that developed syndepositionally as a consequence of unequal loading of the underlying salt during Travis Peak progradation from the northwest.

Near the center of the Sabine Arch, on the eastern side of the study area, the top of the Travis Peak occurs at 5,600 ft (1,707 m) below sea level (fig. 3). The formation dips to the west and southwest on the western side of the Sabine Uplift, and in the southern part of the study area the top of the Travis Peak is at 9,400 ft (2,865 m) below sea level (Tye, 1989). The Travis Peak Formation is generally about 1,800 to 2,200 ft (550 to 670 m) thick in the study area (fig. 4).

METHODS

To assess the stratigraphy and depositional history of the Travis Peak Formation, more than 300 well logs were used to correlate depositional packages and construct regional cross sections (fig. 5) from East Texas into Louisiana (Tye, 1989). Resistivity markers associated with subregionally persistent shale beds were chosen in the basinal region of western Louisiana where the Travis Peak is relatively shaly, and these markers were traced into the updip, more sandstone-rich parts of the basin. Where shales thin or pinch out, the resistivity markers could still be correlated. Sandstone-sandstone contacts at the positions of these resistivity markers are considered to be erosional or unconformable expressions of the equivalent downdip shale beds.

Five lithostratigraphic units were defined (fig. 6). Each unit was mapped to illustrate thickness, net-sandstone, and percent-sandstone trends (Tye, 1989). Portions of the

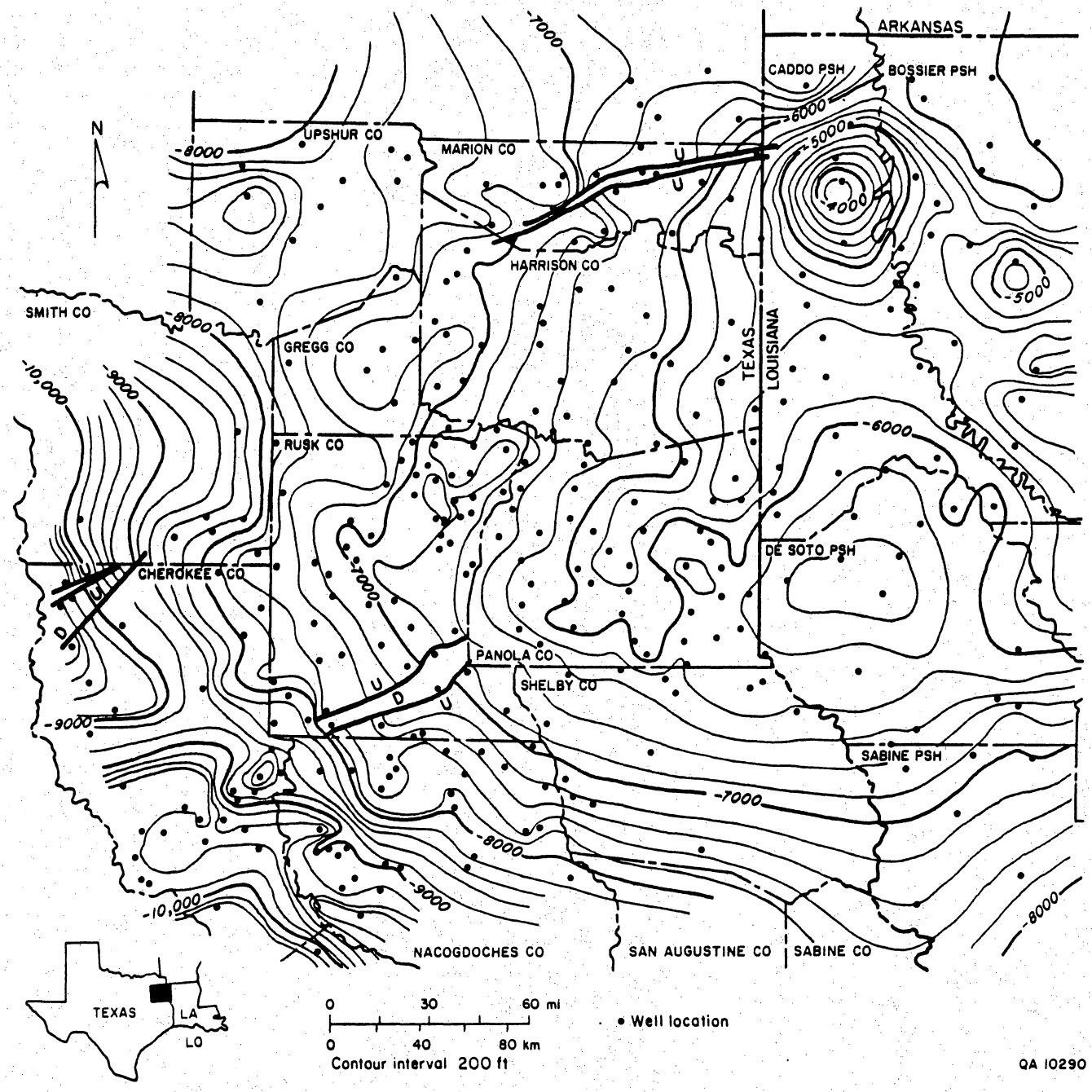

Figure 3. Structure-contour map on the top of the Travis Peak Formation. Subsea depths in the study area range from less than 4,000 ft to greater than 10,000 ft and increase radially, away from the crest of the Sabine Arch.

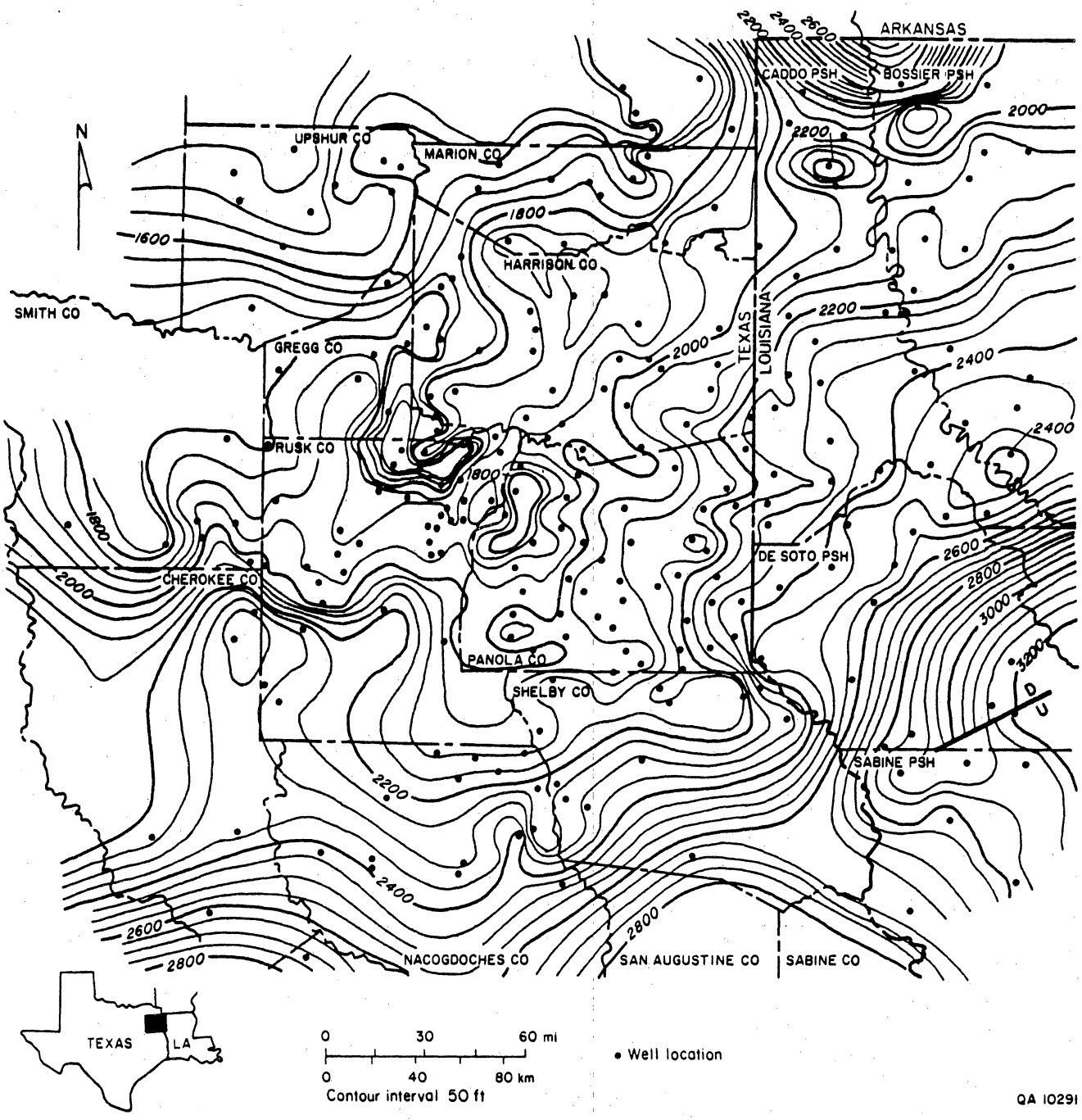

Figure 4. Isopach map of the Travis Peak Formation in the East Texas–West Louisiana study area. Thickness values range from 1,425 ft to 3,190 ft and increase from the northwest to the southeast.

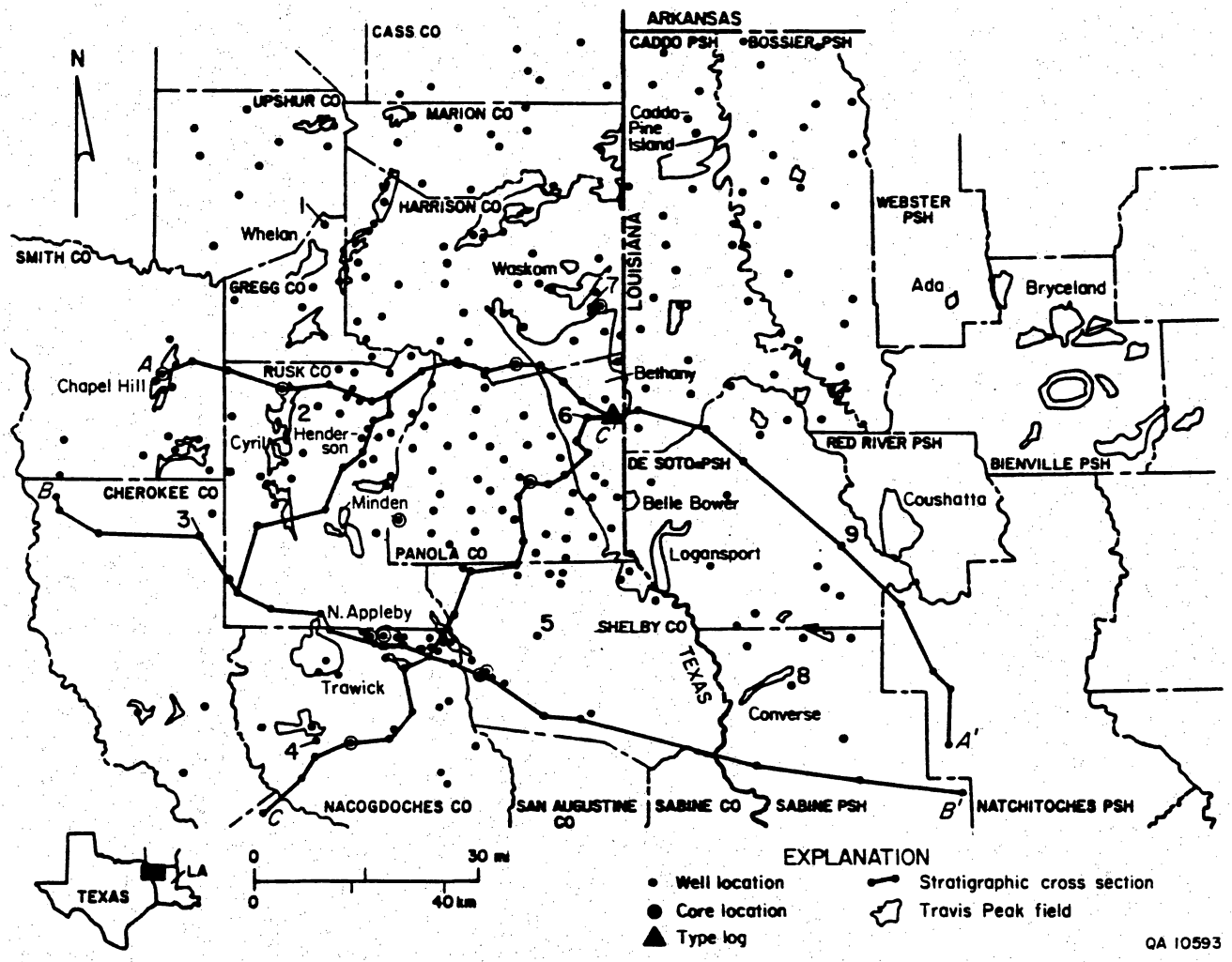

Figure 5. Location of East Texas counties and West Louisiana parishes included in the study of stratigraphy and depositional systems of low-permeability, gas-bearing sandstones in the Travis Peak Formation. Major Travis Peak fields, well locations, and lines of cross section are shown.

TENNECO
Harris-Drummond No. 1
Bethany Field, James Mathews Sur. A-42
PANOLA COUNTY, TEXAS

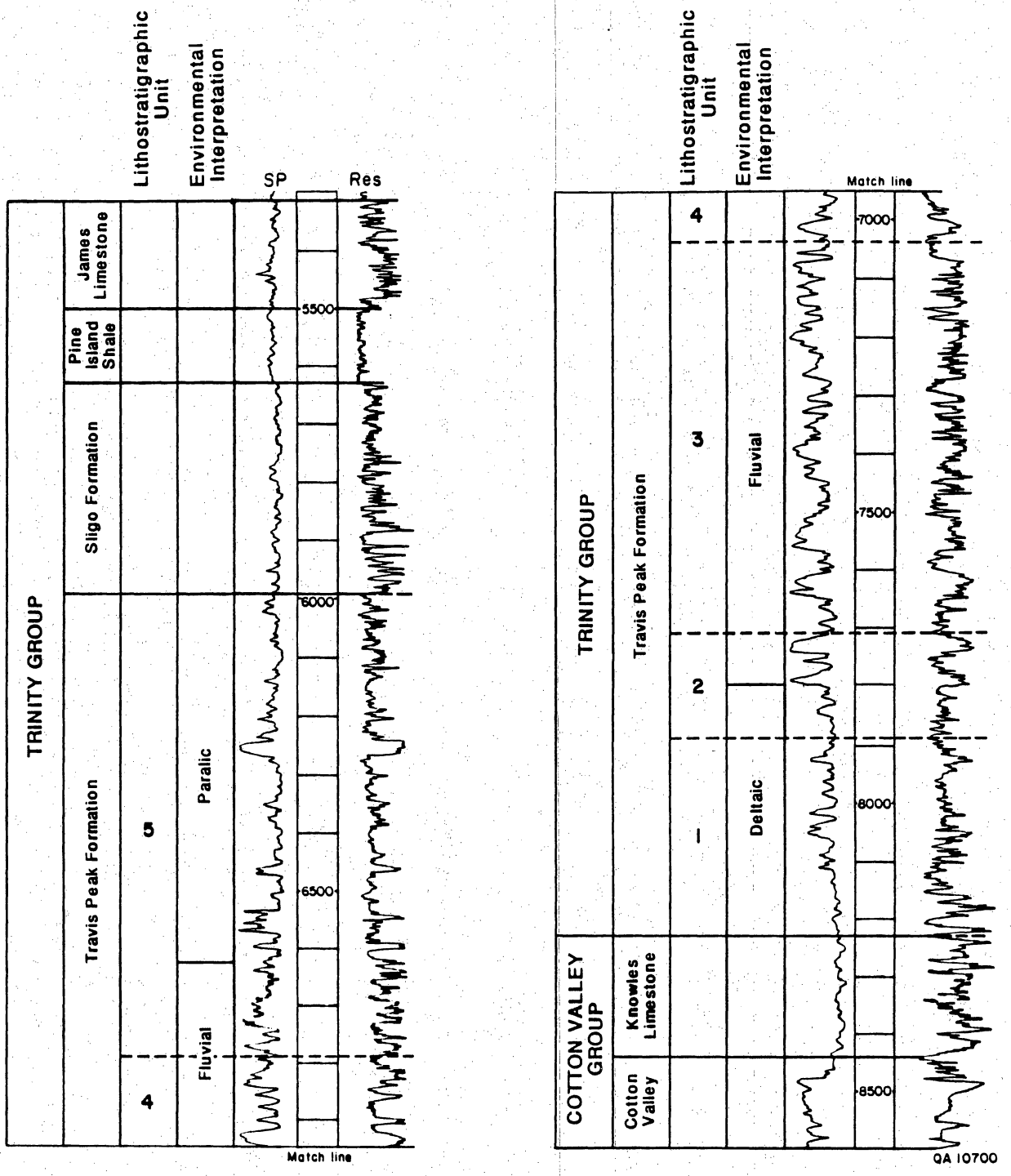

Figure 6. Type log of the Travis Peak Formation from eastern Panola County, Texas. Lithostratigraphic unit divisions and environmental interpretations are illustrated. Location shown in figure 5.

spontaneous potential (SP) well log curve exceeding a 30-percent cutoff value (greater than 30 percent deflection from a shale baseline) denoted sandstone content. Lithologic and depositional interpretations were extended throughout the study area by calibration of well log response to particular rock types and depositional settings inferred from core data. Cores from 26 wells were described for this study (fig. 7); 3,680 ft (1,122 m) of core was from the Travis Peak and 242 ft (74 m) from the Cotton Valley.

The composition of Travis Peak sandstone was determined from thin sections selected from different facies and from the total depth range in each core. Matrix-free sandstones were sampled preferentially because cementation was more extensive in them than in sandstones with abundant detrital clay matrix. Of a total of 431 samples, 226 are clean sandstones with less than 2 percent detrital clay matrix. Most of the remaining 205 samples are silty sandstone, muddy sandstone, and sandy mudstone (textural classification of Folk, 1974).

Standard thin-section petrography, cathodoluminescent petrography, scanning electron microscopy (SEM) with an energy dispersive X-ray spectrometer (EDX), electron microprobe analyses, X-ray diffraction analyses, and isotopic analyses were used to identify and determine the chemical composition of detrital and authigenic components of sandstone and mudstone. Thin sections were stained with sodium cobaltinitrite (potassium feldspars) and with potassium ferricyanide and alizarin red-S (carbonates). Point counts (200 per slide) were performed on a standard petrographic microscope to determine mineral composition and porosity. Grain size and sorting (phi standard deviation) were determined by measurement (50 points) of the long axis of sand- and silt-sized framework grains.

Core analyses from 1,687 sandstone samples form the porosity and permeability data base. All samples were measured under unstressed conditions, that is, under ambient pressure (200 or 800 psi confining pressure), and some were also measured under stressed conditions, at restored in-situ overburden pressure (ResTech, 1989). Permeability measurements were made using nitrogen gas or air as the fluid, and porosity was measured by helium injection (Boyle's Law method). Thin sections were made from the ends of 109 core-analysis plugs, and an additional

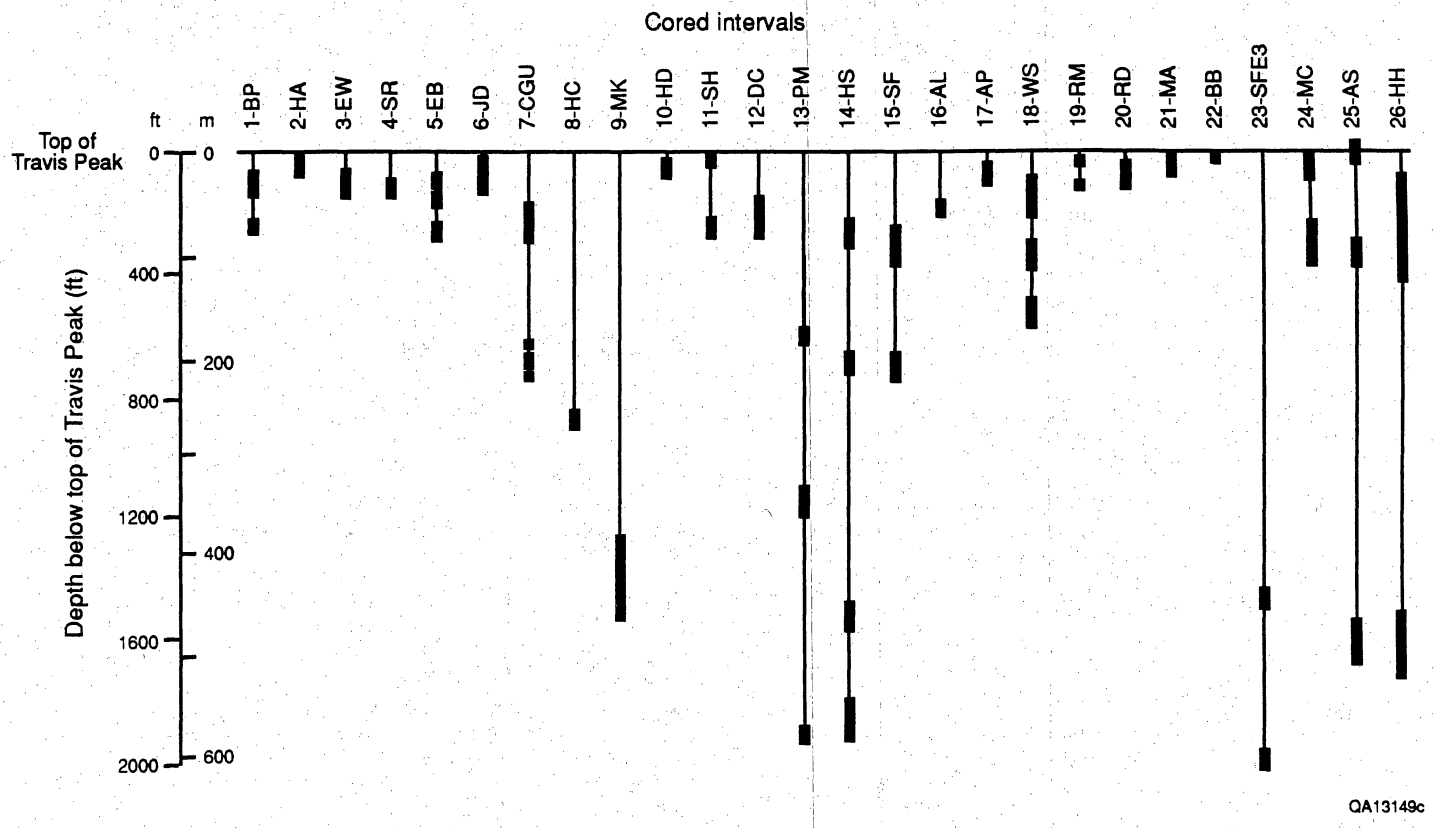

Figure 7. Cored intervals plotted by depth below the top of the Travis Peak. See table 1 for explanation of abbreviations.

125 thin sections were made from samples cut immediately adjacent to core plugs. The latter samples were collected from sandstones with the same apparent lithologic characteristics as the adjacent core plugs. By comparing thin-section point-count data with core analyses, the influence of parameters such as grain size, sorting, compaction, volume of authigenic cements, and pore type (primary versus secondary) on porosity and permeability was evaluated. Only the 234 thin sections that are directly comparable to core-analysis plugs were used to compare petrographic and petrophysical data.

TRAVIS PEAK STRATIGRAPHY AND DEPOSITIONAL SYSTEMS

Stratigraphy

The Travis Peak Formation is not divided into members, and good marker horizons that could facilitate division of the Travis Peak and aid in interpretation of its component depositional environments do not exist (McGowan and Harris, 1984; Saucier and others, 1985). On the basis of the log character and relative distribution of sandstone intervals, studies by Seni (1983), Saucier (1985), and Saucier and others (1985) established a threefold internal stratigraphic framework for the Travis Peak. These researchers described a middle sandstone-rich fluvial sequence that is gradationally underlain and overlain by marine-influenced, relatively mudstone-rich, fluvial-deltaic zones. The fluvial sequence is characterized by blocky SP log traces that suggest stacked sand bodies. In contrast, the lower and upper fluvial-deltaic sequences are generally characterized by more widely separated sand bodies with distinctly bell-shaped, inverse bell-shaped, or irregular-serrate SP log traces (Fracasso and others, 1988).

Tye (1989) divided the Travis Peak into five lithostratigraphic units or bodies of sedimentary rock delimited on the basis of their lithic characteristics and stratigraphic position. Regionally correlative resistivity markers form the lithostratigraphic unit boundaries, and the arrangement and sedimentary characteristics of each unit are shown in figures 8 to 10. A type log from Panola County shows the unit boundaries in addition to general facies interpretation (fig. 6).

Shales divide the distal portions of the Travis Peak into multiple sandstone beds that thicken and merge updip (toward the northwest; figs. 8 and 9). The greater mudstone content of the upper Travis Peak is evident from the lithologic correlations (figs. 8 to 10) and lithofacies maps. A significant lithologic contrast can be found in a comparison of maps of the combined percent-sandstone values for units 1 to 3 with those for units 4 and 5 (figs. 11 and 12). The

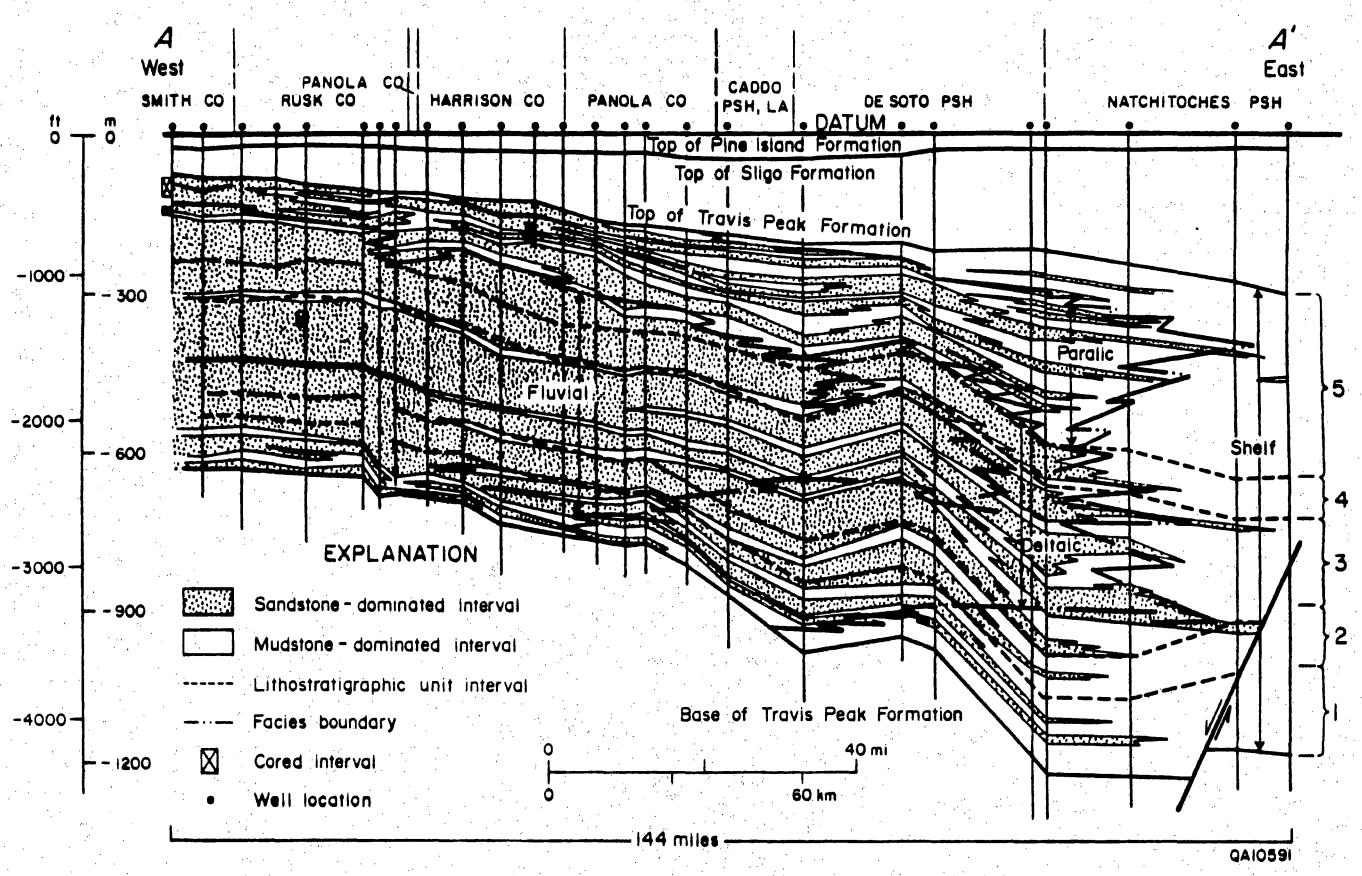

Figure 8. Stratigraphic cross section A-A' extends 144 mi from Smith County, Texas, eastward to Natchitoches Parish, Louisiana. Lithologic correlations (sandstone-mudstone) are illustrated, in addition to the lithostratigraphic units and interpreted depositional facies. Datum is the top of the Pine Island Shale. Line of section shown in figure 5.

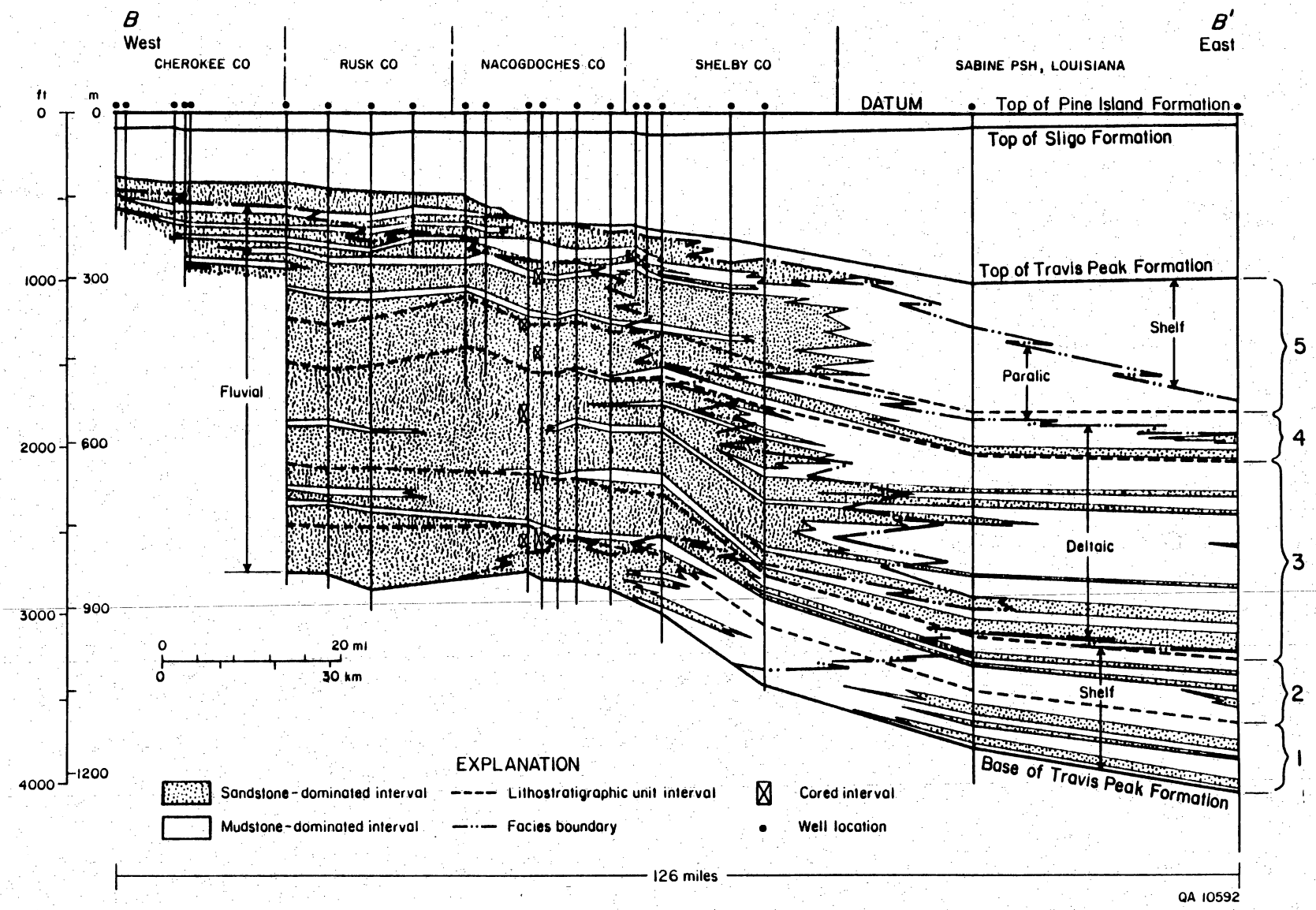

Figure 9. Stratigraphic cross section B-B' extends 126 mi from Cherokee County, Texas, eastward to Sabine Parish, Louisiana. Lithologic correlations (sandstone-mudstone) are illustrated, in addition to the lithostratigraphic units and interpreted depositional facies. Datum is the top of the Pine Island Shale. Line of section shown in figure 5.

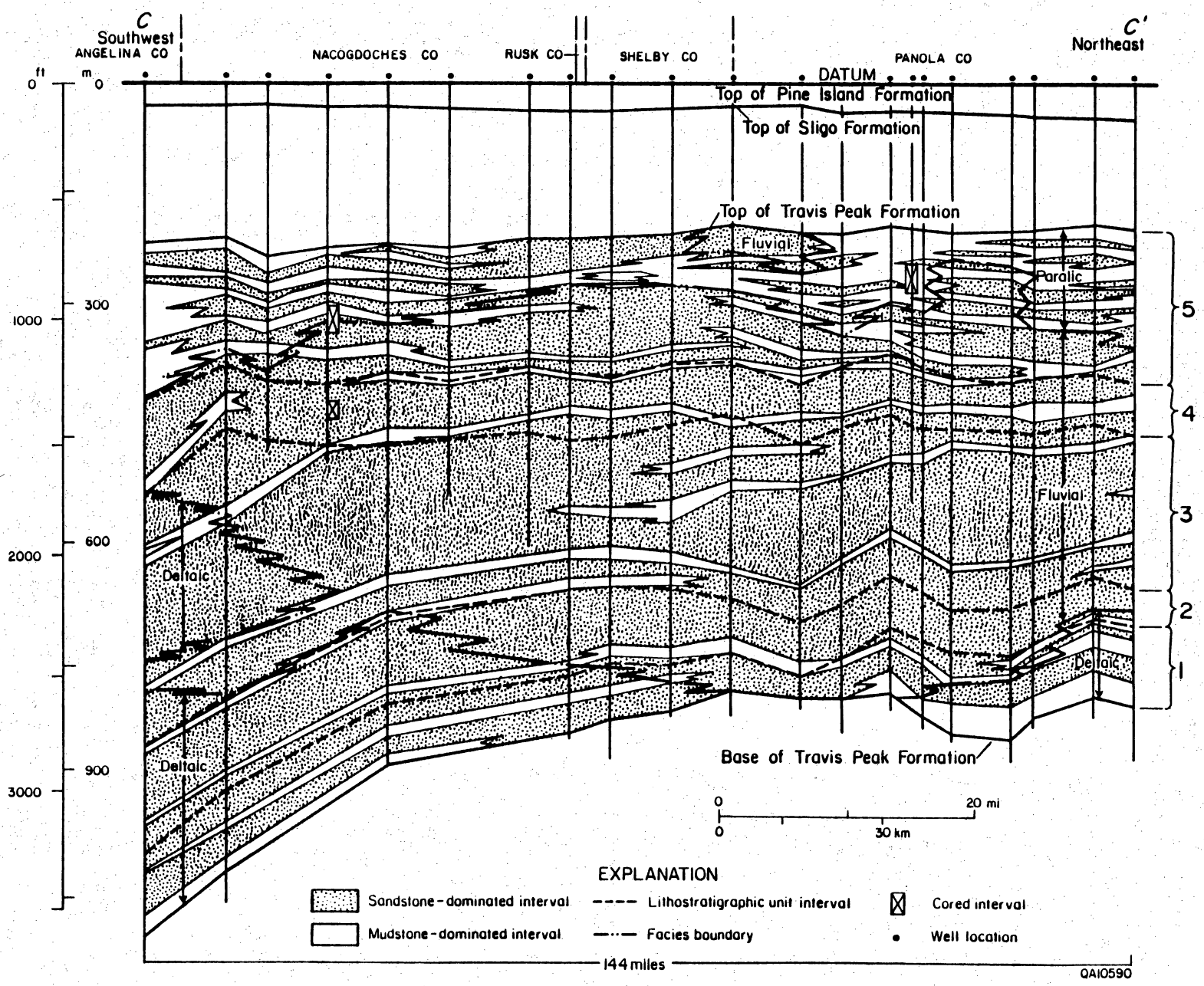

Figure 10. Stratigraphic cross section C-C′ extends 79 mi from Angelina County, Texas, northeastward to Panola County, Texas. Lithologic correlations (sandstone-mudstone) are illustrated, in addition to the lithostratigraphic units and interpreted depositional facies. Datum is the top of the Pine Island Shale. Line of section shown in figure 5.

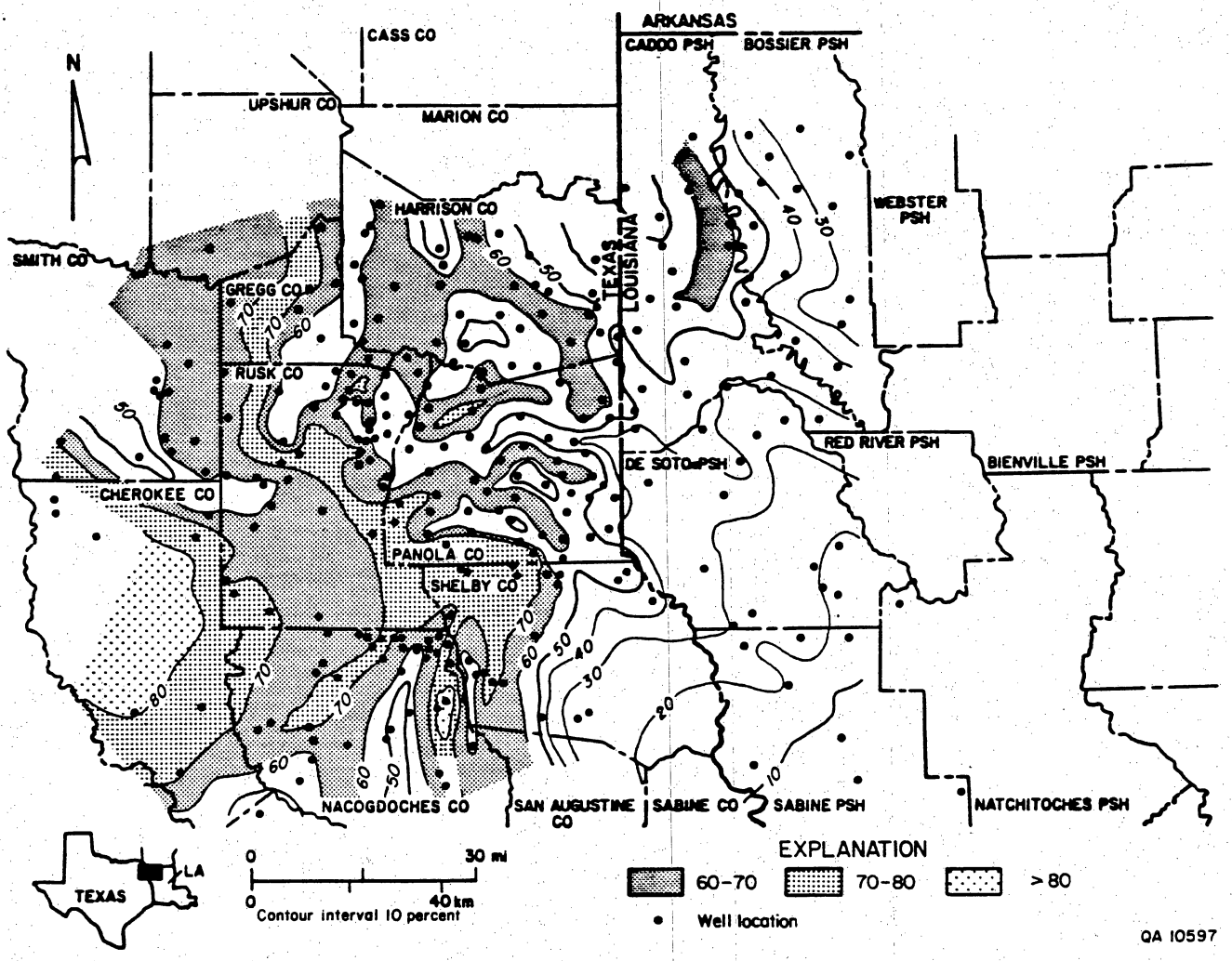

Figure 11. Percent-sandstone map for combined lithostratigraphic units 1 through 3.

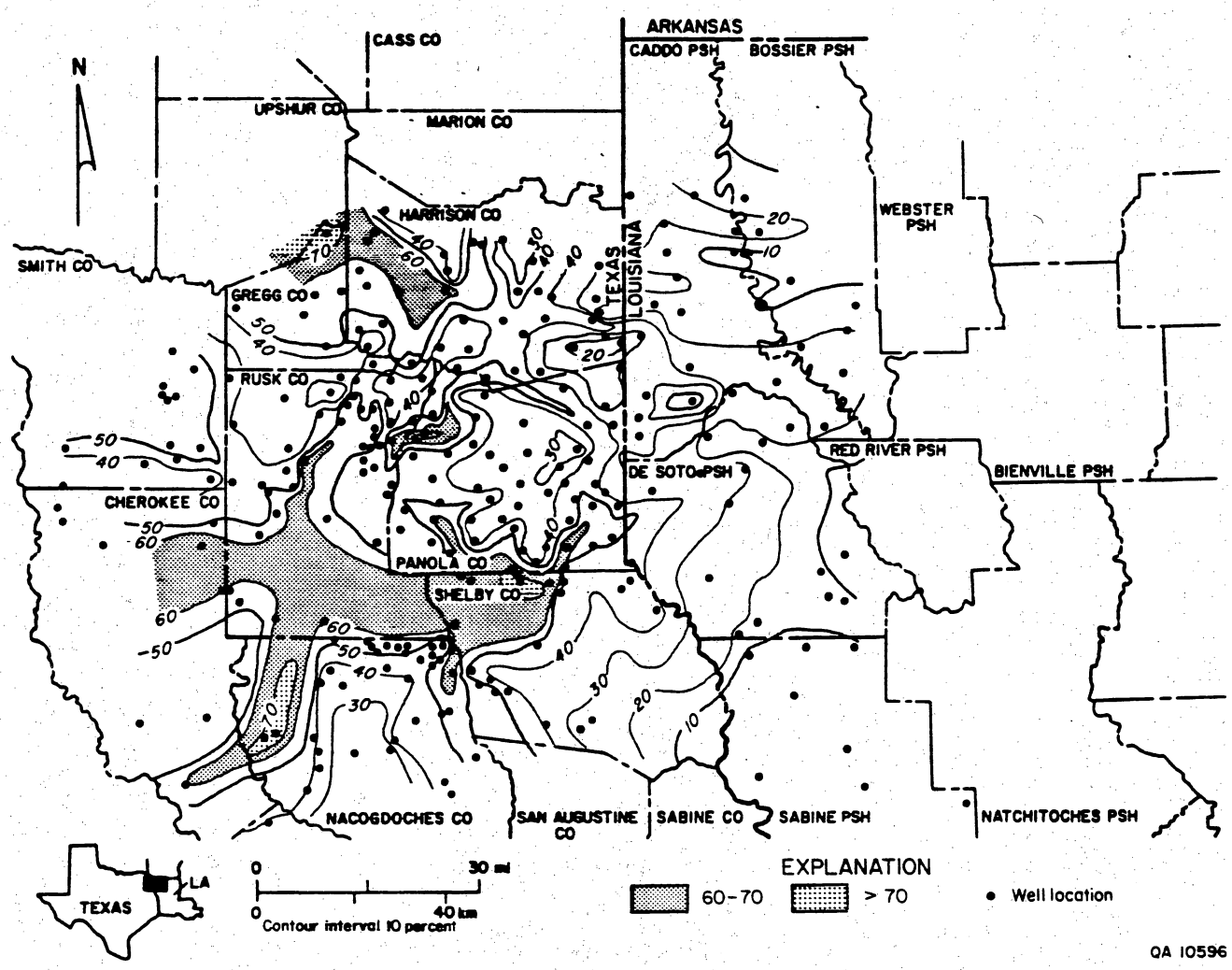

Figure 12. Percent-sandstone map for combined lithostratigraphic units 4 and 5.

upper portion of the Travis Peak (units 4 and 5) contains more mudstone. Areas containing more than 60 percent sandstone in the lower Travis Peak (units 1 to 3) form north-south-oriented bands from Gregg and Harrison Counties through Cherokee, Nacogdoches, and Shelby Counties. Smaller areas of equal sandstone content (more than 60 percent) in the upper Travis Peak occur in pods or narrow bands.

Depositional Systems

Bushaw (1968), Hall (1976), McBride and others (1979), Bebout and others (1981), McGowan and Harris (1984), Finley and others (1985), Saucier (1985), Saucier and others (1985), Dutton (1987), and Tye (1989) utilized data from well logs, cuttings, seismic lines, isopach and net-sandstone maps, cross sections, and cores to characterize the depositional environments represented by Travis Peak deposits. A typical Travis Peak depositional systems tract in East Texas, defined by Tye (1989) and incorporating information from the earlier studies, consists of (1) a braided- to meandering-fluvial system that forms the core of the Travis Peak section, (2) deltaic deposits that are interbedded with and encase the distal portion of the fluvial section, (3) paralic deposits that overlie and interfinger with the deltaic and fluvial deposits near the top of the Travis Peak, and (4) shelf deposits that are present at the downdip extent of the Travis Peak; they interfinger with and onlap deltaic and paralic deposits (figs. 8 to 10).

The sedimentology of each facies that comprises this terrigenous-clastic depositional systems tract is interpreted on the basis of macroscopic descriptions of their lithologic and physical and biogenic sedimentary characteristics in cores. Some of these lithofacies are thought to represent deposition in channel, floodplain, lacustrine, and overbank environments of a braided- to meandering-fluvial system. The remaining lithofacies document the preservation of various paralic environments: (1) coastal plain (channel, floodplain), (2) marsh, (3) estuary or bay, (4) tidal flat, and (5) estuarine shoal. Although the existence of deltaic and shelf

environments has been postulated on the basis of sediment-distribution maps, log character, and facies associations (figs. 8 to 10), no deltaic or shelf sediments in the Travis Peak section were cored for use in this study. Deltas and the shelf over which they prograded were located east and south of the main study area. Therefore, discussions and interpretations of the deltaic and shelf facies are limited to their log response, areal distribution, and lithology determined from logs.

Braided- to Meandering-Fluvial Facies

Braided- and meandering-fluvial deposits form the bulk of the Travis Peak studied. In the proximal Travis Peak depositional system, fluvial deposits form a sequence nearly 2,000 ft (610 m) thick that unconformably overlies the Cotton Valley Formation. Downdip, fluvial deposits overlie and interfinger with the deltaic, paralic, and shelf facies (figs. 8 to 10). On the basis of their sedimentary character, lithofacies representing the following five discrete fluvial depositional environments were recognized: (1) channel, (2) abandoned channel, (3) lacustrine, (4) floodplain and swamp, and (5) overbank. Cores characteristic of the braided-fluvial part of the Travis Peak Formation were recovered from the Prairie Mast No. 1-A well (fig. 13).

Fluvial channel fill—Fluvial channel-fill sandstones are generally fine- to very fine grained, although grain size can reach medium to coarse, and their thickness ranges from 10 to 50 ft (3 to 15 m). Most have scoured bases and commonly exhibit internal scour contacts. All channel-fill sandstones may include clay-clast conglomerates, with clast size ranging up to pebble size (0.2 to 2.5 inch; 0.5 to 6.4 cm). The primary bedding type in the basal portion of these sandstones is planar crossbedding (fig. 13). Above the scoured base, planar crossbed sets form beds 0.5 to 1.0 ft (0.15 to 0.3 m) thick, and they are interbedded with gently inclined, parallel-laminated beds (thickness 1.0 to 2.0 ft; 0.3 to 0.6 m). The thickness of the parallel-laminated beds decreases upward, and in the middle to upper portions of the channel-fill sandstones,

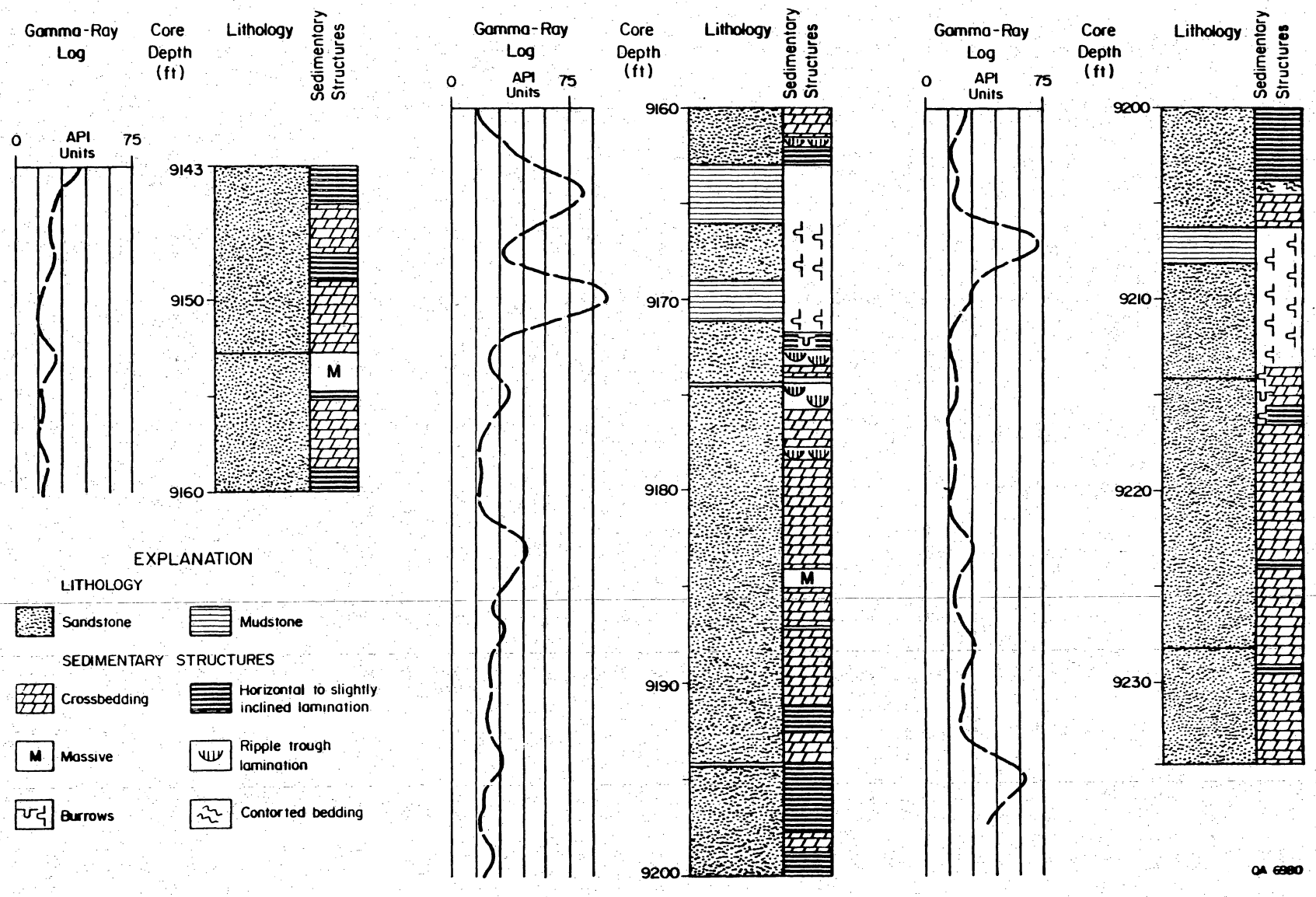

Figure 13. Core description of Prairie Mast No. 1-A well, Nacogdoches County, Texas. This core interval is representative of the braided fluvial deposits in the Travis Peak.

they are replaced by beds (<1.5 ft; 0.5 m thick) of current-ripple laminated sandstone. Near the top of the channel-fill sandstones, planar crossbedding (sets 0.3 to 2.0 ft; 0.1 to 0.6 m thick) grades upward into thinly interbedded (1.0 to 3.0 inches; 2.5 to 7.5 cm) sets of planar crossbeds and current-rippled beds that commonly display climbing ripple lamination. Mudstone is present in the sandstone interval as thin mud drapes on planar crossbeds and ripples (flaser beds) and as rip-up clasts.

Channel-fill sandstones are best developed in the middle and lowermost portion of the Travis Peak (fig. 6). Thickness of channel deposits commonly reflects net thickness of stacked separate channel bodies. On gamma-ray (GR) logs, channel-fill sandstones appear blocky to irregular or serrate in form. Channel bases are generally sharp, but the log in some cases underestimates the actual channel thickness because clay-clast lags on the channel bases are seen as "shales." Many "shaly" breaks noted by GR logs are actually channel lag deposits, and stacking of these channel deposits gives the sandstone a "dirty" appearance.

Abandoned channel fill—Abandoned-channel deposits abruptly to gradationally overlie the channel sandstones and are represented on the GR log by an overall upward-fining serrate pattern. In core, these deposits consist of thin- to medium-bedded (0.5 to 12 in; 1.3 to 30 cm), fine- to very fine grained sandstone, silty sandstone, and mudstone. The prevailing conditions of low sediment input and weak depositional energies in the abandoned channels are reflected in the increased mud content of the sediments and in the greater density of burrows. Trough and planar ripple cross-lamination are common, and ripple foresets are often accentuated by flaser beds and organic drapes. Pyrite associated with the detrital organics is abundant. Contorted, soft-sediment deformed beds as much as 1.5 ft (0.5 m) thick occur within the abandoned-channel deposits. Burrows and somewhat rare rooting structures have obliterated primary structures in the uppermost portion of the abandoned-channel sequences.

Floodplain—Densely rooted and burrowed red to greenish-gray and black sandy mudstones represent the floodplain environment (fig. 13). The thickness of cored floodplain sequences ranges from 2 to 15 ft (0.6 to 4.6 m). Intense biogenic reworking gives these deposits a mottled

appearance, but some sedimentary structures such as laminations or ripples are present. Diagenetic carbonate nodules (Fracasso and others, 1988) and disseminated organic matter are common in the floodplain sediments. Pyrite is absent, suggesting that floodplains were well drained. Floodplain deposits exhibit serrate to uniform shaly patterns on the GR log. The sand and silt content of these deposits is high; therefore, shaly log patterns are not indicative of true shales. More thickly developed floodplain deposits appear serrate on the lithologic log because of the inclusion of thin, muddy sandstones.

Lacustrine—Lacustrine sequences are thin (<6.0 ft; 1.8 m) and not abundant in the cored intervals. They consist of intensely burrowed to laminated and rippled mudstones to silty sandstones. Burrowing is the dominant feature, but lacustrine sediments may also be rooted. Some organic material is preserved. Lacustrine deposits overlie floodplain sediments and are usually overlain by a coarsening- or fining-upward muddy, lacustrine-delta sandstone. This association imparts an upward-fining, shaly character to the lacustrine deposits on the GR log (transition from floodplain to lacustrine). Because the lacustrine deposits are overlain by sandstones, a sharp upper contact is common.

Overbank—Thin (4- to 12-ft; 1.2- to 3.7-m thick), muddy, fine- to very fine grained sandstones deposited in crevasse-splay or lacustrine delta environments commonly overlie or are interbedded with floodplain and lacustrine deposits. These sandstones can form both upward-coarsening and upward-fining sequences. Because these sandstones appear to have been deposited by traction processes during flood events and then to have been later reworked by biogenic processes on the floodplain, their internal stratification can be complex. Planar crossbeds, planar- and trough-ripple laminations, and distorted beds (slumps and dewatering structures) are the most abundant physical structures. Normal-graded and reverse-graded beds 0.5 to 3.0 ft (0.15 to 0.9 m) thick are common. Depending on the intensity of the physical processes and the rate of burial, organisms may have burrowed through the entire sequence and destroyed primary stratification. Overbank sandstones commonly appear as sharp-based and sharp-topped beds on the GR log.

Deltaic Facies

Deltaic deposits are identified in the Travis Peak Formation on the basis of progradational (upward-coarsening) well-log profiles. Additionally, cross sections (figs. 8 to 10) and the isopach and percent-sandstone map patterns (Tye, 1989) reveal that the braided-fluvial facies grades basinward into lobate depocenters. These depocenters are primarily located to the south and east of the study area.

Upward-coarsening deltaic cycles consist of stacked shales, mudstones, and sandstones deposited in prodelta through distributary-mouth bar environments. Well developed cycles reach thicknesses of between 100 and 200 ft (30 and 60 m), indicating that rivers deposited sediments onto a fairly shallow, stable shelf. Through sea-level fluctuations, slow basin subsidence, or both, multiple deltaic cycles were stacked. During the initial phases of Travis Peak deposition, deltas built out over the pre-Travis Peak shallow shelf formed by the Knowles Limestone. Through subsequent deposition, the deltas extended to the south and east as they prograded over, and interfingered with, laterally equivalent shale and sandstone deposited on the Travis Peak shelf (figs. 8 to 10). In the later stages of Travis Peak deposition, the locations of deltaic depocenters shifted progressively updip (north and northwest); transgressed deltaic deposits are overlain by the paralic facies (figs. 8 to 10).

Paralic Facies

Interbedded sandstones and mudstones in the uppermost portion of the Travis Peak Formation are characterized by spiky and upward-fining or upward-coarsening well log responses. These sediments are thought to have been deposited in a paralic depositional setting that consisted of coastal-plain (fluvial meanderbelt, floodplain) and marginal-marine (estuarine, bay, marsh, tidal-channel, shoal) environments. In the proximal regions of the study

area, paralic facies gradationally overlie and interfinger with the fluvial facies. Farther downdip, they overlie deltaic deposits and grade into the shelf facies (figs. 8 to 10).

Cores of paralic deposits reveal the most diverse assemblage of lithofacies in the Travis Peak, and their diversity is strongly apparent along depositional dip (figs. 8 and 9). Coastal plain environments dominate in the updip regions of the study area and grade downdip (south to southeast) into estuarine and marine deposits. Cores that are characteristic of the paralic part of the Travis Peak Formation were recovered from the Clayton Williams Sam Hughes No. 1 well (fig. 14).

Coastal plain—Sandstones in coastal-plain fluvial channels are fine- to very fine grained and vary from 5 to 15 ft (1.5 to 4.6 m) in thickness. An example is the sandstone at 7,088 to 7,101 ft (2,160 to 2,164 m) in the Clayton Williams Sam Hughes No. 1 core (fig. 14). These sandstones have sharp to scoured bases that may be overlain by thin (<0.5 ft; 0.15 m) normally graded beds of sandstone and mudstone. Mud rip-up clasts (clast size may exceed 1.0 inch; 2.5 cm) may be present at their base. Ripples are common; planar crossbeds are present but not as abundant as in the braided-fluvial sandstones. A prominent stratification style is the alternation of low-amplitude current ripples with massive-appearing beds. Soft-sediment deformation (faults, slumps, load and water-escape structures) that resulted in contorted bedding is pronounced in the channel-fill sandstones (fig. 14). Bed thickness decreases and soft-sediment deformation structures increase in abundance approaching the tops of sandstones, where they grade upward into abandoned-channel deposits.

Thin (average thickness 5.0 ft; 1.5 m) sandstone and mudstone intervals overlie the channel-fill sandstones. These fine-grained deposits accumulated in channels abandoned through avulsion or meander cutoff. Trough cross-laminated, wave-rippled, and burrowed sandstone beds less than 1.0 ft (0.3 m) thick are interbedded with laminated, burrowed, and rooted mudstones. Because of the initially high water content of the unstable sediments, soft-sediment deformation features are abundant.

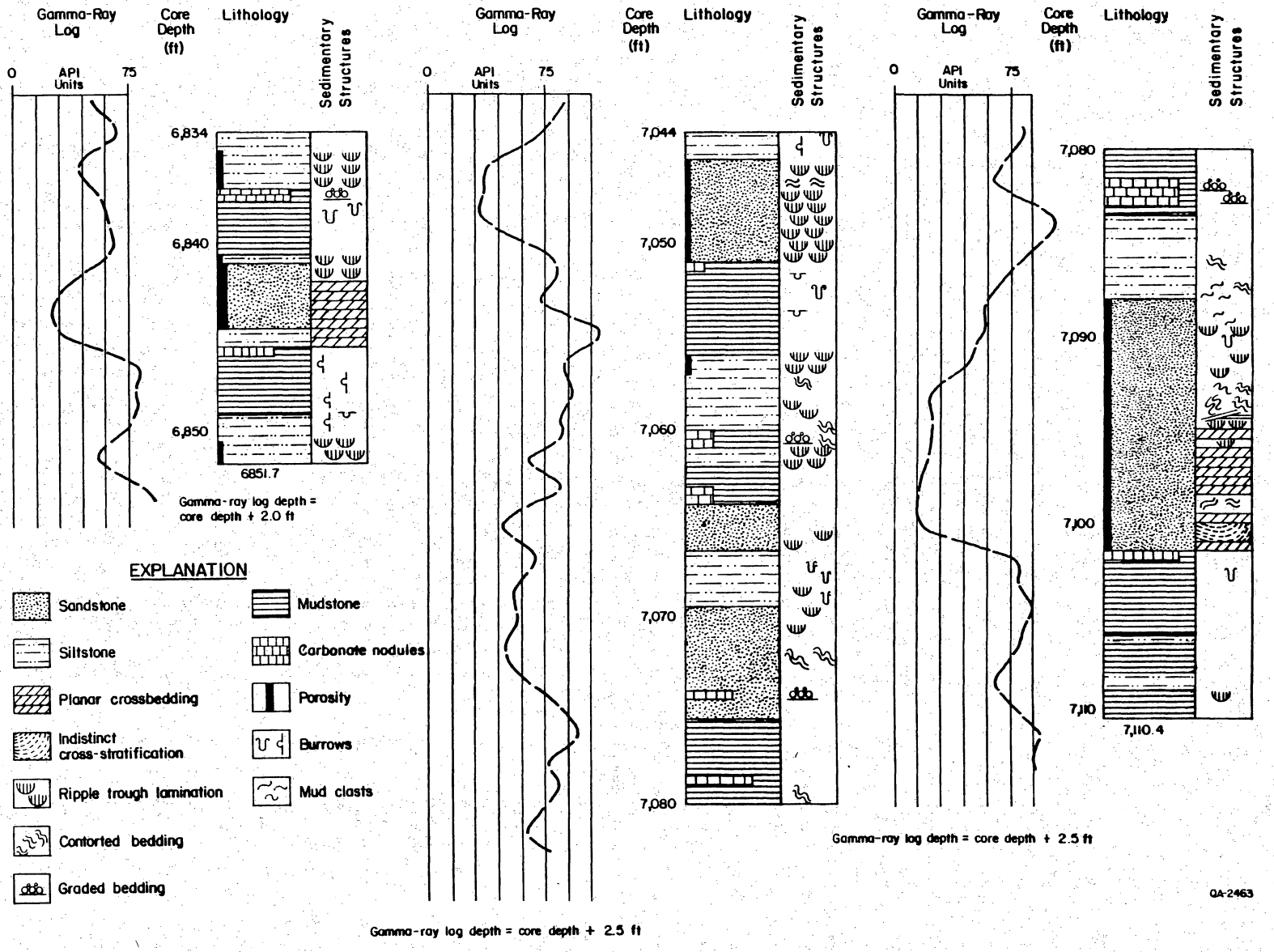

Figure 14. Core description of Clayton Williams Sam Hughes No. 1 well, Panola County, Texas. This core interval is representative of the paralic deposits in the upper Travis Peak.

Interbedded sequences of rooted and burrowed mudstone and thin beds of rippled to cross-laminated sandstone separate the coastal-plain channel deposits and represent deposition in floodplains adjacent to the meanderbelts (for example, fig. 14, 7,044 to 7,088 ft; 2,147 to 2,160 m). Sandstone beds denote episodic periods of overbank deposition in natural-levee, crevasse-splay, or lacustrine environments.

Floodplain and overbank deposits are thicker (2 to 25 ft; 0.6 to 7.6 m) and more laterally continuous than comparable deposits in the braided-fluvial facies of the Travis Peak. Biogenic structures dominate, and burrows of multiple sizes and orientations are more abundant than root traces. Preserved physical sedimentary structures include ripple and flaser bedding in the sandstone beds and parallel laminations, wave ripples, and starved ripples in the sandy mudstones. Soft-sediment deformation is common in the sandstones and mudstones. Pedogenic features, diagenetic carbonate mineralization associated with soil formation (fig. 14), burrows, root traces, and evidence of alternating oxidizing and reducing conditions are characteristic of floodplain deposits.

Marginal marine—Many sandstones and mudstones of the paralic facies, especially in the distal depositional system, are interpreted to have been deposited in marginal-marine depositional environments. These sediments are finer grained and relatively mudstone-rich as compared with the rest of the Travis Peak section, and their log response is highly variable. Evidence of increased biogenic activity, indications of wave and tidal processes, and a greater content of fine-grained sandstone and mudstone indicate a depositional transition from coastal-plain to estuarine conditions. Estuaries occupy zones of gradation containing both continental and marine facies. The lithologic, sedimentologic, and biogenic attributes of the fluvial-channel, tidal-flat, tidal-channel, and estuarine-shoal environments record the contrasting and dynamic depositional processes in estuaries.

Blocky to upward-fining marginal-marine sandstones 10 to 25 ft (3 to 7.5 m) thick are composed of medium bedded (1.0 to 2.0 ft; 0.3 to 0.6 m) trough- and planar-ripple cross-laminated beds. Except in thicker, sharp-based sandstones in which trough and planar cross-

stratification prevail, current- and symmetrical-ripple laminations (0.2- to 1.2-inch [0.5- to 3-cm] sets; 2.0 to 4.0-inch [5- to 10-cm beds), as well as horizontal laminations, are the most common physical sedimentary structures. Soft-sediment deformation, flaser beds, mud drapes, and rip-up clasts occur throughout the marginal-marine sandstones. Planar cross-stratification in several sandstone beds suggests the existence of bidirectional cross-stratification induced by opposing tidal currents, and mud drapes that separate foreset laminae into tidal bundles (Visser, 1980; Reineck and Singh, 1986) are present.

All sandstones in this facies are burrowed, and most are densely burrowed at their tops. Burrow traces are predominantly vertical to obliquely oriented (escape burrows), but many traces are horizontal (grazing burrows). Coal streaks, organic debris, and rare shell material (gastropod and bivalve fragments) are present.

Mudstones and thin sandstones (0.5 to 2.5 ft [0.15 to 0.75 m] thick) are intercalated in intervals that average 5.0 ft in thickness (maximum thickness 10 to 15 ft; 3 to 4.5 m). These intervals do not exhibit upward-coarsening or upward-fining tendencies. Sandstone beds may have scoured bases, but many of the bedding contacts are burrowed. Shell debris (gastropod and bivalve) and clay clasts are concentrated in the coarser-grained beds. Howard and Frey (1973) described Georgia estuaries as having only a small amount of shell material, but they observed some local concentrations.

Owing to less energetic depositional conditions, biogenic sedimentary structures dominate in the mudstones and poorly sorted sandstones. Rooting and burrowing activity destroyed most physical sedimentary structures; those preserved include horizontal laminations, ripple cross-laminations, lenticular beds, and soft-sediment deformation (convoluted beds). Symmetrical ripples and starved ripples are evident. Burrow traces are primarily vertical, and some mudstones contain disseminated organic debris and possible algal laminations.

Howard and Frey (1973), Howard and others (1973), Greer (1975), Freeman (1982), and McCants (1982) have described modern estuarine depositional sequences and assemblages of physical and biogenic sedimentary structures from Georgia and South Carolina that compare

favorably with the Travis Peak paralic cores. Because estuaries are stratigraphically and sedimentologically complex, interpretations of the Travis Peak deposits are somewhat general. However, thick, sharp-base sandstones in the Travis Peak paralic facies are inferred to be deposits of tidal channels and fluvial channels that drained into large estuaries. Other thick sandstones that have sharp to gradational bases are believed to the tidal-flat and estuarine-shoal deposits. Thinner sandstones accumulated in small tidal channels and in tidal flats (for example, 6,840 to 6,844 ft [2,085 to 2,086 m], fig. 14). Mudstones in this sequence represent deposition in swamp, marsh, and lagoon or bay environments.

Shelf Facies

The shelf is the most basinal of the depositional environments examined in this study, and it forms the distal equivalent of the deltaic and paralic facies (figs. 8 to 10). Shelf deposits are thought to occur at the base of the Travis Peak and onlap paralic deposits at the top of the formation. On the basis of logs, shale has been found to be the main sediment type in the shelf facies, and it exhibits a high gamma-ray response. Some sandstone beds of highly variable thickness (less than 2 to 60 ft [less than 0.6 to 18 m]) occur in the shelf facies. Stratigraphic correlations indicate that most of the sandstones are not continuous with the updip deltaic deposits, but instead are separated by an expanse of mudstone 8 to 10 mi (5 to 6 km) wide (fig. 9).

Travis Peak Paleogeographic Evolution

Two prominent Early Cretaceous depocenters are present in the vicinity of the Sabine Arch and the Monroe Uplift along the Gulf Basin arc between East Texas and Mississippi (Cullom and others, 1962; McFarlan, 1977; Saucier, 1985). These depocenters were formed by alluvial systems that were confined within elongate basins oriented parallel to regional

structural dip and perpendicular to the margins of the East Texas Basin. McFarlan (1977) attributed the Lower Cretaceous Travis Peak regression to uplift of the Appalachian and Ouachita Mountains. Saucier (1985) referred to the fluvial system that fed the northwestern corner of the East Texas Basin as the ancestral Red River. It was localized in a structural break or downwarp between the Dallas, Texas, region and the Arbuckle Mountains in southern Oklahoma.

Thinning of the Travis Peak to the northwest (fig. 4) suggests that the Ouachita, Arbuckle, and Wichita highlands were among the sources of Travis Peak sediments (McGowan and Harris, 1984; Saucier, 1985). The large volume of sediment in the Travis Peak Formation, however, indicates that these areas were not the only source of sediments. Contemporary highlands in the Rocky Mountains and Triassic and Jurassic sedimentary terranes to the southwest may have been additional sources of Travis Peak sediments (Saucier, 1985). Moreover, textural and mineralogical maturity of Travis Peak sandstones (Dutton, 1987) implies a reworked sedimentary (multi-generation) source.

Despite rising sea level, rivers debouching into the basin initially had sufficient discharge and an ample supply of sediment with which to construct the Travis Peak depocenters. A series of maps (fig. 15) schematically illustrates the evolution of the East Texas depocenter during Travis Peak time. Each map depicts the occurrence and distribution of sedimentary facies during a particular time period of Travis Peak deposition. The time interval that each map represents is variable and cannot be ascertained because no dated stratigraphic markers divide the Travis Peak. Refer to figure 15 to supplement the following discussion of Travis Peak evolution.

Paleogeography: Time 1

Initial Travis Peak development is marked by the progradation of the shoreline that was supplied sediment by north-south- to northwest-southeast-oriented braided fluvial systems. Channelbelts were separated by elongate interfluves that ranged from 10 to 20 mi (16 to 32

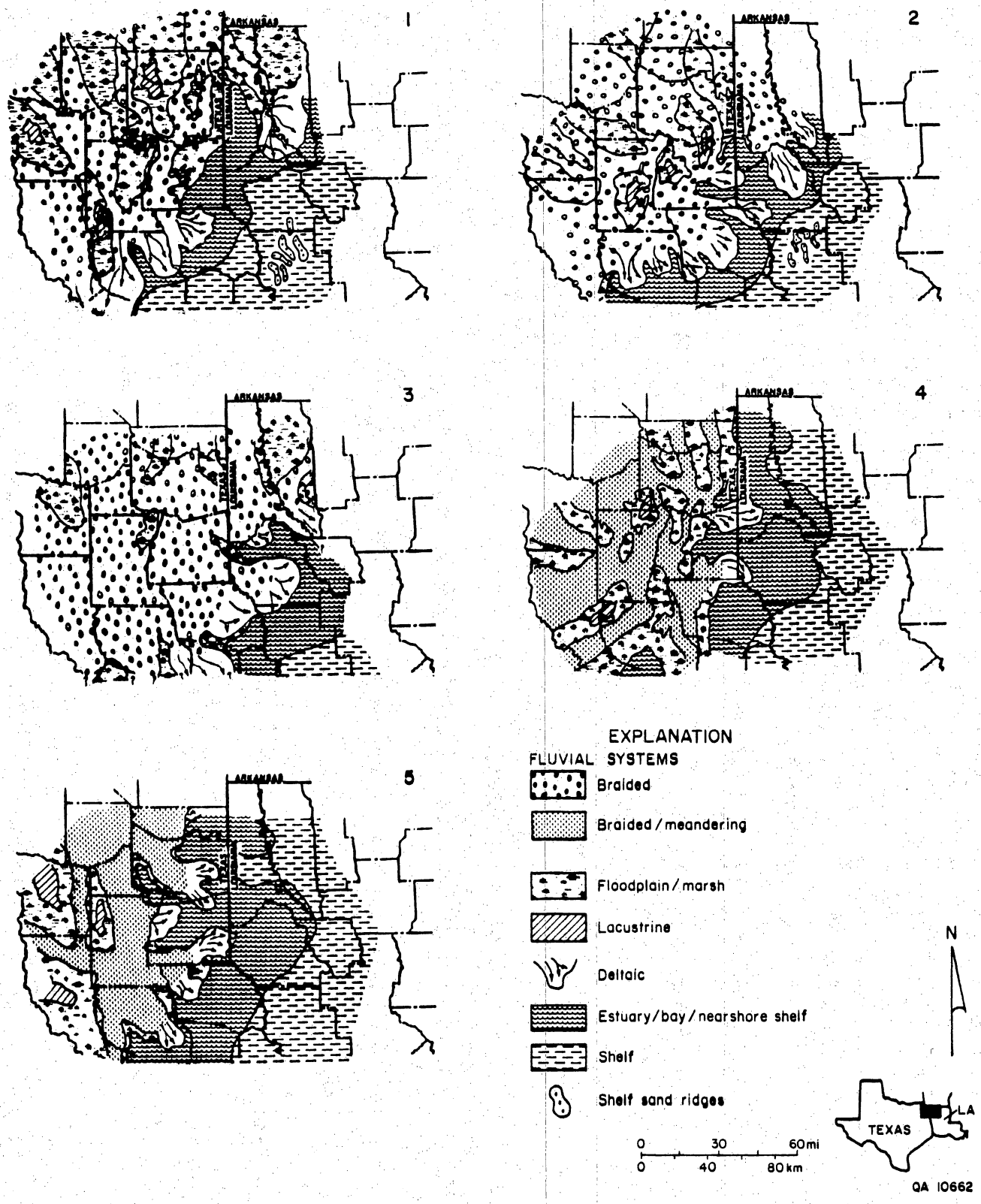

Figure 15. Hypothetical paleogeographic reconstructions for five time periods during Travis Peak deposition. Note initial development and progradation of fluvial-deltaic systems, followed by shoreline transgression. Interpretations are based on sedimentary patterns observed in isopach, net-sandstone, and percent-sandstone maps of lithostratigraphic units 1 through 5 (Tye, 1989) and core from wells shown in figure 5. Actual time span represented by each period is variable and unknown.

km) in width. Floodplain (swamp), lacustrine and lacustrine-delta, and overbank (levee, crevasse-splay) environments occupied the interfluves. Large, elongate delta lobes fed by the braided channelbelts covered hundreds of square miles (fig. 15). Shallow estuaries and bays separated delta lobes. To the east, a muddy shelf extended basinward, but in north-central Sabine Parish, shelf-sandstone ridges, perhaps representing reworked deltaic deposits, were present.

Paleogeography: Time 2

Increased development of the braided-fluvial system and progradation of the shoreline is evident during Time 2 (fig. 15). Floodplains decreased in size, perhaps by channel migration and reworking, but also through overbank deposition and filling of swampy areas. Concurrently, estuaries were drained and filled, thus creating floodplains and marshes between delta lobes.

Deltas increased in size and extended farther basinward during Time 2. Existing deltaic deposits at the end of Time 1 were partially cannibalized during this phase of fluvial progradation and delta enlargement. Additional deltas developed near the Louisiana border. As in Time 1, a marine shelf was present eastward of Shelby County and DeSoto Parish, and shelf-sandstone deposits (derived from marine-reworked deltas and delta-front sediment-gravity processes) accumulated in north-central Sabine Parish.

Paleogeography: Time 3

The distribution of sedimentary facies during Time 3 illustrates the farthest basinward advance of the Travis Peak shoreline. Continued development of braided channelbelts from Time 1 through Time 3 resulted in much fluvial reworking (erosion and redeposition) and a sharp reduction of floodplain deposits. During Time 3, most of the western portion of the study area was occupied by a braided channelbelt (fig. 15). Previously deposited deltas in southern

Cherokee, Nacogdoches, and San Augustine Counties were abandoned (they subsided or were reworked, or both), and the braided-fluvial and deltaic systems extended south of the study area. Estuarine, nearshore, and shelf environments were present in a very small portion of the study area at this time.

Paleogeography: Time 4

Time 4 records a marked change in the geomorphology of the Travis Peak that was induced by the rising Cretaceous Sea (fig. 15). Dominantly north-south and northwest-southeast-oriented fluvial systems were present as braided to meandering channelbelts that were smaller than the previously deposited braided channelbelts. Floodplains, lakes, and marshes occupied interfluves between channelbelts.

The extent of deltaic deposition decreased drastically during Time 4. As river valleys were drowned, estuaries covering tens to hundreds of square miles developed between the delta lobes. Shelf environments became more widespread, but because of decreased sediment input and rising sea-level conditions, no sand-size sediment was transported to the shelf.

Paleogeography: Time 5

Maximum flooding of abandoned deltas and river courses and formation of large estuaries characterizes the final stages of Travis Peak deposition. Fluvial systems that were present during early Time 5 deposition appear to have been larger than those present in Time 4. They fed a series of small deltas and were separated laterally by floodplain and lacustrine environments (fig. 15). At the end of Travis Peak deposition, the entire study area consisted of marginal-marine to marine environments.

STAGED FIELD EXPERIMENTS—STRUCTURAL AND DEPOSITIONAL SETTINGS

Geologic study of the Travis Peak involved extensive collection of core and production data, requiring operator activity and cooperation. A total of 1,280 ft (390 m) of Travis Peak core was drilled by GRI in seven cooperative wells, and an additional 1,440 ft (439 m) of existing core was loaned or donated by operators (fig. 7; table 1). Information gained from the cooperative wells, combined with detailed geologic characterization of two smaller fairways within the East Texas study area, led to the drilling of three GRI Staged Field Experiment (SFE) wells. SFE No. 1 was drilled in Waskom field, Harrison County, Texas, in August 1986, and SFE No. 2 was drilled in North Appleby field, northern Nacogdoches County, Texas, in September, 1987. The research focus in these two wells was on productive sandstones near the top and base of the Travis Peak Formation. SFE No. 3 was drilled in September, 1988, in Waskom field. In this well, the research focus was the low-permeability Taylor Sandstone in the lower Cotton Valley Formation. The objective of this well was to test the transfer of technologies, techniques, and models developed during study of the Travis Peak Formation to the Cotton Valley. Almost 960 ft (293 m) of Travis Peak core and 242 ft (74 m) of Cotton Valley core were recovered in the three SFE wells and were used in geologic analyses.

Cores taken in the three SFE wells provide examples of several Travis Peak depositional systems. A brief description of the geology of each SFE well follows; more detailed discussion of the interpretation of cores from the SFE wells are found in Dutton and others (1988), Laubach and others (1989b), and Dutton and others (in press).

SFE No. 1

SFE No. 1 is located in Waskom field, Harrison County, Texas, on the northwest flank of the Sabine Arch. The Waskom structure is a gentle north-trending structural dome with

Table 1. Travis Peak cores used in this study.

Well no. (Fig. 1)	Well	Well abbrev.
1	ARCO B. F. Phillips No. 2 (cooperative well)	BP
2	ARCO S. F. Hammon No. 2	HA
3	Delta E. Williams No. 1-A	EW
4	Stallworth Renfro No. 2	SR
5	Stallworth Everett No. 2-B	EB
6	Sun Janie Davis No. 2	JD
7	Amoco Caldwell Gas Unit No. 2	CGU
8	Henderson Clay Products Christian No. B-2A	HC
9	Amoco M. Kangerga No. 1-C	MK
10	Henderson Clay Products M. J. Doerge No. 2	HD
11	Clayton Williams Sam Hughes No. 1 (cooperative well)	SH
12	Sun D. O. Caudle No. 2	DC
13	Prairie Mast No. 1-A (cooperative well)	PM
14	Holditch SFE No. 2	HS
15	Ashland S.F.O.T. No. 1 (cooperative well)	SF
16	Arkla Alton Lilly No. 2	AL
17	Arkla Pate No. 1	AP
18	Marshall Werner Sawmill No. 5 (cooperative well)	WS
19	Reynolds Marshall No. 1	RM
20	Reynolds Duncan No. 1	RD
21	Marshall Abney No. 2	MA
22	Brasfield Bradshaw Heirs No. 1-A	BB
23	Mobil Cargill No. 15 (SFE No. 3)	SFE3
24	Mobil Cargill No. 14 (cooperative well)	MC
25	Arkla T. P. Scott No. 5 (cooperative well)	AS
26	Holditch Howell No. 5 (SFE No. 1)	HH

approximately 120 ft (37 m) of relief on the top of the lowest carbonate bench in the Sligo Formation (fig. 16). At least one well, the Arkla Waskom-Smackover No. 1, penetrated salt at a depth of 11,341 ft (3,457 m) over the Waskom structure. At SFE No. 1 the top of the Travis Peak occurs at approximately 6,000 ft (1,830 m) below sea level and beds dip northwestward.

Two main intervals of the Travis Peak were cored in SFE No. 1 (fig. 17). The cores from the lower Travis Peak interval (7,395.3 to 7,562.8 ft; 2,254 to 2,305 m) contain sandstone beds up to 28 ft (9 m) thick, interbedded with red and gray mudstones. The three sandstones in the interval, informally called the X, Y, and Z sandstones, have been mapped as single depositional units across Waskom field (fig. 18). These sandstones exhibit multiple fining-upward cycles, the upper sections of which are commonly truncated. The sandstones generally have scoured lower contacts and high-angle crossbeds and planar laminations near the base, and they are capped by rippled and burrowed muddy sandstone. The best reservoir quality occurs in the crossbedded and planar laminated sandstones at the base of each cycle. Natural fractures are present in producing intervals in this well.

Most mudstones in the lower Travis Peak are thin, but a 15-ft-thick (4.6 m) mudstone occurs at 7,474.5 to 7,490.0 ft (2,278 to 2,283 m). This red mudstone has a burrowed, disturbed texture and contains abundant carbonate nodules. The rocks in the lower Travis Peak section of core are interpreted to have been deposited in a proximal fluvial environment. The crossbedded and planar-laminated sandstones may be longitudinal and transverse-bar deposits and channel fills from a sand-rich, low-sinuosity braided stream system. The tops of many of the sandstones are burrowed, which probably took place after the waning of floods. The mudstones interbedded with these sandstones are interpreted as overbank floodplain deposits. Three intervals in the X sandstone were perforated for production in SFE No.1 (fig. 17).

The upper cored interval (5,950.0 to 6,311.0 ft; 1,814 to 1,923 m) contains sandstones interbedded with thicker red and gray mudstones than in the lower cored interval. The sandstones in the lower part of this cored interval have sharp bases, and the highest-energy sedimentary structures (i.e., crossbeds and parallel to slightly inclined laminae) occur in the

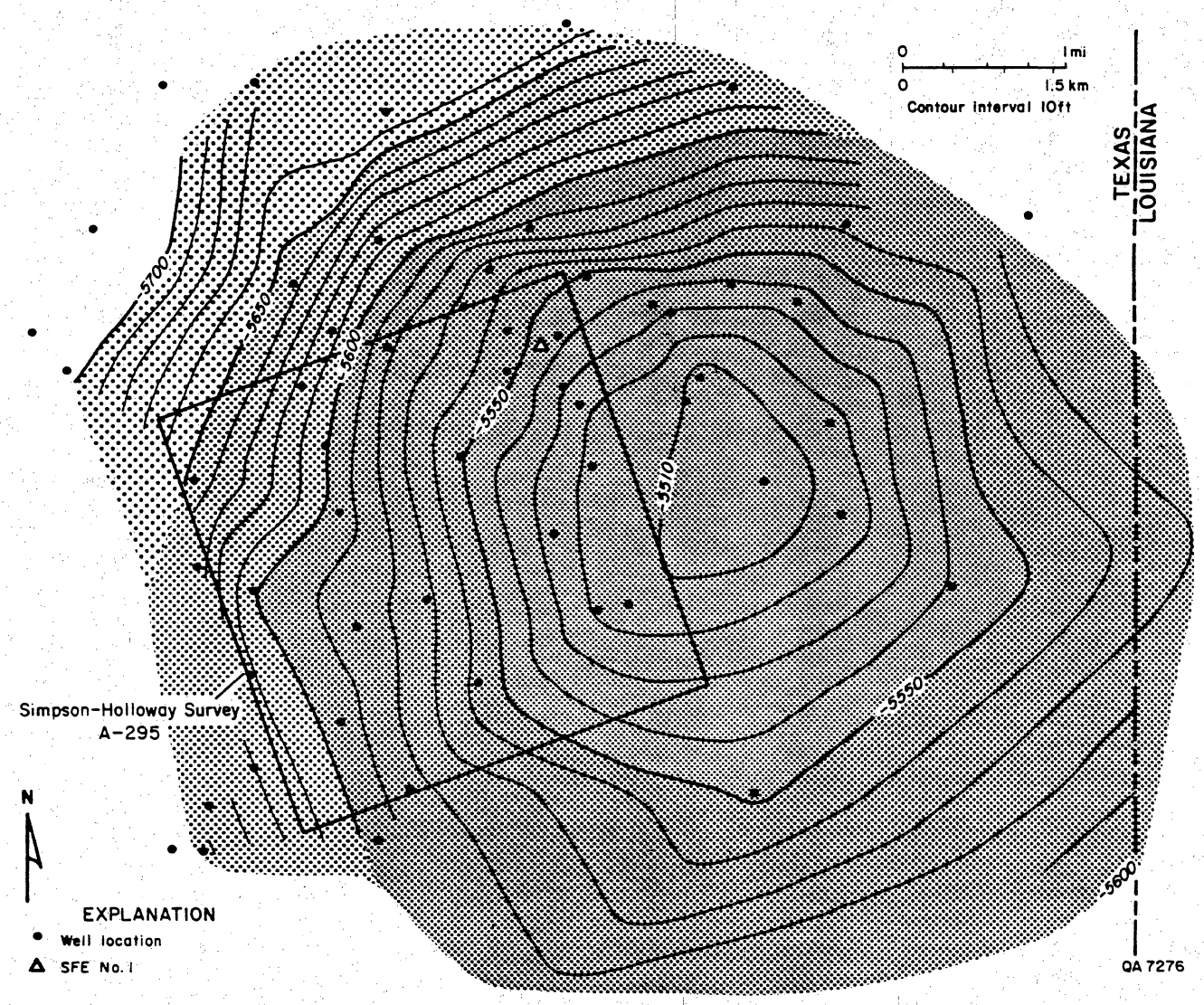

Figure 16. Structure map of the top of the lowest carbonate bench in the Sligo Formation, Waskom field, Harrison County, Texas. Location of SFE No. 1 (Holditch & Associates Howell No. 5) is shown.

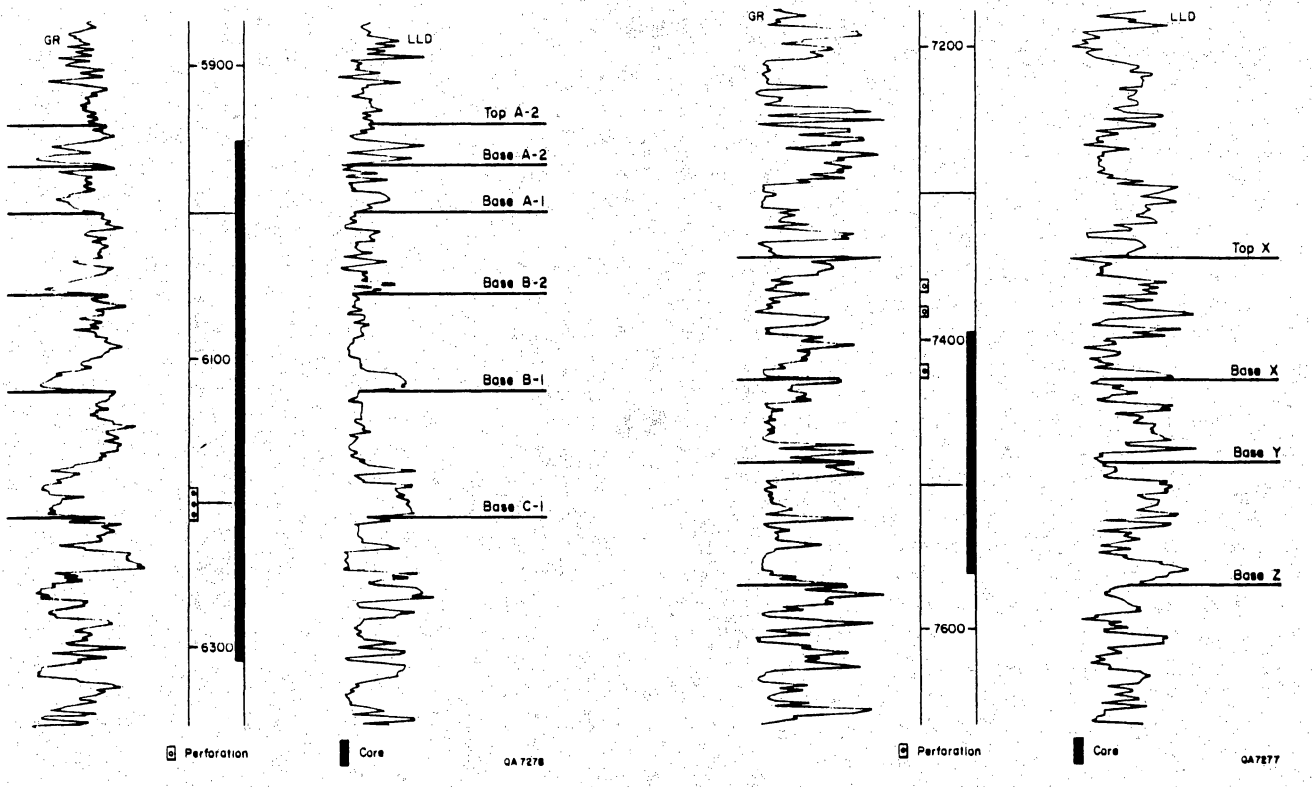

Figure 17. Informal nomenclature of lower and upper Travis Peak producing sandstones, SFE No. 1 well. Cored and perforated intervals are shown.

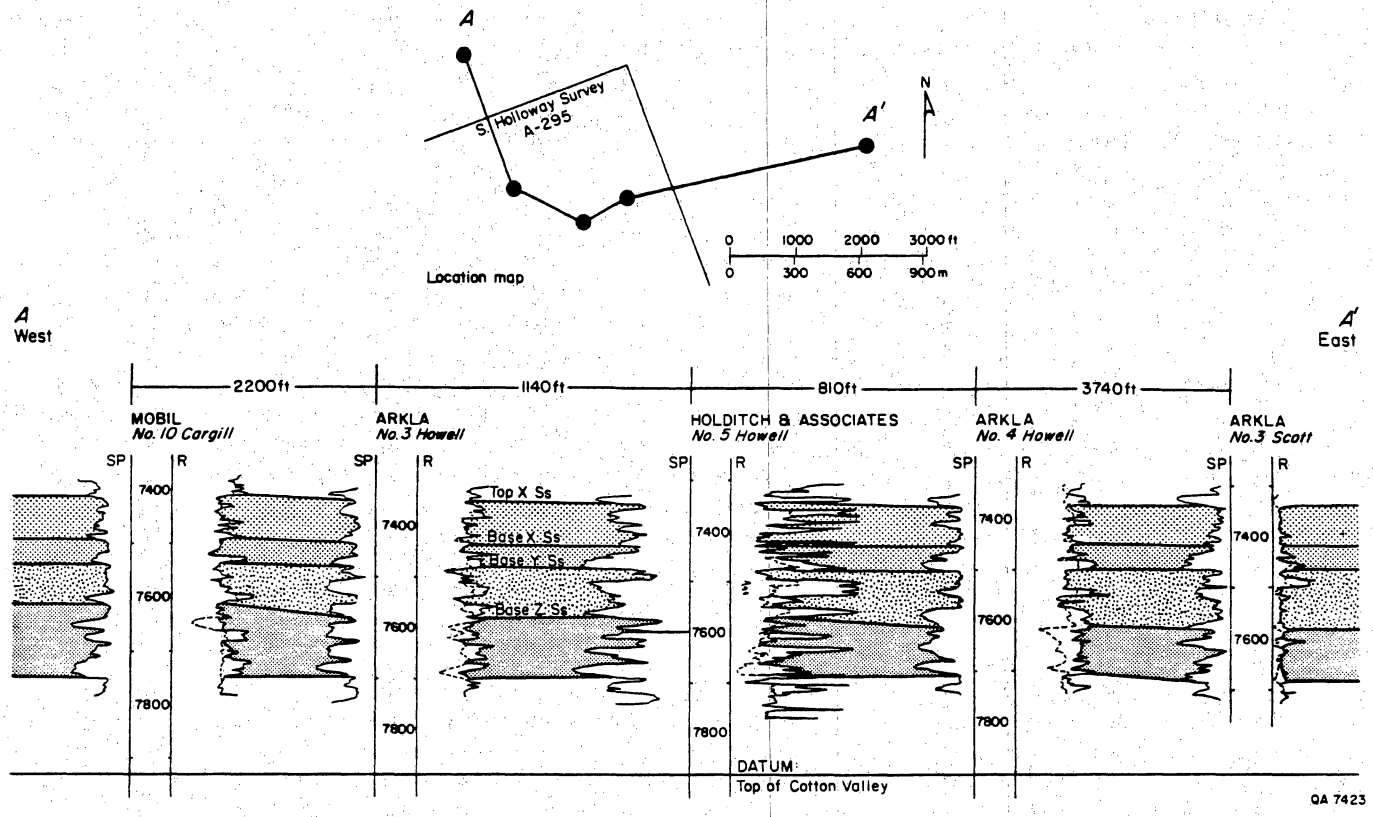

Figure 18. Cross section of lower Travis Peak producing sandstones in the area around the SFE No. 1 well.

lower part of the sandstones, which have the best reservoir quality. The sandstones fine upward, and the upper parts are extensively burrowed. An example is the B-1 sandstone at 6,110 to 6,125 ft (1,862 to 1,867 m) (fig. 17). Many of the burrows are highlighted by reservoir bitumen. Calcareous nodules are common in the mudstones and at the base of sandstones. Most mudstones are red, but some mudstones are gray and contain pyrite associated with organic matter.

Above 6,010 ft (1,832 m) in the upper cored interval, all mudstones are gray. Sandstones are thin, extensively burrowed, and cemented by carbonate. In the upper part of the cored interval, limestones are interbedded with siliciclastic mudstones. The limestones are packstones, that is, they are composed of skeletal fragments and carbonate mud. Oyster, pelecypod, and gastropod shell fragments are the most common skeletal grains. Thin stringers of terrigenous clastic mud are common within limestone beds.

The upper cored interval records the transition from continental to shallow-marine deposition. The lower part of this interval lacks evidence of marine deposition, and the rocks probably represent small fluvial-channel and crevasse-splay deposits in the adjacent floodplain. This environment represents a more distal fluvial setting compared with the rocks of the lower core. The red and gray mudstones are interpreted as overbank floodplain deposits. Mudstones are relatively thick in this core, suggesting that the streams carried bedload and suspended load, and overbank floodplain deposits were preserved in the system. The upper part of the cored interval is interpreted as having been deposited in a paralic setting, such as a lower delta plain to interdistributary bay environment. Periodic marine incursions in the upper Travis Peak are recorded by the limestones near the top of the formation.

Upward-fining sandstones in the upper 300 ft (90 m) of the Travis Peak are largely continuous around SFE No. 1 (fig. 19) and have been mapped as single depositional units. The bases of three of these sandstones in the upper Travis Peak have been used to arbitrarily define larger-scale operational stratigraphic units. The sandstone sequences, from top to base, are known as A, B, and C (figs. 17 and 19). The C sandstone sequence is approximately 95 ft (29 m)

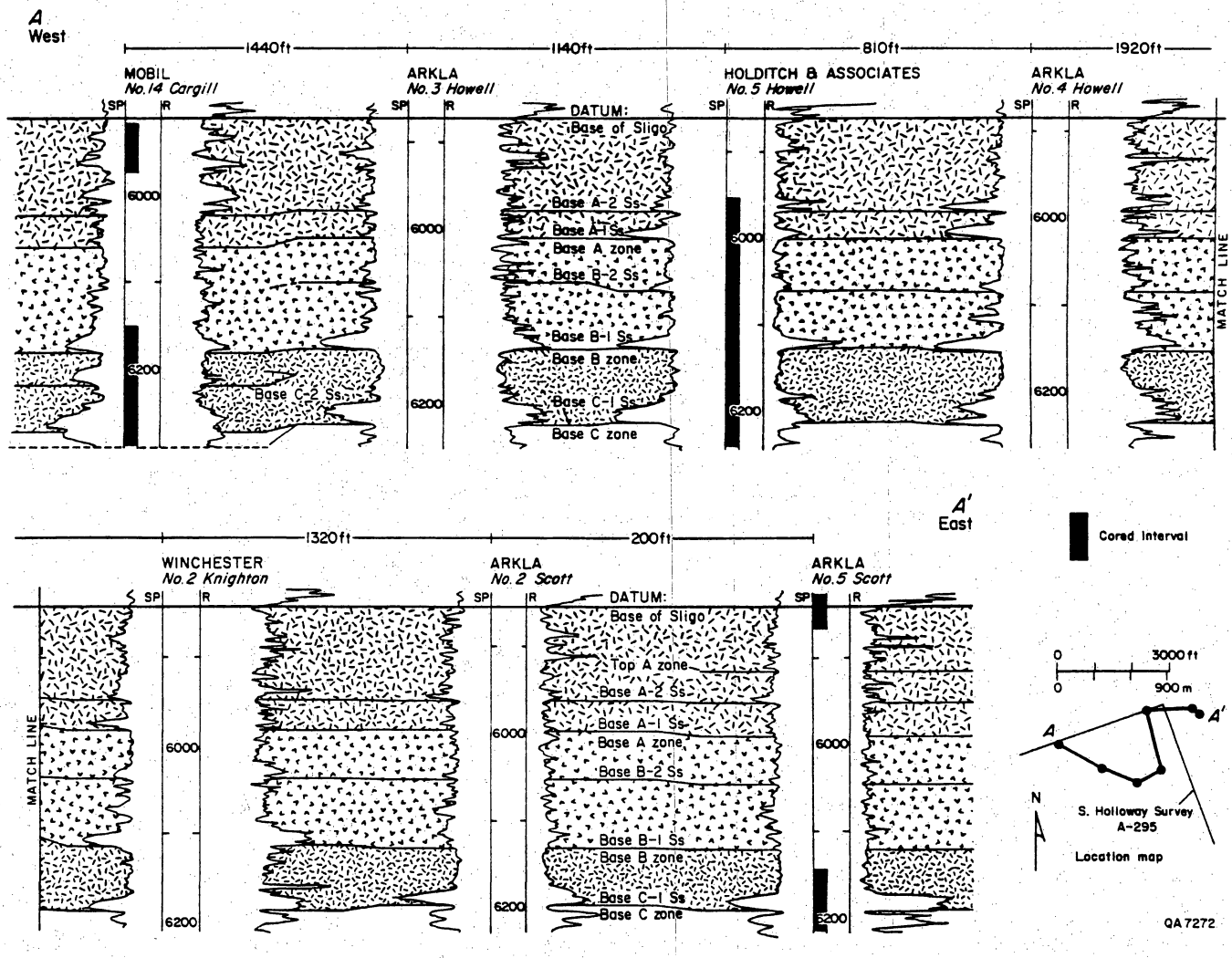

Figure 19. Cross section of upper Travis Peak producing sandstones in the area around the SFE No. 1 well.

thick and is comprised of two generally well-developed fining-upward sandstones, designated the C-1 and C-2. The C-1 was perforated for production in the SFE No. 1 well (fig. 17).

Upward-fining sandstones dominate the upper Travis Peak producing interval in the Waskom play. The mapped distributions of individual upward-fining sandstones delimit moderately sinuous, branching fluvial channelbelts (fig. 20). Channelbelts range from approximately 1,500 ft (457 m) (A-1 sandstone) to greater than 12,000 ft (3,657) wide (A-2 sandstone).

SFE No. 2

SFE No. 2 was drilled in North Appleby field, in a domain of uniform, gentle (80 ft/mile; 14 m/km) southwesterly dip. North Appleby field, which is located on a homocline with no structural closure (fig. 21), has produced approximately 7 Bcf of gas from combined stratigraphic and diagenetic traps. Production in North Appleby field is from sandstones throughout the Travis Peak, but most production occurs within the fluvial facies of the formation. Within the 2,000-ft-thick (610-m-thick) Travis Peak interval, fluvial deposits dominate in all but the upper 300 ft (90 m). Depth to the top of the Travis Peak averages 8,000 ft (2,438 m). Figure 22 shows the gamma ray and resistivity (SFL) logs from SFE No. 2, in addition to the cored and perforated intervals. Sandstones completed for gas production in SFE No. 2 are within Zones 1 and 4 (fig. 22).

The thickest and most continuous discrete sandstones within Zones 1 and 4 represent channelbelts deposited in a fluvial depositional environment. Although these sandstones are laterally persistent, they exhibit vertical and lateral discontinuities. Four channelbelts are present in Zone 1 (only three of which occur in SFE No. 2: C, B, A, in descending order; figs. 22 and 23). In Zone 1, multilateral fluvial channel sandstones occur in broad flat-lying lenses. They reach maximum thicknesses of 25 to 40 ft (8 to 12 m), and their widths range from 1 to 6 miles (1.6 to 9.6 km). Sandstones are separated vertically by floodplain deposits, and mudstones

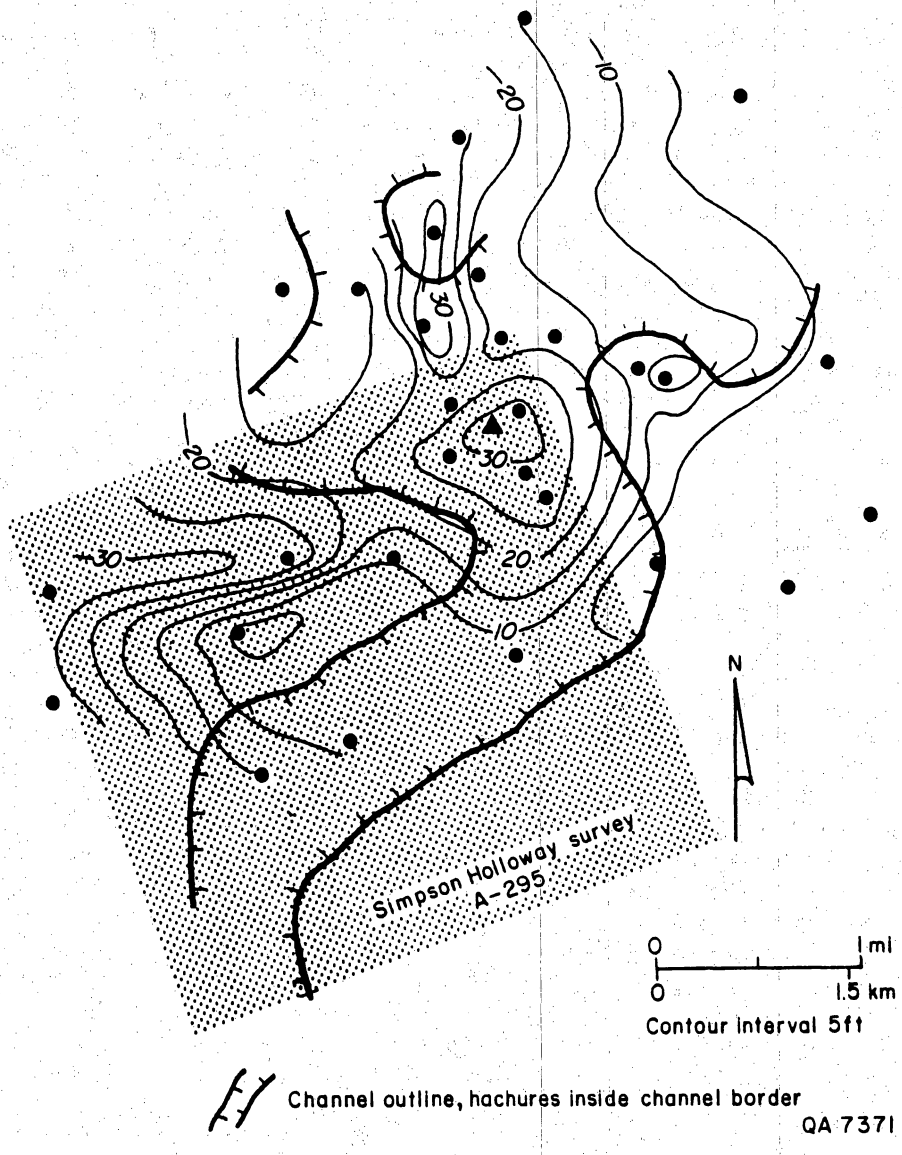

Figure 20. Net-sandstone map of upper Travis Peak C-1 sandstone with channel borders superimposed.

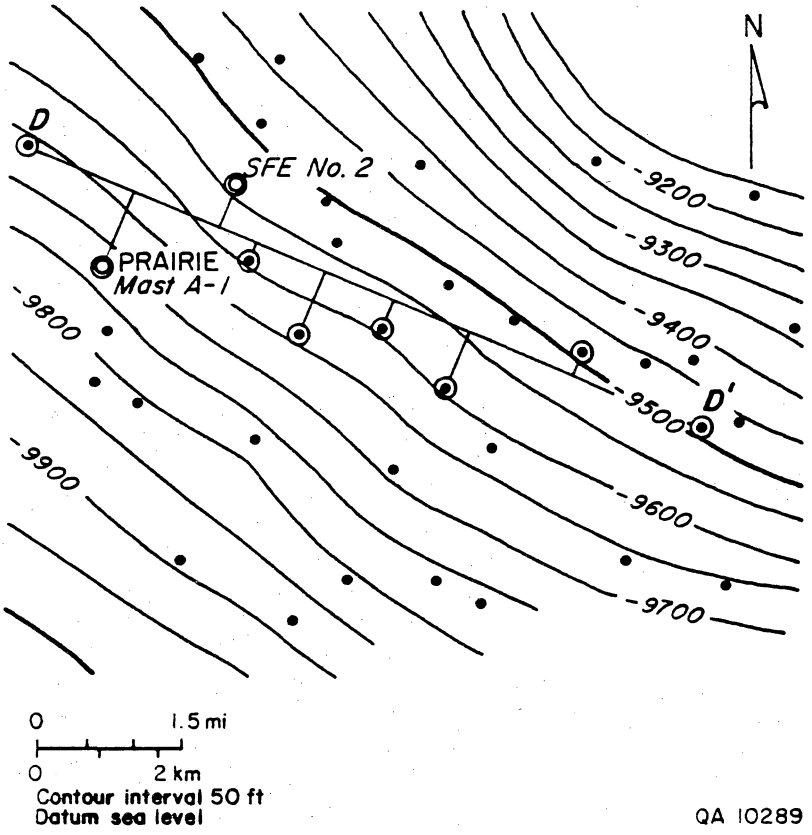

Figure 21. Structure-contour map on the top of the Cotton Valley Formation, North Appleby field, showing the Prairie Mast No. A-1 cooperative well and SFE No. 2. Cross section D-D' shown in figures 23 and 24.

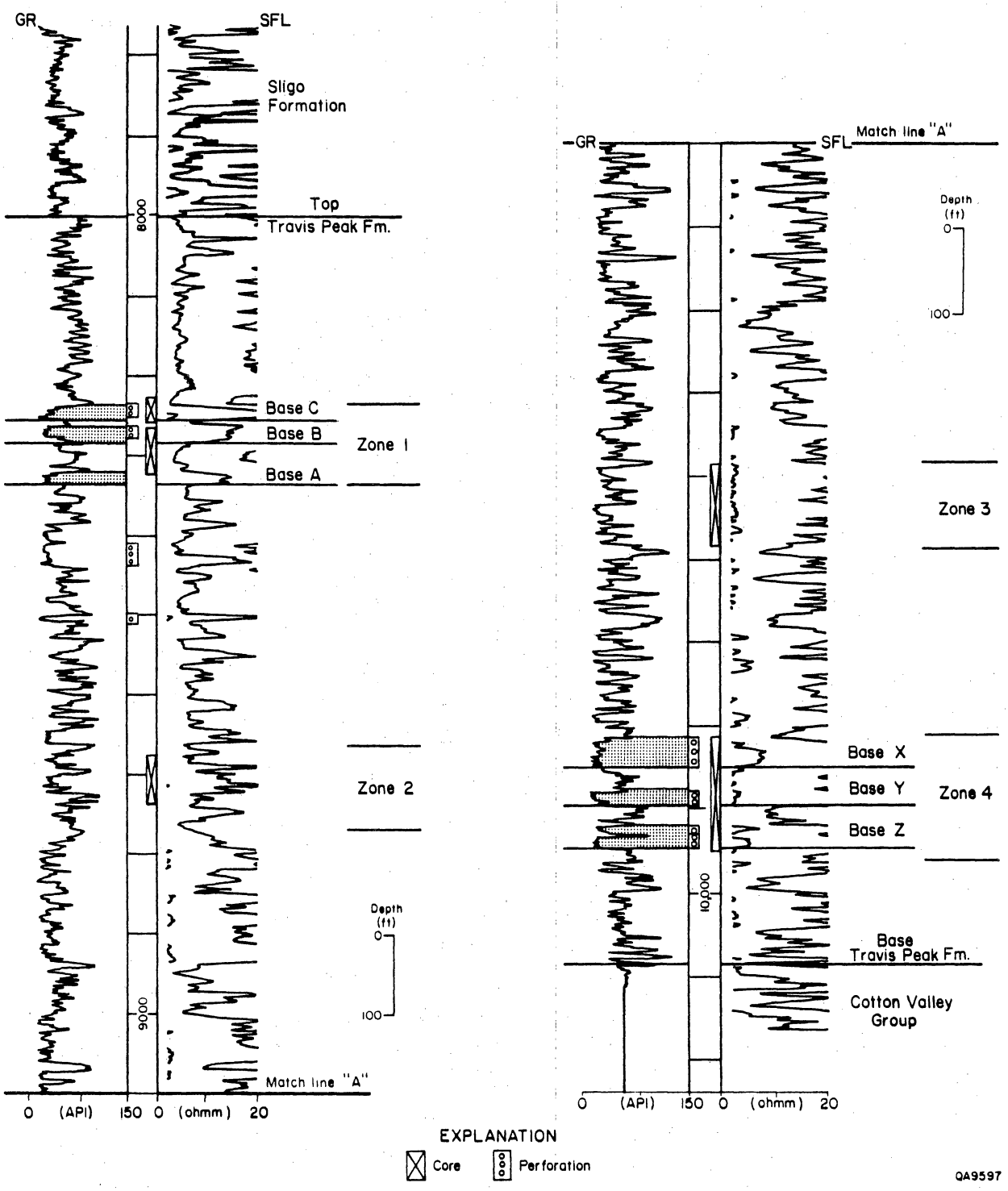

Figure 22. Gamma-ray and resistivity (SFL) logs and informal nomenclature for the Travis Peak Formation in SFE No. 2. Cored and perforated intervals are shown.

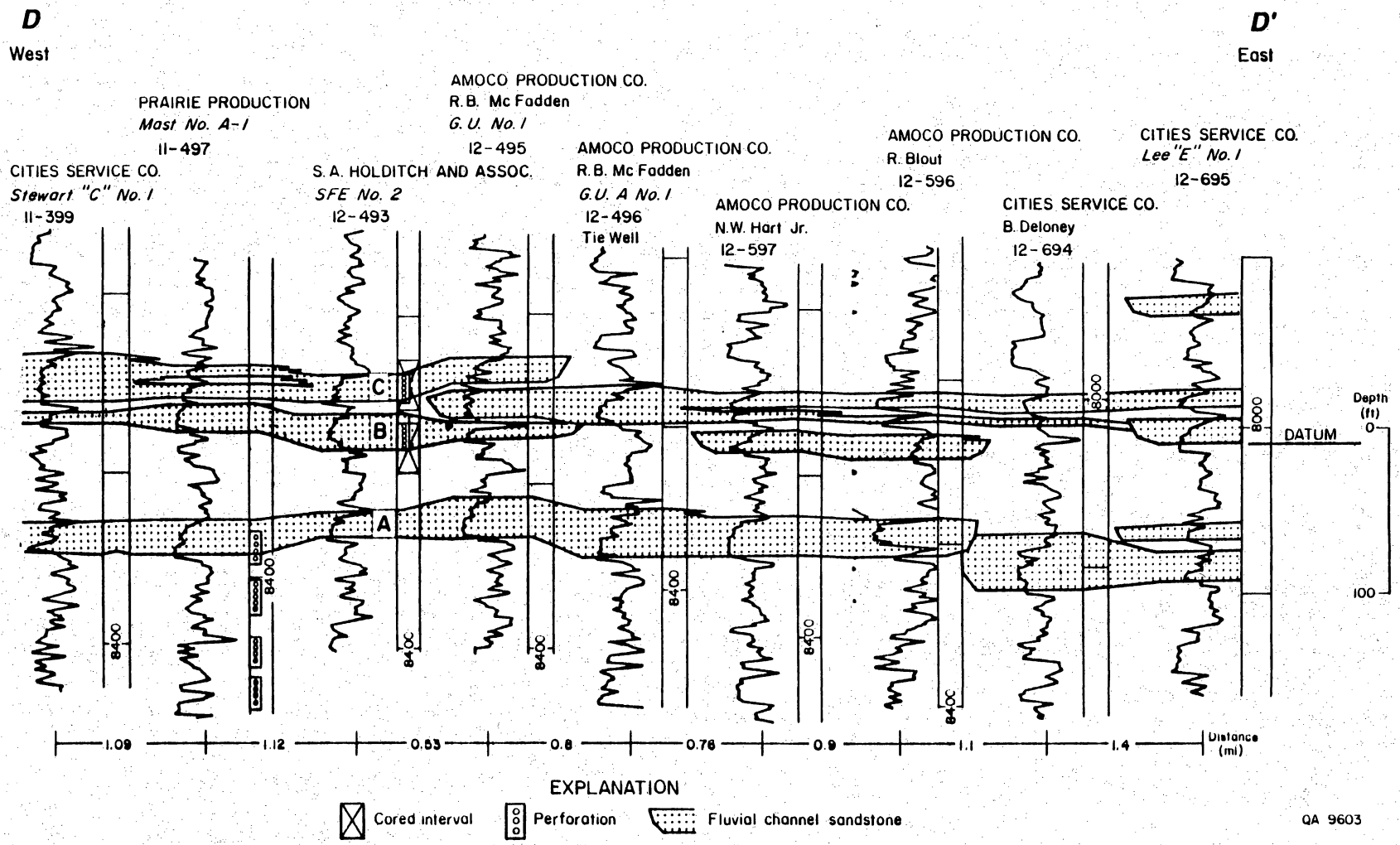

Figure 23. Stratigraphic cross section D-D' illustrating the occurrence and geometry of channelbelt sandstones in upper Travis Peak Zone 1, North Appleby field. Multilateral fluvial channel sandstones occur in broad lenses. Discrete sandstone lenses may be in horizontal contact due to lateral channel migration. Gamma-ray log curves are shown. Line of section shown in figure 21.

interfingering with the channel deposits result in some internal lithologic heterogeneity. Discrete sandstone lenses may be in horizontal contact due to lateral channel migration. Channelbelts B and C, the two uppermost sandstones in Zone 1, were perforated (figs. 22 and 23). In Zone 4, eight channelbelts are present, and three of these channelbelts occur in SFE No. 2 (X, Y, Z, in descending order; figs. 22 and 24). The X, Y, and Z sandstones were all perforated in SFE No. 2. There is a relative increase in multilateral fluvial channel sandstones in Zone 4 as compared to Zone 1. The braided channelbelt sandstone deposits reach maximum thicknesses of 35 to 45 ft (11 to 14 m), and their widths range from 2.5 to 5 miles (4 to 8 km). Erosional juxtaposition of discrete sandstone lenses is greater in Zone 4 than in Zone 1, thus indicating a higher degree of channel scour and lateral migration.

Channelbelt sandstones appear as sharp-based and sharp-topped packages on SP and gamma-ray logs. Channelbelt thicknesses range from 8 to 29 ft [2.4 to 8.8 m] (average = 20 ft [6.1 m]) in Zone 1, and from 8 to 44 ft [2.4 to 13.4 m] (average = 27 ft [7.1 m]) in Zone 4. Log correlations indicate that single channelbelts have widths that exceed 3.5 to 5 mi (5.6 to 8 km), and their thickness-to-width ratios are approximately 1:800. Individual channelbelt sandstones can generally be correlated over an area encompassed by as many as 20 wells that are drilled on 640 acre-spacing.

Net sandstone maps of Sandstone B, Zone 1, and Sandstone X, Zone 4 (figs. 25 and 26), depict the range of channelbelt thicknesses and orientations. These sandstones were deposited by numerous braided-fluvial channels that formed and migrated within the 3- to 5-mile-wide (5- to 8-km-wide) channelbelts. Sandstone X has a northeast-southwest orientation, whereas Sandstone B trends north-south.

In summary, the best quality reservoir sandstones in SFE No. 2 occur in wide channelbelts oriented parallel to depositional dip. These channelbelts form a network of overlapping, broad, tabular sandstones with thickness-to-width ratios of 1:850 (8 to 44 ft thick [2.4 to 13.4 m]; widths exceeding 4 to 5 miles [6.4 to 8 km]). Reservoir quality decreases at channel margins (levees), tops (abandoned channel deposits), and in interchannel areas where siltstone and

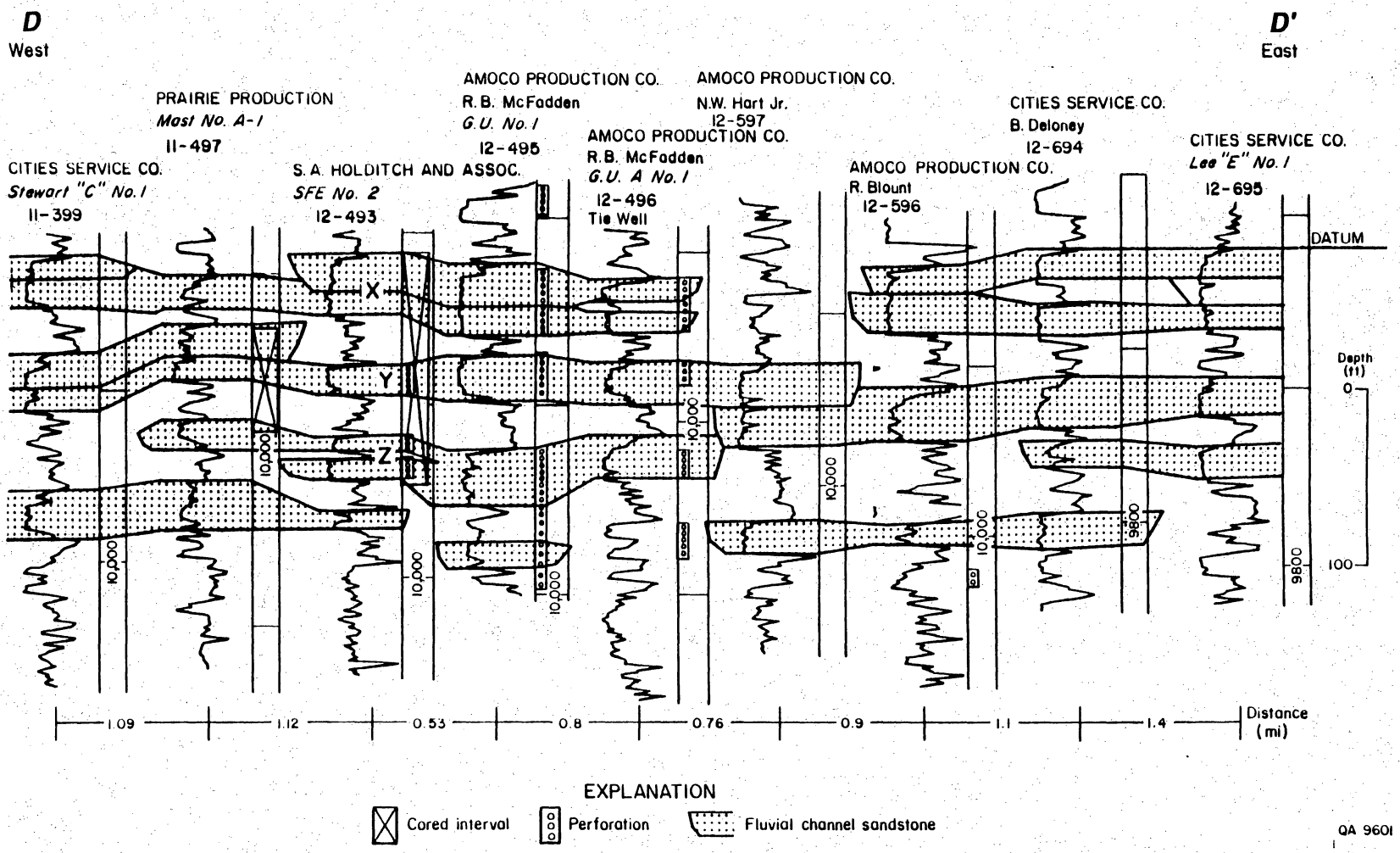

Figure 24. Stratigraphic cross section D-D' illustrating the occurrence and geometry of channelbelt sandstones in lower Travis Peak Zone 4, North Appleby field. Note the relative increase in multilateral fluvial channel sandstones in Zone 4 as compared to Zone 1 (fig. 23). Erosional juxtaposition of discrete sandstone lenses is greater in Zone 4 than in Zone 1, thus indicating a higher degree of channel scour and lateral migration. Gamma-ray log curves are shown. Line of section shown in figure 21.

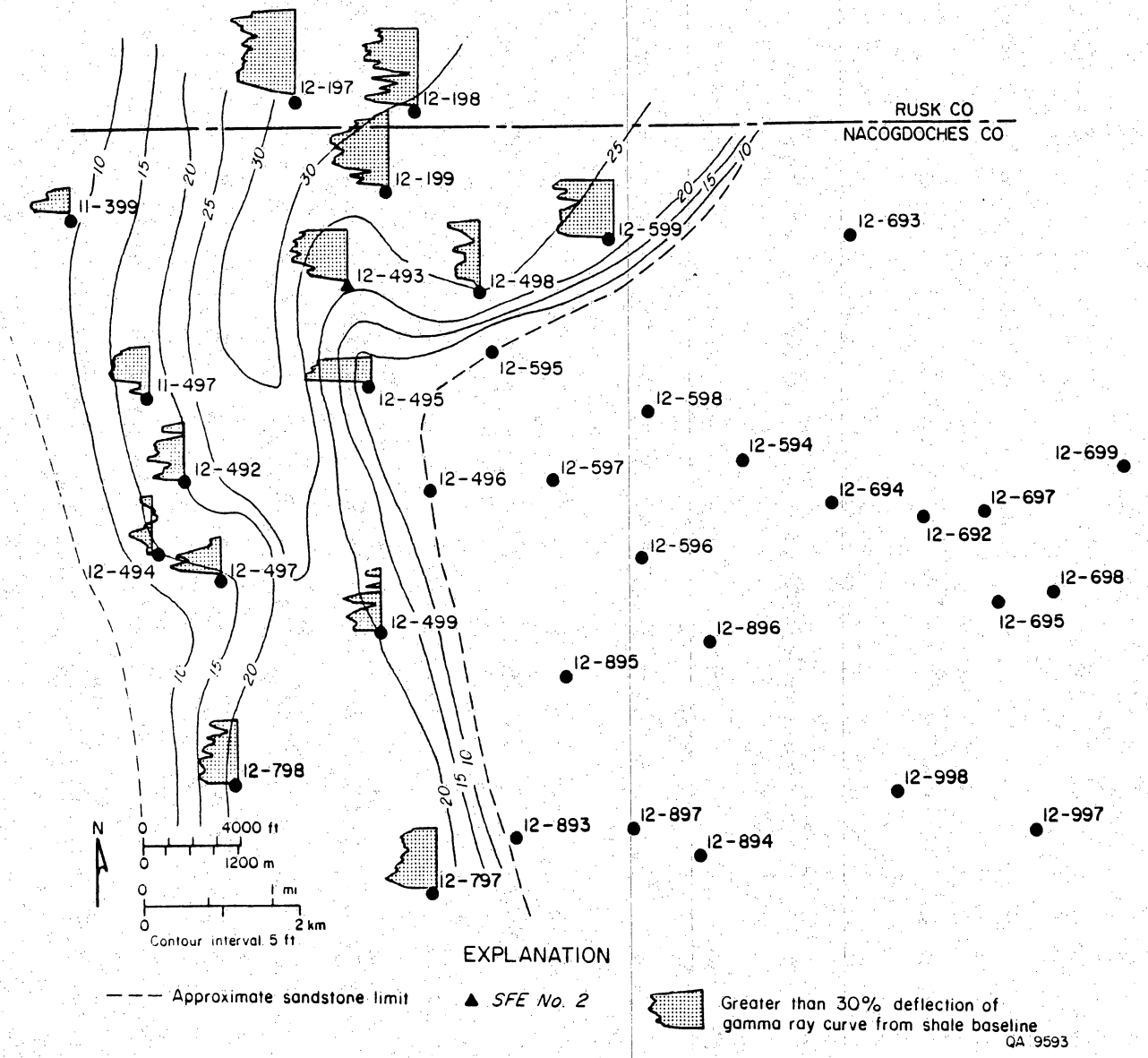

Figure 25. Net-sandstone map for Sandstone B, upper Travis Peak Zone 1, North Appleby field. Core, log, and map data indicate that this sandstone was deposited in a north/south oriented channel belt. Gamma-ray log signatures are generally blocky to upward-fining.

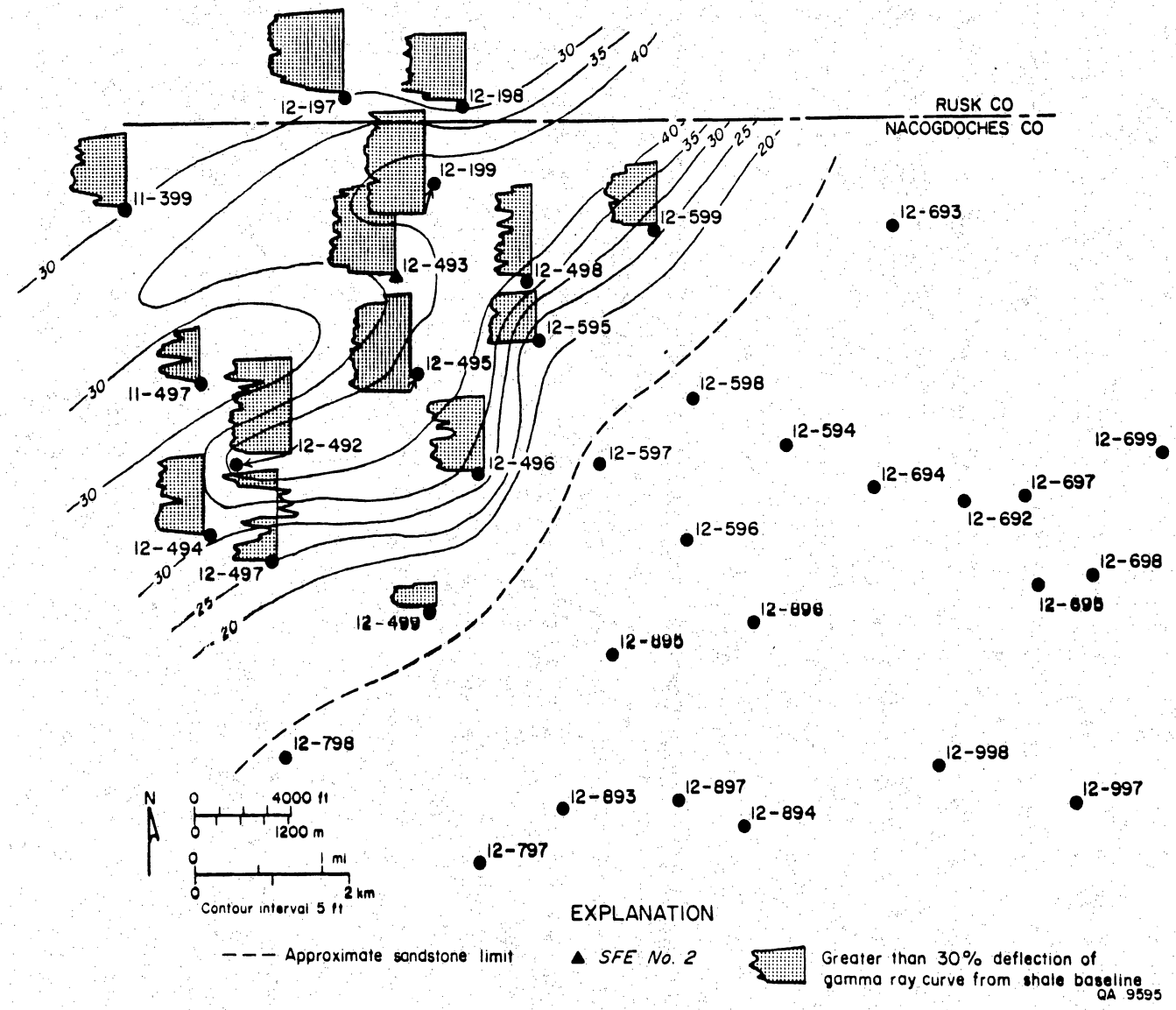

Figure 26. Net sandstone map for Sandstone X, lower Travis Peak, Zone 4, North Appleby field. Core, log, and map data indicate that this sandstone was deposited in a northeast/southwest-oriented channel belt. Gamma-ray log signatures are generally blocky to upward-fining.

mudstones accumulated. Channel sandstones in both the upper and lower Travis Peak in SFE No. 2 contain numerous natural fractures (Laubach and others, 1989b). Fractures are particularly common and closely spaced in the deeper sandstones, where matrix permeability is lowest.

Stratigraphic correlation of channelbelt sandstones and interbedded mudstones provides a basis for identifying reservoirs and estimating their extent and geometry. Although one producing sandstone may cover more than 25,000 acres (10,000 ha), maximum drainage areas in North Appleby field are less than 80 acres (32 ha) (Holditch and others, 1988). Hydraulic-created fracture half-lengths range from 100 to 200 ft (30 to 60 m) (Holditch and others, 1988), well below the lateral dimensions of the sandstones. A well would have to be located within 100 ft (30 m) of a channelbelt margin for the artificial fracture to laterally propagate out of the reservoir and into an adjacent mudstone or channelbelt. However, due primarily to uniform stresses and a lack of vertical barriers to fracture growth, circular east-west oriented fractures will form (S. A. Holditch, personal communication, 1988) that will connect as many as six to eight vertically stacked sandstones (CER Corporation and S. A. Holditch & Associates, 1988; Holditch and others, 1986; Holditch and others, 1988b). Vertical communication could enhance or detract from production depending on the amount of water in vertically adjacent sandstones.

SFE No. 3

SFE No. 3 was drilled in Waskom field, less than one mile from SFE No. 1. Intervals of the Travis Peak Formation, Cotton Valley Sandstone (also called the Schuler Formation, fig. 2), and Bossier Shale were cored in SFE No. 3 (fig. 27). The environments of deposition range from fluvial (Travis Peak) to marginal marine (Travis Peak and Cotton Valley) and marine (Bossier) (Tye and others, 1989b).

Core from the lower part of the Travis Peak in SFE No. 3 (7,351.0 to 7,409.8 ft; 2,240.6 to 2,258.5 m) is similar to core from the nearby SFE No. 1 well. Sandstones and mudstones represent deposition in fluvial channels and laterally adjacent floodplain environments (Tye

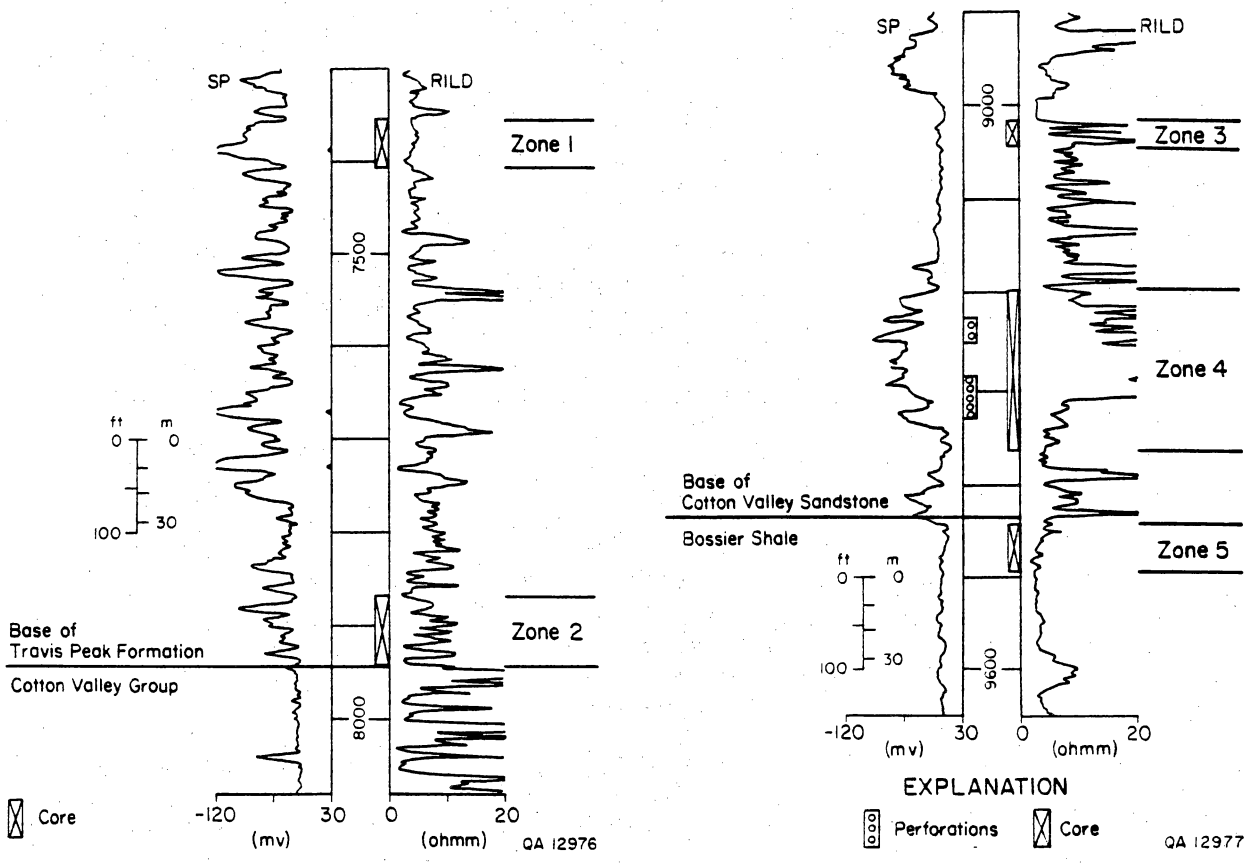

Figure 27. Gamma-ray and resistivity logs of lower Travis Peak Formation, lower Cotton Valley Sandstone, and Bossier Shale, SFE No. 3 well, showing cored and perforated intervals.

and others, 1989b; Dutton and others, in press). Rippled and planar crossbedded sandstones were deposited by current flow through fluvial channels. The dominance of ripple-laminated sandstone and the upward-fining log and lithologic character imply deposition in a meandering fluvial system. The basal crossbedded sandstone probably was formed by the migration of sand waves or transverse bars along the channel bottom. Planar and trough ripple-lamination, parallel lamination, and rare root traces are indicative of deposition in upper channel reaches (point bar) and levee environments.

Mudstones and muddy sandstones separating the two sandstones are indicative of abandoned-channel, lacustrine, and overbank deposits. These finer grained sediments cap the channel deposits and accumulated in response to the abandonment of the channels. The lacustrine deposits may represent a small pond or ox bow lake. Muddy sandstone overlying the lacustrine deposits was probably formed by flood-induced processes that resulted in deposition of a prograding crevasse splay or lacustrine delta. Burrowed to laminated mudstone formed during channel abandonment.

The Travis Peak-Cotton Valley transition was cored in SFE No. 3 at a depth of 7,868.0 to 7,943.4 ft (2,398.2 to 2,421.1 m) (fig. 27). The lithologic and sedimentary character of interbedded sandstones and mudstones in this cored interval are indicative of sediments deposited in paralic environments that developed during early stages of Travis Peak deposition (Tye, 1989). Fossil content and sedimentary attributes of the finer-grained facies imply deposition in a semi-protected bay. Preservation of articulated and unabraded mollusk shells, the predominance of grazing burrows, and presence of wave-formed ripple laminations indicate low-energy marginal-marine to marine deposition. Faunal diversity in the mudstones and sandstones is low, therefore fluvial systems may have emptied into this area and produced brackish to marine conditions, indicating that the bay was actually an estuary.

A well-developed 3-ft-thick (1-m-thick) oyster bioherm is present between 7,901.7 and 7,905.0 ft (2,408.4 and 2,409.4 m). The mudstone matrix of the bioherm and the scarcity of

wave- or current-formed structures in the mudstones indicate deposition in a protected environment.

Sandstone beds abruptly overlie the bay mudstones and fine upward. Ripple cross-laminated sandstone at the base grades upward into burrowed and wavy bedded sandstone. These sediments were deposited by relatively high-energy processes (wave, tidal current, storm) that formed thin shoals within the bay. An upward increase in burrows in the shoal sandstones and the presence of root traces at the top of shoal sandstones indicate a progressive decrease in depositional energy and subaerial exposure of the shoal top. A thin marsh deposit and a storm-emplaced fossiliferous silty sandstone (7,874.0 to 7,876.0 ft; 2,400.0 to 2,400.6 m) cap the uppermost sandstone in the cored interval.

The stacked bay-shoal sequences imply that consistent depositional processes operated within a slowly subsiding basin. Perhaps because of progradation during early Travis Peak deposition, shoal sandstones thicken and are somewhat better sorted at the top of the cored interval.

Two intervals of the Cotton Valley were cored in SFE No. 3 (fig. 27); the upper interval consists of lower Cotton Valley mudstone, and the lower interval contains the lower Cotton Valley Taylor sandstone and interbedded mudstones. A cross section of the lower Cotton Valley in SFE No. 3 and adjacent wells is shown in figure 28. The upper mudstone interval was deposited in a semi-protected or low-energy bay (Tye and others, 1989b). Faunal evidence and sparse wave-formed physical sedimentary structures indicate that oyster bioherms grew in a low-energy marine bay. The Taylor Sandstone in Waskom field can be subdivided into an upper sandstone that is up to 100 ft (30 m) thick and a lower sandstone up to 25 ft (8 m) thick. In SFE No. 3, the division between upper and lower Taylor sandstones occurs at a depth of 9,360 ft (2,853 m) (fig. 27). Both the upper and lower Taylor sandstones form elongate trends that are oriented northeast-southwest across Waskom field (fig. 29). Numerous fractures occur in the Taylor Sandstone (Dutton and others, in press).

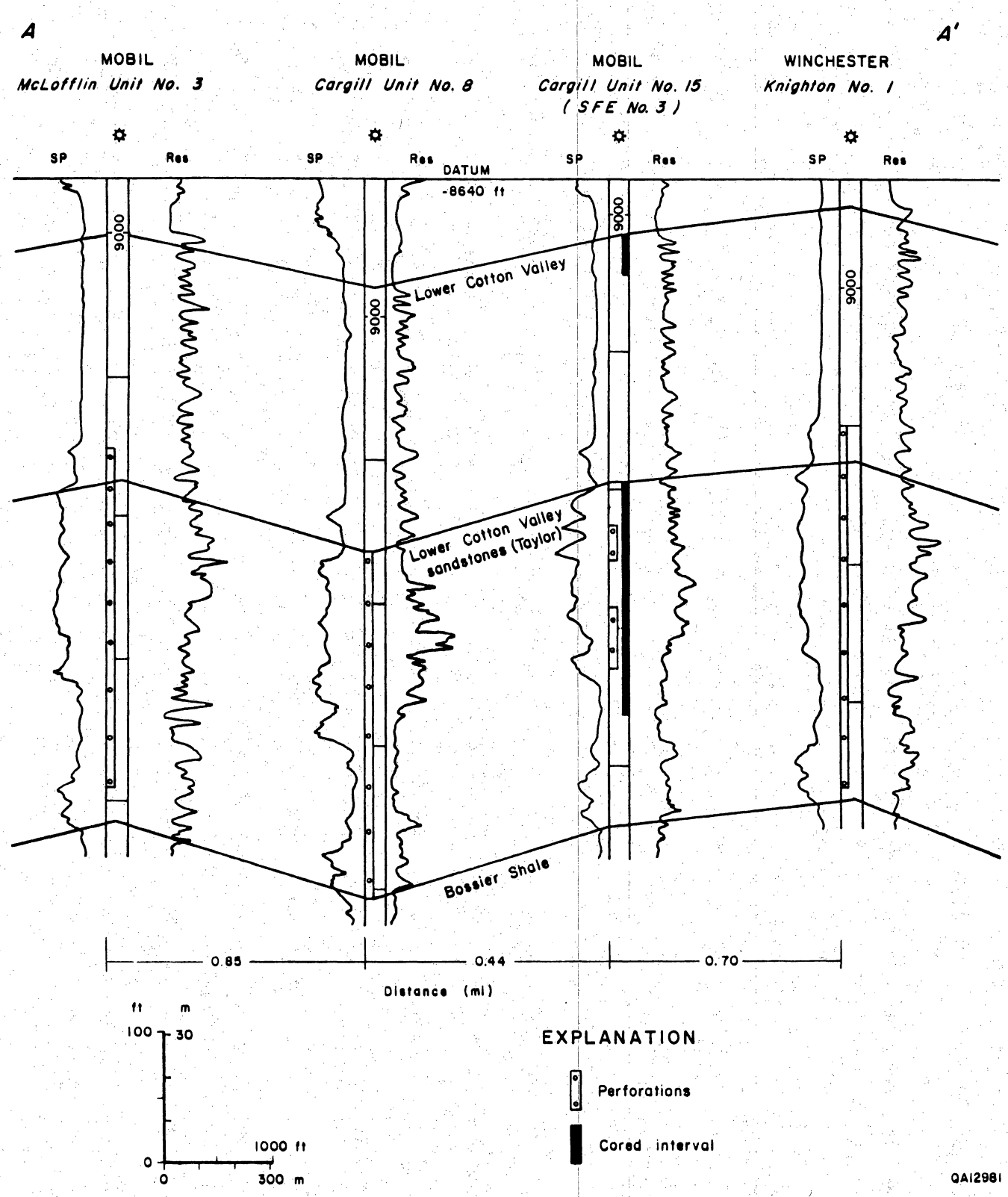

Figure 28. Cross section of lower Cotton Valley Taylor Sandstone interval in the area around the SFE No. 3 well. Cross section modified from a section provided by M. R. Poffenberger, Mobil Exploration & Producing U.S., Inc., Houston, Texas.

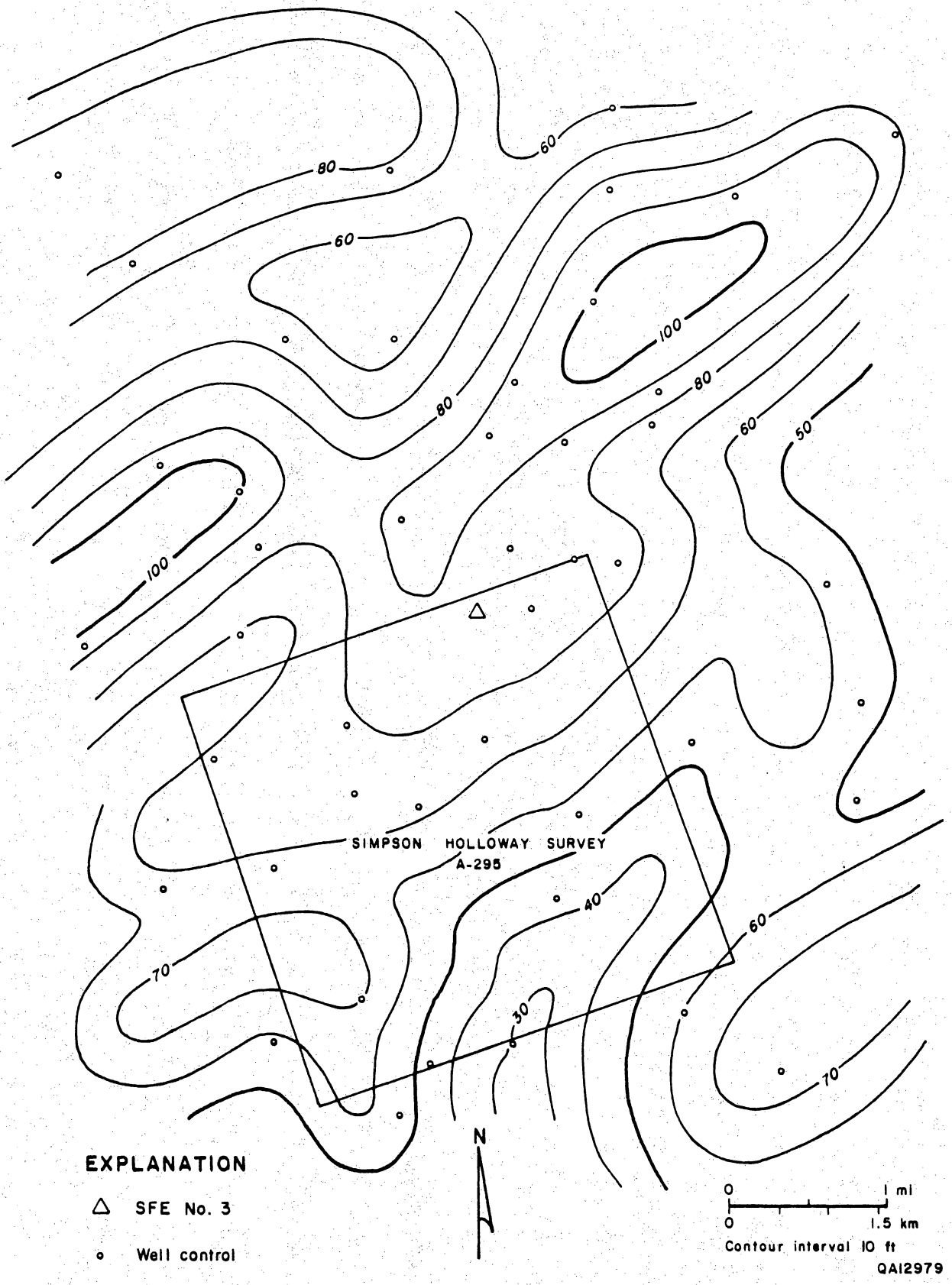

Figure 29. Net sandstone map of upper Taylor Sandstone (Cotton Valley), Waskom field, Harrison County, Texas. Map provided by M. R. Poffenberger, Mobil Exploration & Producing U.S. Inc., Houston, Texas.

Lithologic and sedimentologic characteristics of the mudstones and sandstones in the cores from the lower Cotton Valley Taylor Sandstone imply that these sediments were deposited in a marine-shoreline setting. In an upward direction, the environments represented in this core include: (1) shoreface, (2) microtidal barrier island, (3) lagoon and washover deposits, (4) microtidal barrier island, (5) tidal inlet, and (6) marsh-lagoon (Tye and others, 1989b; Dutton and others, in press). This vertical sequence was formed by an initial shoreline regression, a subsequent transgression, and later relative sea level stillstand as indicated by the stacking of barrier and tidal-inlet deposits.

The basal 22-ft-thick (6.7-m) upward-coarsening sandstone is a regressive barrier-island deposit that prograded over a low-energy shoreface (fig. 27). Shoreline regression and submergence resulted in the development of 10-ft-thick (3-m) back-barrier mudstone deposits (lagoon and washover) over the first barrier island. The mudstones are overlain by a 120-ft-thick (37-m) sandstone that consists of more barrier-island deposits (figs. 27 and 28). Progradation of a second barrier island was initiated because of a decrease in the rate of sea-level rise or increased sedimentation, or both. The barrier islands were probably similar to the microtidal barrier islands that line the coast of North Carolina and the U.S. Gulf Coast. Physical sedimentary structures structures indicate wave processes were important in reworking the sandstones, but tidal influences were minimal by comparison (Tye and others, 1989b).

Tidal inlets eroded and reworked the second barrier-island deposit. Inlet migration and shoreline subsidence resulted in the incorporation of stacked tidal-inlet sequences in the uppermost portion of the Taylor Sandstone. Interbedded with the tidal-inlet deposits are beds of abandoned-inlet deposits. These deposits account for the upward-fining log character and emphasize the ephemeral nature of the tidal-inlet channels. Marsh and lagoon deposits cap the cored portion of the Taylor Sandstone.

Cores from the Bossier Shale consist of fossiliferous silty and sandy mudstone (fig. 27). The mudstones were deposited in a low-energy shelf environment. Rare ripple laminations and normally graded shell beds indicate that this environment was below normal wave base but

storm processes affected sedimentation. Association with a prograding shoreline (Taylor Sandstone) is implied by the upward increase in sand.

The best reservoir sandstones in the Cotton Valley in SFE No. 3 are barrier-island deposits that are oriented parallel to depositional strike and tidal-inlet sandstones oriented perpendicular to depositional strike. Highest permeability in barrier-island sandstones occurs in well-sorted fine-grained sandstone with low-angle planar crossbeds, gently inclined to horizontally oriented parallel laminae, and current and wave ripple lamination. Other permeable zones occur at the base of tidal-inlet channels. Planar-ripple cross lamination is the prevailing sedimentary structure. Reservoir quality decreases vertically in lagoon and washover deposits above barrier-island sandstones and in abandoned-inlet deposits above tidal-inlet sandstones. Marsh and lagoon mudstone deposits cap the Taylor Sandstone and form a seal for hydrocarbons.

DIAGENESIS

Travis Peak sandstones have undergone extensive modification by compaction, cementation, and pressure solution since they were deposited. These diagenetic changes have had an important effect on the physical characteristics and reservoir properties of Travis Peak sandstones. The following sections summarize Travis Peak composition, organic geochemistry, burial and thermal history, diagenetic history, and reservoir quality.

Travis Peak Composition

The Travis Peak Formation in East Texas is composed mainly of fine-grained to very fine grained sandstone, silty sandstone, muddy sandstone, and sandy mudstone. True claystones (as defined by Folk [1974] as being composed primarily of clay-sized particles) that could provide stress barriers to contain hydraulic fracture growth are rare. Matrix-free sandstones are moderately to well sorted and texturally mature, according to the definition of Folk (1974). Sandstone composition can be expressed by framework grains, matrix, cement, and porosity.

Framework Grains

Travis Peak sandstones are quartzarenites and subarkoses, and the average composition is $Q_{95.0}R_{3.8}R_{1.2}$ (Dutton, 1987). Quartz is the most abundant detrital mineral in all Travis Peak samples. It composes an average of 65.5 percent of the total sandstone volume and forms between 82 and 100 percent of the essential framework constituents (quartz, feldspar, rock fragments).

Detrital feldspars compose an average of 2.7 percent of the total sandstone volume and 0 to 15 percent of the essential constituents. Plagioclase is more abundant than orthoclase in

most samples, and microcline is rare. Feldspar content was greater at the time of deposition because some feldspar has been lost by dissolution and by replacement by carbonate cements. The original feldspar content may have been about 9 percent, and the original sandstone composition was approximately $Q_{90}F_9R_1$ (Dutton, 1987).

Plagioclase grains vary from fresh to sericitized and vacuolized. Partial dissolution of plagioclase along cleavage planes results in delicate honeycombed grains and secondary porosity. Plagioclase grains in the Travis Peak have been extensively albitized. Feldspars from 18 Travis Peak samples were analyzed by electron microprobe to determine major element composition. Plagioclase composition ranges from An_0 to An_{24}, but 74 percent of the grains that were analyzed are less than An_2, and 86 percent are less than An_5 (Dutton, 1987).

Lithic components of the Travis Peak are primarily chert and low-rank metamorphic rock fragments. Each is generally present in volumes of less than 1 percent. Clay clasts are common, but they were derived locally when partly consolidated mud layers were ripped up and redeposited with the sand. Clay clasts compose an average of 1.2 percent of the total sandstone volume and range from 0 to 13.7 percent.

Travis Peak sandstones are mineralogically mature; either unstable grains were scarce in the source area (perhaps because of dissolution during weathering) or they were removed during transportation, deposition, and burial, or both. Saucier (1985) indicates that the Travis Peak was derived from a large area of the southwestern United States that was exposed in Early Cretaceous time. This source area in the Texas Panhandle, Oklahoma, New Mexico, and Colorado included sedimentary, metamorphic, and igneous rocks. The high percentage of quartz in the Travis Peak is probably caused at least in part by the abundance of quartz-rich terrigenous sedimentary rocks in the source area.

Matrix

Detrital matrix occurs in sandstones that either were deposited in an alternating high- and low-energy environment (such as rippled sandstones with clay drapes on ripple faces) or had clay mixed into an originally well-sorted sandstone by burrowing organisms. X-ray diffraction analysis of detrital matrix indicates that it is composed primarily of illite and chlorite, mixed with varying amounts of fine quartz (Dutton, 1987). Mixed-layer illite-smectite with approximately 5 percent smectite layers occurs in the Ashland S.F.O.T. No. 1 core and in trace amounts in the Prairie Mast No. 1-A core (David K. Davies and Associates, 1985a, 1985b).

Cements

Cements and replacive minerals constitute between 0 and 70 percent of the rock volume in the Travis Peak samples. The volume of rock composed of authigenic minerals has a normal distribution with an average of 22.5 percent. The most important control on the total volume of cement in sandstones is the amount of detrital matrix; the correlation coefficient between between matrix volume and total cement volume is -0.61 (Dutton and Diggs, in press). Large amounts of detrital matrix lowered the porosity and permeability of the sediment, so that a smaller volume of mineralizing fluids passed through matrix-rich sandstones than through clean sandstones. Furthermore, in the matrix-rich sandstones, less primary porosity was available for cements to fill. Finally, abundant detrital matrix probably reduced the availability of nucleation sites on detrital grains, and in particular inhibited the precipitation of quartz cement.

Quartz, illite, chlorite, ankerite, and dolomite are the most abundant authigenic phases in Travis Peak sandstones. Less abundant authigenic minerals include calcite, kaolinite, feldspar, pyrite, barite, and anhydrite. Finally, reservoir bitumen, a solid hydrocarbon residue that occurs in some sandstones, was also considered a cement. On the basis of petrographic evidence, the

relative order of occurrence of the major authigenic phases is (1) illite rims, (2) dolomite, (3) quartz overgrowths, (4) albite, (5) illite (a second generation) and chlorite, (6) ankerite, and (7) reservoir bitumen.

Quartz—Authigenic quartz is the most abundant cement in Travis Peak sandstones, having an average volume of 13.8 percent (σ = 7.2 percent). In clean sandstones the average volume of quartz cement is 16.9 percent (σ = 5.5 percent). In samples with abundant quartz cement, the overgrowths completely occlude primary porosity and form an interlocking mesh of quartz crystals. In samples with less authigenic quartz, the overgrowths did not grow together; thus some primary porosity remains between crystal faces.

The volume of quartz cement in clean Travis Peak sandstones increases significantly with present burial depth (fig. 30). The predicted value of quartz cement at 6,000 ft (1,829 m) is 14.6 percent, compared with 20.0 percent at a depth of 10,000 ft (3,048 m) (Dutton and Diggs, in press). Trends of increasing quartz cement with present burial depth in fluvial and paralic sandstones are nearly identical.

Oxygen-isotopic composition of authigenic quartz was measured by using 33 selected samples that contain a wide range in percentage of quartz overgrowths (Dutton, 1986; Dutton and Land, 1988). Many possible combinations of temperature and water composition could have resulted in precipitation of quartz overgrowths with the measured $\delta^{18}O$ values of +20 ‰ to +24 ‰. Constraints on the timing and temperature of feldspar dissolution and ankerite precipitation, which clearly occurred after most quartz cementation, were used to estimate the temperature and $\delta^{18}O$ composition of fluids that precipitated the quartz cement (Dutton and Land, 1988). Based on these constraints, the quartz cement is interpreted as having precipitated from meteoric fluids ($\delta^{18}O$ = -5 ‰) at temperatures of 130° to 165°F (55° to 75°C), at depths of 3,000 to 5,000 ft (900 to 1,500 m).

Authigenic Clay Minerals—Authigenic clays that have been identified in the Travis Peak sandstones are illite, chlorite, kaolinite, and mixed-layer illite-smectite. Illite and chlorite are by far the most abundant authigenic clays, constituting a combined average of 3.0 percent of the

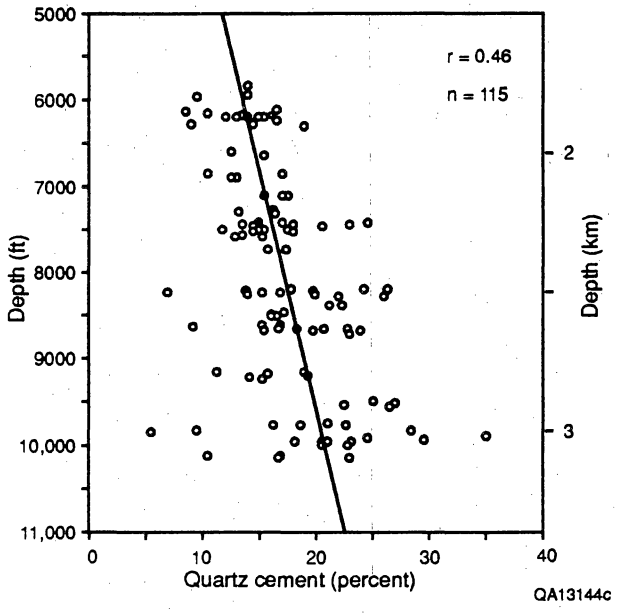

Figure 30. Quartz cement volume in clean sandstones as a function of present burial depth, which is a measure of maximum burial depth. (Maximum burial depth was approximately 450 m greater than present burial depth throughout the study area.) Quartz cement increases significantly with depth.

sandstone based on point counts, although as much as half of that volume is probably microporosity. In thin sections, microporosity cannot be distinguished from clay flakes, but by SEM it can be seen that abundant porosity occurs between individual clay flakes.

Some of the illite in Travis Peak sandstone occurs as rims of tangentially oriented crystals that coat detrital grains. In most samples the illite rims are thin, and quartz cement precipitated over them, so the illite now forms distinct boundaries between detrital grains and overgrowths. Where the illite rims are sufficiently thick, they prevented nucleation of quartz overgrowths. An extreme example of this occurs in a sandstone at 7,442 to 7,462 ft (2,268.3 to 2,274.4 m) in the Arkla T. P. Scott No. 5 well (Dutton, 1987). This is a crossbedded and planar-laminated fluvial sandstone near the base of the Travis Peak; it is overlain by muddy sandstone and red mudstone with mottled soil texture and root traces. The upper part of the sandstone (7,442 to 7,453 ft; 2,268.3 to 2,271.7 m) is porous and poorly indurated, whereas the lower part (7,453 to 7,462 ft; 2,271.7 to 2,274.4 m) is well indurated. Samples from the upper interval contain as much as 14 percent by volume clay rims around detrital grains, and volumes of quartz overgrowths are as low as 0.5 percent. Some chorite as well as illite occurs in the rims. The deeper part of this sandstone has much thinner clay rims (1 to 3 percent) and correspondingly more abundant quartz cement (15 percent). Resistivity varies between the upper and lower zones as well. The upper zone, with the thick clay cutans, has deep-induction resistivity of 1 to 2 ohm-m, compared with resistivity of 6 to 10 ohm-m in the lower, quartz-cemented zone. Abundant bound water in the clay rims probably is responsible for the low resistivity. The depositional setting of this sandstone and the distribution of cutans within the sandstone suggest that most of the clay entered the sandstone by mechanical infiltration from the soil above and subsequently was recrystallized during burial diagenesis.

True authigenic illite occurs as delicate fibers inside both primary and secondary pores. Illite is commonly associated with altered and leached feldspars and thus was a relatively late diagenetic phase compared with the precipitation of quartz overgrowths. Authigenic chlorite occurs as individual flakes and rosettes inside both primary and secondary pores, and, like illite,

is commonly associated with altered feldspars. No difference in the timing of precipitation of illite and chlorite could be distinguished. Both illite and chlorite cements in the Travis Peak are iron rich.

Studies have shown that when fibrous illite is present in core samples, the method of sample preparation can alter fundamental petrophysical properties, including permeability (Waal and others, 1988; Pallatt and others, 1984). SEM analysis indicates that air-drying drastically alters illite morphology in Travis Peak sandstones (Tye and others, 1989a; Dutton and others, in press). Illite fibers in freeze-dried samples are long, delicate thin fibers, which is how the illite naturally occurs in Travis Peak reservoirs. However, illite fibers in air-dried samples have either matted together to form thick "ropes" of illite or else the illite has completely collapsed and plated out against the walls of the pores. This change in illite morphology by air drying has been shown to significantly increase measured permeability in Travis Peak core-analysis plugs (Dutton and others, in press). Permeability to brine in core plugs that were never dried is an average of 1.5 times lower than in plugs that have undergone Dean-Stark extraction, methanol leaching, and oven drying, the process that core plugs routinely experience before core analysis. Thus, permeability measurements in Travis Peak sandstones made during routine core analysis may be too high because of the change in illite morphology during core-plug preparation.

Carbonate Cements—Dolomite, ankerite, and calcite cements all occur in Travis Peak sandstones, but only dolomite and ankerite are common. Calcite cement was observed only in sandstones adjacent to limestone beds near the top of the formation. In most samples that contain calcite cement, the calcite appears to be the first cement that precipitated, and thus it would have prevented the later nucleation of quartz cement.

The average volume of dolomite cement is 1.1 percent, but a few samples contain abundant dolomite. Three samples contain more than 25 percent dolomite pore-filling cement and framework-grain replacement. Dolomite rhombs commonly precipitated within detrital clay matrix or clay clasts, and from petrographic evidence they appear to have precipitated early in

the diagenetic history of the Travis Peak sandstones. Dolomite is most abundant in the paralic facies in the upper part of the Travis Peak; samples from the deeper, fluvial sections of the Travis Peak contain little or no dolomite.

Ankerite is also most abundant in the paralic facies near the top of the Travis Peak Formation, and its abundance decreases with depth into the braided fluvial section. The mean volume of ankerite is 2.4 percent (σ = 4.4 percent), but a few samples contain abundant ankerite. Fourteen samples contain more than 15 percent ankerite pore-filling cement and framework grain replacement. Ankerite cement is commonly zoned, the most iron rich ankerite being at the edges of rhombs. For all ankerite cements, the composition ranges from $(Ca_{1.06}Mg_{0.88}Fe_{0.02}Mn_{0.03})(CO_3)_2$, which is really a ferroan dolomite, to $(Ca_{1.10}Mg_{0.44}Fe_{0.43}Mn_{0.03})(CO_3)_2$ (Dutton, 1987).

Carbon and oxygen isotopic compositions of dolomite and ankerite cements were determined for 16 samples (Dutton, 1986 and 1987). The average of all values for dolomite is a $\delta^{18}O$ composition of +1 ± 3 ‰ (PDB) and an average $\delta^{13}C$ composition of –4.8 ± 1.9 ‰. Ankerite $\delta^{18}O$ compositions range from –6.2 ± 0.1 ‰ to –10.9 ‰ (PDB). Carbon isotopic composition averages –6.9 ‰ and ranges from –4.8 ‰ to –9.3 ‰ (PDB). The measured variation in $\delta^{18}O$ composition reflects changing fluid conditions during precipitation of ankerite cement.

Solid Hydrocarbons—Solid hydrocarbon accumulations that line pores in some sandstones were observed in most cores. Because it was emplaced in the sandstones during burial diagenesis, this material is considered to be a cement. It is interpreted to be reservoir bitumen, which was defined by Rogers and others (1974, p. 1806) as "black, solid asphaltic or graphitic coatings and particles within reservoir porosity." Reservoir bitumen occurs primarily within the paralic facies and is most abundant in the upper 300 ft (90 m) of the Travis Peak Formation (fig. 31). Most hydrocarbon production from the Travis Peak Formation to date has occurred in the same interval as the reservoir bitumen, that is, from the upper part of the paralic facies.

Reservoir bitumen fills both primary and secondary pores and commonly coats quartz overgrowths. Emplacement of reservoir bitumen appears to have been a late diagenetic event that occurred after both quartz and ankerite precipitation.

The volume of reservoir bitumen in Travis Peak sandstones is as high as 19 percent. Among samples that contain reservoir bitumen, the average volume is 4.1 percent. Where reservoir bitumen occurs, it significantly reduces porosity. Samples that contain bitumen had an average of 7.5 percent porosity prior to bitumen emplacement (calculated as total thin-section porosity + bitumen volume), therefore the bitumen filled an average of 55 percent of the existing pore space (4.1/7.5). Reservoir bitumen apparently filled only pore space that existed at the time it was emplaced and did not cause dissolution of framework grains or earlier cements (Dutton, 1987).

Within the paralic facies, permeability differences apparently controlled the distribution of reservoir bitumen (Dutton and Finley, 1988). Intervals of well-sorted, rippled and crossbedded sandstones now contain the most reservoir bitumen. Burrowed and other poorly sorted sandstones contain little or not reservoir bitumen. Thus, many zones that originally had relatively high porosity and permeability may now be tight because of reservoir bitumen.

Reservoir bitumen affects both neutron and density log response. Bitumen has an estimated hydrogen index of 0.89 to 0.99, which means that 90 to 99 percent of the bitumen volume will be measured as porosity by the neutron log (Dutton and others, 1987). In a sample containing the average volume of bitumen (4.1 percent), the neutron log porosity will be too high by 3.7 to 4.1 porosity units. In some intervals the volume of bitumen is as high as 19 percent, which could potentially result in a very large overestimation of porosity.

The presence of bitumen also affects density log response. The range of bitumen density from 1.01 to 1.20 gm/cm^3 brackets the mud filtrate density of 1.03 gm/cm^3 in the Travis Peak (E. Hunt, personal communication, 1987). The density log is therefore unable to distinguish bitumen from mud filtrate. Unless a correction is added for the presence of reservoir bitumen as

part of the matrix, density-log calculations for porosity will be too high by 0.89 to 1.01 porosity units times the volume of the bitumen present.

The presence of bitumen can also affect the porosities determined by conventional core analysis. When the cores are cleaned by Soxhlet extraction, varying amounts of bitumen are dissolved, and the measured porosities will be in error by a variable and unknown amount. In the ARCO Phillips No. 1 core, porosities measured by the Dean Stark method after extraction with toluene were an average of 1.1 (maximum of 2.7) porosity units higher than the porosities that were measured before extraction. Therefore, determination of porosity and permeability in intervals containing bitumen should be done prior to extraction.

The effect of reservoir bitumen on sandstone permeability varies. In the ARCO Phillips No. 1 well, a sandstone at 8,216.5 ft (2,504.4 m) that lacks bitumen has porosimeter porosity of 11.6 percent, in situ permeability of 22.5 md, and average grain density of 2.65 gm/cm^3. Less than 1 ft (0.3 m) away, at 8,217.2 ft (2,504.6 m), the sandstone contains reservoir bitumen; porosimeter porosity is 5.4 percent, permeability is 0.0004 md, and average grain density is 2.51 gm/cm^3. Interpreted log porosity at this depth is about 13 percent, which is almost 8 porosity units too high. However, in another example from the same well, the presence of bitumen decreases porosity only 1.4 porosity units (from 12 percent to 10.6 percent), and permeability decreases from 25 md to 4.9 md. However, these decreases in permeability may be minimum estimates because the bitumen probably formed in the most porous and permeable intervals. Therefore the initial permeability of a bitumen-bearing sandstone was probably higher than the permeability of an adjacent bitumen-free sandstone.

Other Authigenic Minerals—Albite overgrowths on plagioclase grains are present in most samples, both as external overgrowths and as internal overgrowths within partly dissolved grains. Overgrowths have compositions of very pure albite, approximately $An_{0.001}$. Pyrite, barite, and anhydrite are the other authigenic mineral phases present in the Travis Peak. Most samples contain either no anhydrite or less than 1 percent, but one sample from the Prairie Mast No. 1-A core (9,212 ft; 2,807.8 m) has 9 percent anhydrite. Petrographic evidence

indicates that it precipitated after quartz overgrowths and probably after ankerite. Anhydrite nodules and fracture fillings were observed in core from the Ankla T. P. Scott No. 5 well. Both anhydrite occurrences are interpreted as late, diagenetic features.

Barite is less abundant than anhydrite, having a maximum volume of 0.5 percent in a few samples. In most thin sections, no barite cement was observed. Bladed barite crystals occur in secondary pores, indicating that they were a relatively late stage cement.

Pyrite is present in small amounts in most cores, but it is more abundant in wells that contain coalified wood fragments. Pyrite nodules in the Prairie Mast No. 1-A core extensively replace framework grains.

Porosity

The amount of porosity in Travis Peak sandstones is variable, ranging from 0 to 18.5 percent measured by point counts of thin sections. Thin-section porosity was divided into primary and secondary types; secondary porosity results from dissolution of framework grains or cements. Average primary porosity in clean Travis Peak sandstones is 1.4 percent, and average secondary porosity is 2.8 percent.

Most of the secondary porosity appears to have formed by dissolution of detrital feldspar grains, based on the remnants found within some secondary pores. There is no evidence that dissolution of carbonate cement was responsible for generation of secondary pores in the Travis Peak. Corrosion of early dolomite cement has been observed, but the corroded dolomite has been replaced by iron-rich dolomite or ankerite.

The true average value of secondary porosity is actually somewhat higher than 2 percent because many secondary pores contain authigenic clay minerals having abundant microporosity between clay crystals. When these areas of clay-filled secondary pores were intersected on a point-counting traverse, they were counted as authigenic clay. Microporosity between clay

crystals was not counted unless it was large enough to be distinguished in thin section. There is no evidence of compaction of secondary pores.

Organic Geochemistry

Analysis of the different types of organic matter in the Travis Peak provides information about the origin of Travis Peak hydrocarbons, timing of hydrocarbon migration, and the diagenetic and thermal history of the formation (Dutton, 1987; Dutton and others, 1987). Organic matter in the Travis Peak exists as (1) dispersed detrital organic matter that occurs primarily in mudstones, (2) mobile gas, condensate, and oil, and (3) immobile, solid hydrocarbon residue that lines pores in some sandstones.

Kerogen in Travis Peak mudstones is mainly vitrinite, and most mudstones contain less than 0.5 percent total organic carbon, indicating that these are poor hydrocarbon source rocks. Vitrinite reflectance (R_o) values generally range from 1.0 to 1.2 percent, although mudstones in the deeper, downdip part of the formation have R_o values as great as 1.8 percent. Oil in Travis Peak reservoirs, and probably gas as well, was most likely generated in a source rock other than the interbedded Travis Peak mudstones (Dutton and others, 1987).

Samples of Travis Peak oil from Chapel Hill Field in Smith County show a range of maturity of API gravity from 45° to 58°. The oils were probably all derived from the same source but have since undergone varying amounts of thermal alteration and cracking. The $\delta^{13}C$ composition of the saturate fraction of the oils is –26.6 ‰ (PDB), which suggests that the oil may have come from Jurassic source rocks (W. Dow, personal communication, 1985; Dutton, 1987). Bossier shales and lower Smackover carbonates appear to be the most probable source rocks for Travis Peak oil based on available data (Dutton and others, 1987).

Reservoir bitumen fills and lines pores in some sandstones, mainly in the upper 300 ft of the Travis Peak (fig. 31). Elemental analyses of insoluble kerogen concentrate give H/C ratios of 0.79 to 0.90, which suggests that the bitumen formed by deasphalting of pooled oil after

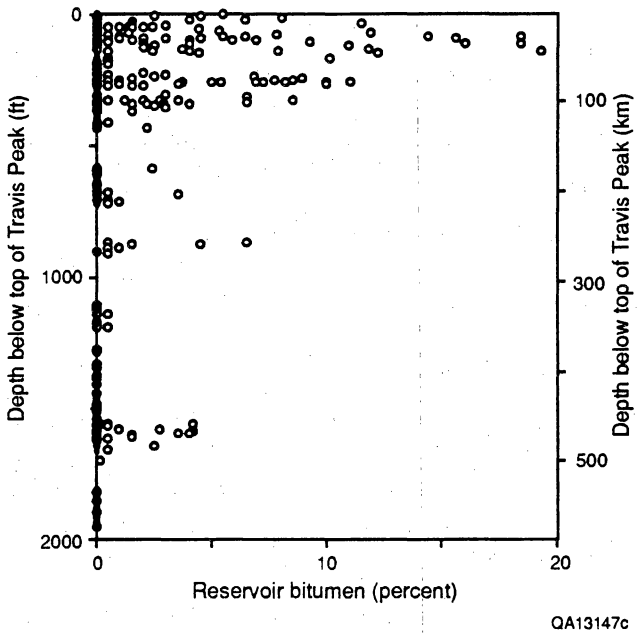

Figure 31. Plot of reservoir bitumen volume with depth below the top of the Travis Peak.

solution of gas into the oil (Rogers and others, 1974). The soluble fraction of reservoir bitumen is similar to normal producible oil but enriched in saturates and depleted in aromatics and polars. The $\delta^{13}C$ composition ranges from -25.9 to -27.1 ‰ (PDB). The bitumen was probably derived from oil similar to that currently in some Travis Peak reservoirs. After oil migrated into Travis Peak reservoirs, gas went into solution in the oil, causing deasphalting of the heavy molecules in the oil and the filling of much of the remaining porosity in some zones with reservoir bitumen. Gas in the Travis Peak may have migrated from the same Jurassic source rocks as did the oil, or it could be derived from thermal maturation of oil in Travis Peak reservoirs. The level of kerogen maturity in mudstones interbedded with Travis Peak sandstone reservoirs indicates that the pooled oil reached sufficiently high temperatures to undergo thermal alteration and gas generation.

Burial and Thermal History

To more completely interpret the diagenetic history of the Travis Peak, it is necessary to estimate the burial depth and temperature of the formation through time. By combining burial-history information with geochemical data, the approximate time when various authigenic cements precipitated can be estimated.

Stratigraphic information was used to reconstruct the burial history, and models for crustal extension and resulting heat-flow elevation (Royden and others, 1980) were combined with data on the modern geothermal gradient to estimate the paleogeothermal gradient since deposition (Dutton, 1987). With this information, it is possible to construct burial-history curves that estimate when the formation reached a given temperature. Representative curves of the tops of the Travis Peak and Cotton Valley Formations were plotted for wells on the crest of the Sabine Arch and on its southwestern flank (fig. 32). Burial-history curves for the top of the Bossier Shale and the top of the Smackover Formation, possible sources of Travis Peak hydrocarbons (Dutton and others, 1987), were also plotted. These burial-history curves plot

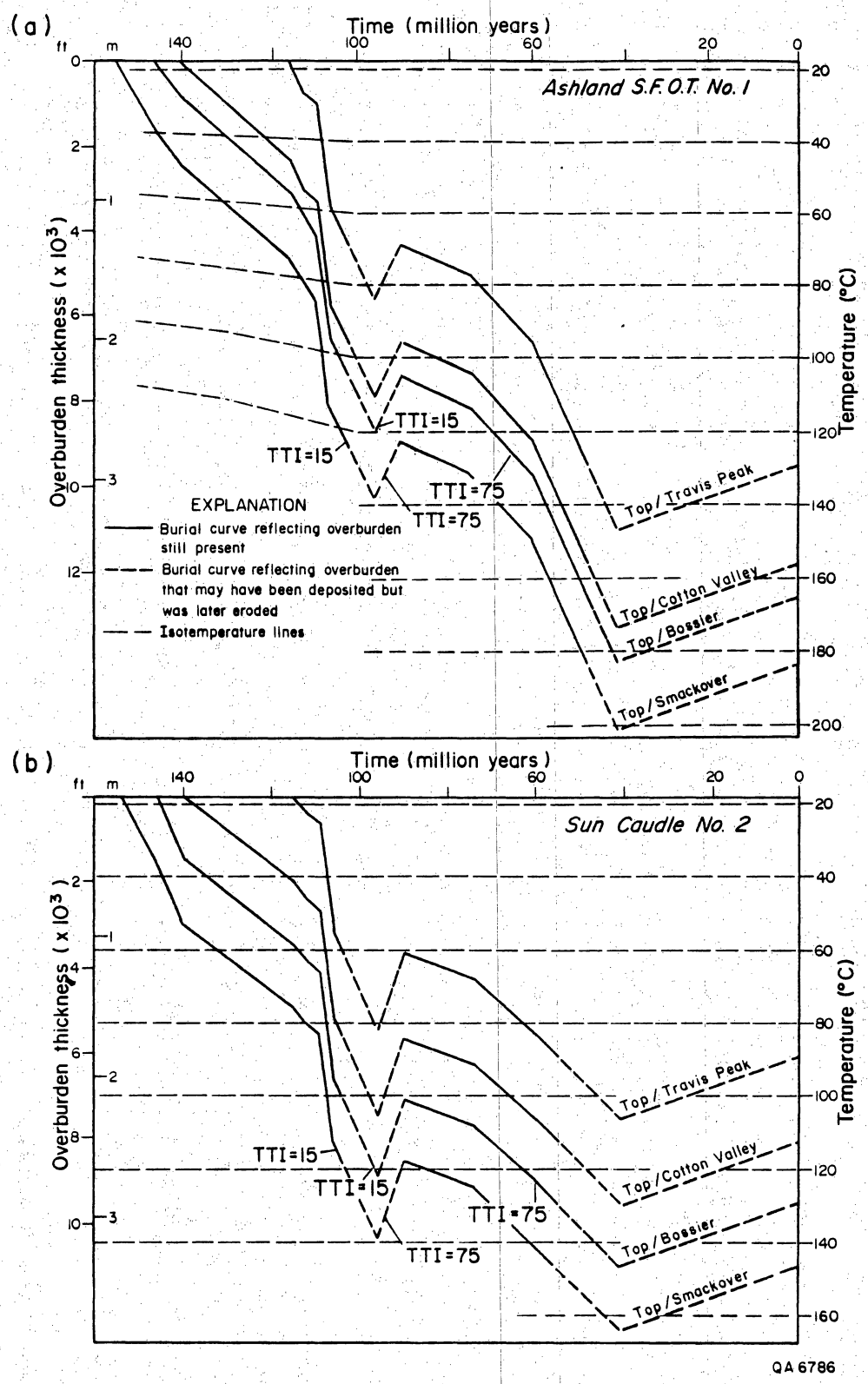

Figure 32. Burial-history curves for the tops of the Travis Peak Formation, Cotton Valley Group, Bossier Shale, and Smackover Formation in (a) Ashland S.F.O.T. No. 1 and (b) Sun D. O. Caudle No. 2 wells. Time-temperature index (TTI) values were calculated according to the method of Waples (1980). The times at which the Bossier and Smackover reached TTI values of 15 (onset of oil generation) and 75 (peak oil generation) are shown.

total overburden thickness versus time, using present-day compacted thicknesses of the stratigraphic units. Sediment compaction through time was omitted from the curves because no thick shale sections occur in this area. Two episodes of erosion were incorporated into the burial-history curves. The first episode involves movement of the Sabine Arch at the beginning of the Late Cretaceous; the other period of uplift and erosion is inferred to have taken place after the middle Eocene, 41 mya (Halbouty and Halbouty, 1982; Dutton, 1987; Jackson and Laubach, 1988).

Interpreted isotherms have been superimposed on the burial-history curves. The present-day geothermal gradient in the study area is approximately 2.1°F/100 ft (38.3°C/km) (Dutton, 1987). In the northern part of the study area, the Late Cretaceous paleogeothermal gradient probably was equal to that of the present. The geothermal gradient in the southern part of the study area was probably higher in the past than it is now because of increased heat flow related to rifting of the Gulf of Mexico. Fluctuations in geothermal gradient (or heat flow) may also have accompanied the Late Cretaceous and Tertiary alkaline volcanic event that affected the Gulf basin (Phipps, 1988), but thermal pulses may have been short lived and localized near volcanic vents. No vents or plutons have been recognized near any of the study wells. For the two wells in Nacogdoches County, higher paleogeothermal gradients were calculated (Dutton, 1987) based on the elevated heat flows derived from the crustal-extension model of Royden and others (1980). Isotemperature lines were added to the burial-history curves, so that the temperature of a given horizon on the curve can be determined for any time throughout its burial history.

Diagenetic History

The major events in the diagenetic history of the Travis Peak Formation, and the interpreted time at which they occurred, are summarized as follows (fig. 33) (Dutton, 1987; Dutton and Land, 1988):

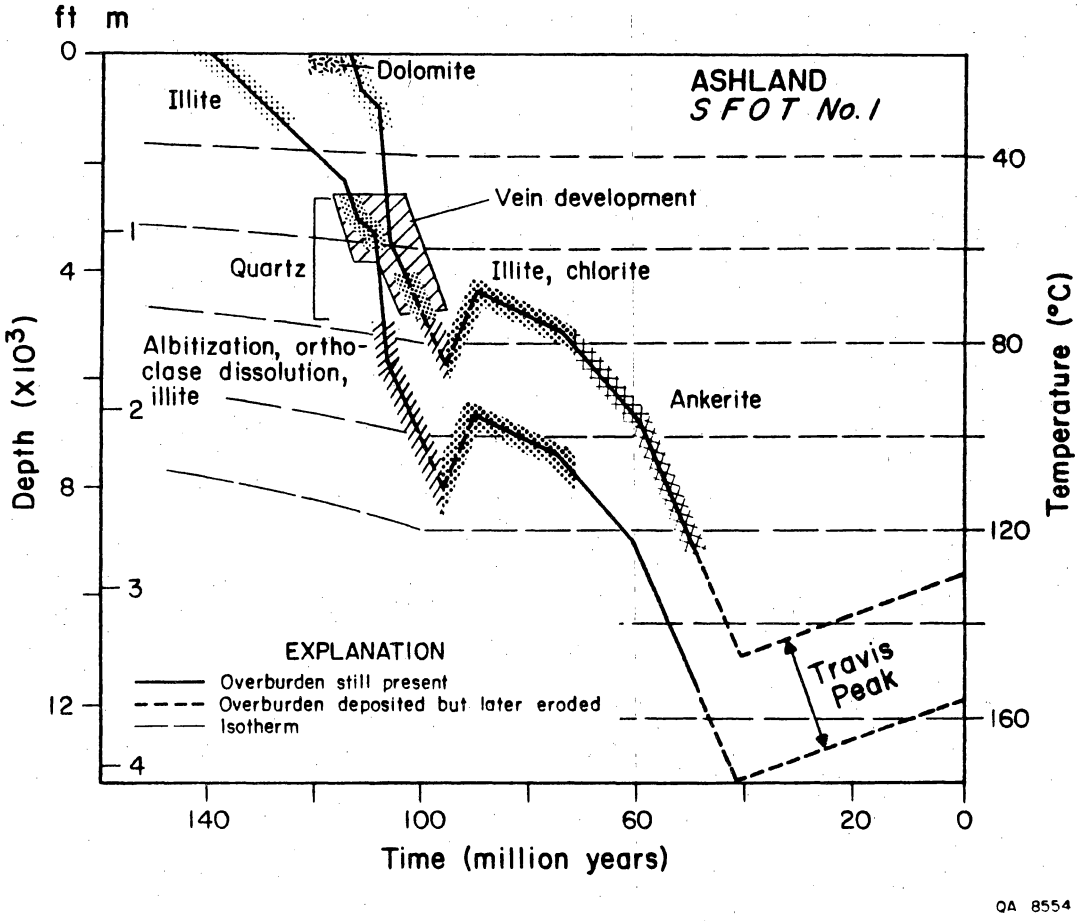

Figure 33. Burial-history curve for the Ashland S.F.O.T. No. 1 well showing when major diagenetic events may have occurred.

(1) The first authigenic cement to precipitate was illite, which coated detrital grains with tangentially oriented crystals. Dolomite cement also formed shortly after deposition at about 77°F (25°C) from a fluid with a $\delta^{18}O$ composition near SMOW.

(2) Next, extensive quartz cement, averaging 17 percent of the rock volume in clean sandstone, occluded much of the primary porosity. Quartz cement is most abundant in the deepest Travis Peak sandstones. Oxygen-isotopic composition of quartz overgrowths indicates that they precipitated from meteoric fluids at temperatures of 130° to 165°F (55° to 75°C). These temperatures occur at depths of 3,000 to 5,000 ft (900 to 1,500 m).

(3) Dissolution of orthoclase and albitization of plagioclase followed quartz cementation and occurred before movement of the Sabine Arch in the mid-Cretaceous. Illite (a second generation), chlorite, and ankerite precipitated after feldspar diagenesis; these late authigenic phases incorporate ferrous iron released by thermal reduction of iron compounds. The ankerite probably precipitated over a range of temperatures from about 175° to 250°F (80° to 120°C), from fluids with $\delta^{18}O$ composition of about +2 ‰ (SMOW); +2 ‰ is the average present composition of Travis Peak water.

(4) Most diagenesis ended when oil migrated into the Travis Peak. Later deasphalting of the oil by solution of gas filled much of the remaining porosity with reservoir bitumen in some zones near the top of the formation.

RESERVOIR QUALITY

All the diagenetic modifications Travis Peak sandstones have undergone during their burial history have significantly affected reservoir quality. Most reservoir sandstones in the Travis Peak Formation in East Texas have low permeability and require hydraulic fracture treatment to produce gas at economic rates. Porosity and permeability are not uniform throughout the formation, however. Porosity in clean sandstones decreases with depth at a rate of 2.4 percent per 1,000 ft (305 m), starting from an average of 13.8 percent at 6,000 ft (1,829 m). Permeability decreases by more than three orders of magnitude between 6,000 and 10,000 ft (1,829 and 3,048 m), from 10 to 0.001 md. Permeability at any given depth varies by about 4 orders of magnitude.

Porosity Distribution

Core porosity was measured by porosimeter, which determines effective pore volume using the principle of Boyle's Gas Law. Porosimeter porosity ranges from 1.0 to 21.1 percent and generally decreases with increasing depth, from an average of 11 percent at 6,000 ft (1,829 m) to 4.3 percent at 10,000 ft (3,048 m) (fig. 34). The 1,687 samples plotted in figure 34 include mudstones and siltstones as well as sandstones, as identified by core description. The large range in porosity at any given depth is in part caused by the textural variation. Porosity also decreases significantly in the smaller subset of sandstones for which thin-section data are available. In clean sandstones only, which contain detrital clay matrix, porosity decreases from an average of 13.8 percent at 6,000 ft (1,829 m) to 4.1 percent at 10,000 ft (3,048 m) (figure 35).

The correlation coefficient between porosity determined by thin-section point counts and porosimeter-measured porosity is 0.51 in clean sandstones (n = 117; significant at the 99

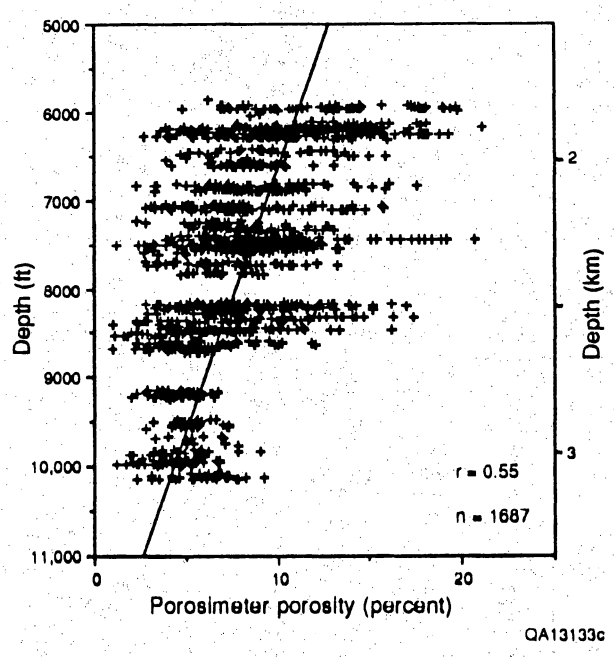

Figure 34. Plot of porosimeter porosity versus depth for 1,687 Travis Peak sandstone samples. Both the mean and range of porosity values decrease with depth.

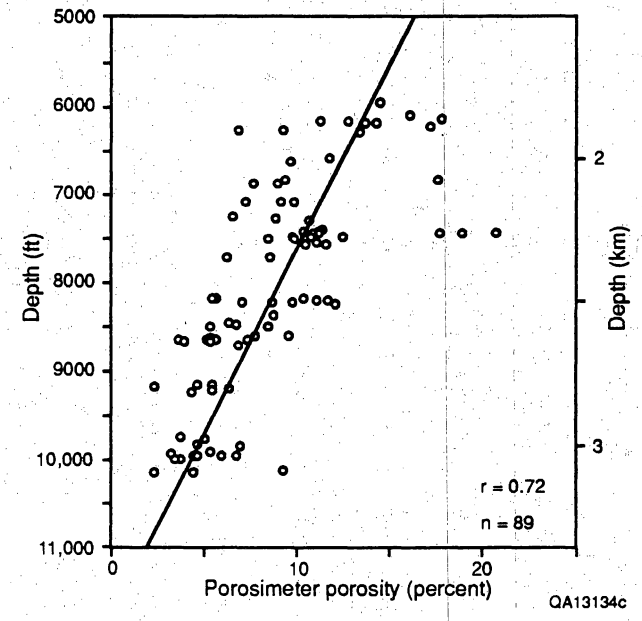

Figure 35. Plot of porosimeter porosity versus depth for 89 clean Travis Peak sandstones (average of 13.8 percent at 6,000 ft to 4.1 percent at 10,000 ft).

percent confidence level). Thin-section porosity is generally lower than porosimeter porosity because of the difficulty of accurately identifying the volume of microporosity in thin section. Primary, secondary, and total porosity identified in thin section all decrease significantly with increasing depth in clean sandstones. Primary porosity decreases from an average of 2.4 percent at 6,000 ft (1,829 m) to 0.5 percent at 10,000 ft (3,048 m), and average secondary porosity in all clean sandstones decreases from 3.9 percent to 1.6 percent over the same depth interval. The decline in secondary porosity with depth is most pronounced in fluvial sandstones (fig. 36); secondary porosity does not significantly change with depth in paralic sandstones.

Average porosimeter porosity is the same in clean fluvial and clean paralic sandstones. Clean fluvial sandstones average 8.64 percent ± 4.1 percent porosimeter porosity (n = 97), whereas clean paralic sandstones average 8.61 percent ± 3.5 percent porosity (n = 52). However, average thin-section porosity in clean fluvial sandstones is 4.9 percent, compared with 3.2 percent in clean paralic sandstones, suggesting that macroporosity is more abundant in fluvial sandstones. Secondary porosity is the most common type of macropore in both fluvial and paralic sandstones. Secondary pores average 64 percent of the total thin-section porosity in clean fluvial sandstones and 69 percent in clean paralic sandstones.

Minus-cement porosity, which is the amount of porosity that remained after compaction but before cementation (Rosenfeld, 1949; Heald, 1956), has no significant trend with present burial depth. Average minus-cement porosity in clean Travis Peak sandstones is 25.6 percent; clean fluvial sandstones average 23.9 percent, and clean paralic sandstones average 28.0 percent. Paralic sandstones probably retained higher average minus-cement porosity because they contain significantly more dolomite cement than do fluvial sandstones. Dolomite precipitated early in the burial history and probably reduced the amount of mechanical compaction experienced by paralic sandstones.

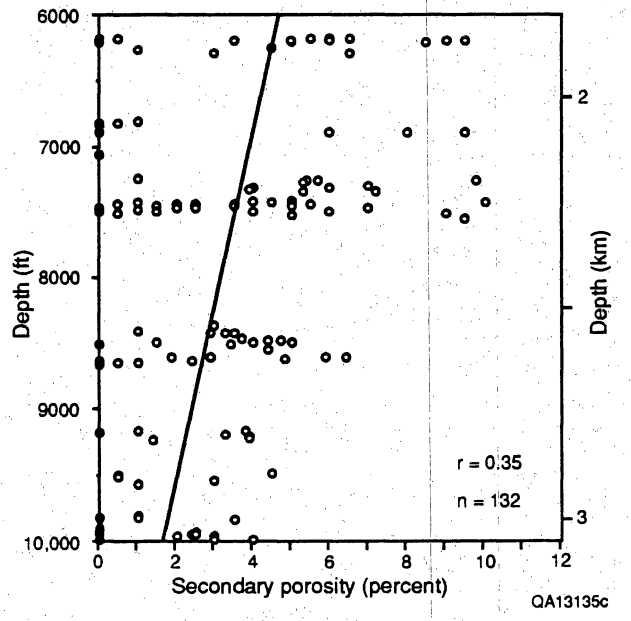

Figure 36. Plot of secondary porosity measured in thin section versus depth in clean fluvial sandstones. Secondary porosity decreases from an average of 4.7 percent at 6,000 ft to 1.6 percent at 10,000 ft.

Permeability Distribution

Permeability is extremely variable in the Travis Peak Formation. Several factors, including compaction, cementation, secondary porosity development, overburden pressure, and depositional environment all have contributed to the present permeability distribution in the Travis Peak.

Among all Travis Peak samples, average stressed permeability decreases by more than three orders of magnitude between 6,000 and 10,000 ft (1,829 and 3,048 m), from 10 to 0.001 md (fig. 37). However, permeability at any given depth varies by more than four orders of magnitude. In the smaller sample set of clean sandstones only, permeability also significantly decreases with increasing depth and shows a wide variation at any given depth (fig. 38). Some of the permeability variation is due to differences in permeability between fluvial and paralic sandstones; at a given depth, average permeability in paralic sandstones is almost an order of magnitude lower than in fluvial sandstones (fig. 39). The average log stressed permeability for all clean paralic sandstones is 0.013 md, compared with an average of 0.162 md for clean fluvial sandstones.

The main control on permeability in Travis Peak sandstones is porosity. A linear relationship that is significant at the 99 percent confidence level ($r = 0.81$) exists between porosimeter porosity and log stressed permeability in Travis Peak samples (fig. 40). Part of the scatter in these data may be caused by the presence of small hairline fractures in some core-analysis plugs. All core-analysis plugs from cooperative wells and SFE wells were inspected by binocular microscope for the presence of microscopic induced fractures, and about half of them were determined to be unsuitable for valid permeability measurements (Luffel and others, 1989; ResTech, 1989). The unsuitable plugs were omitted from the porosity and permeability data presented here. However, core plugs from the donated cores were not available and could not be examined for fractures. Thus, some of the scatter in the relationship between porosity

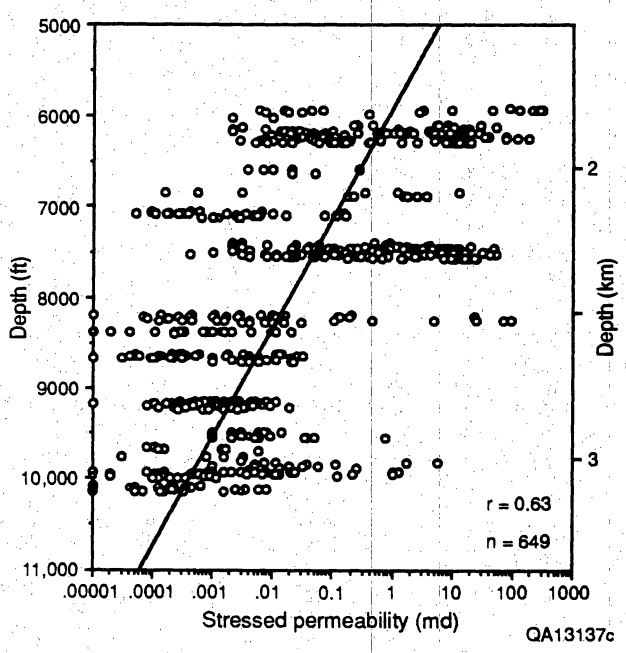

Figure 37. Plot of stressed permeability versus depth for 649 Travis Peak sandstones.

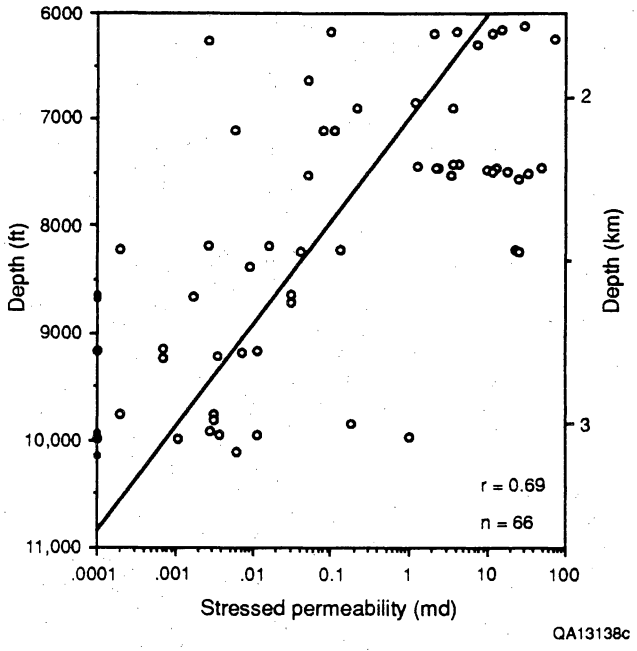

Figure 38. Plot of stressed permeability versus depth for 66 clean Travis Peak sandstones (from 10 md at 6,000 ft to 0.001 md at 10,000 ft).

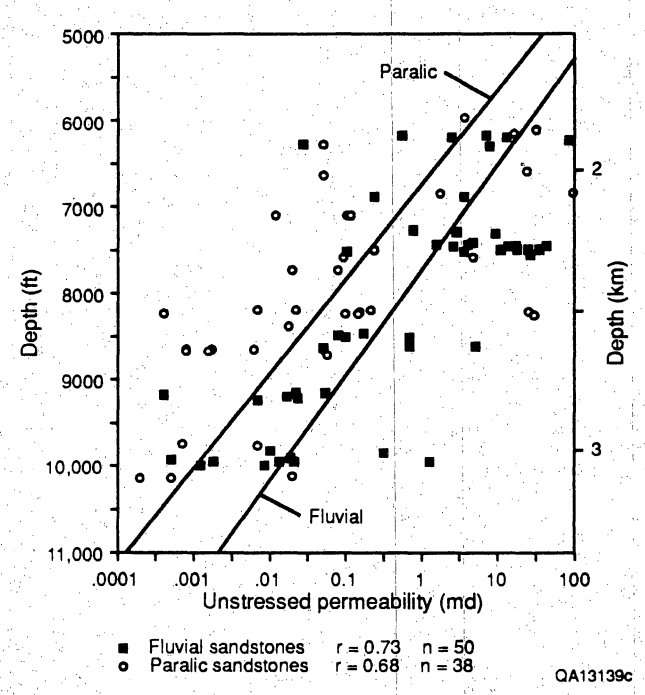

Figure 39. Plot of unstressed permeability versus depth for 176 clean Travis Peak sandstones. Paralic sandstones have an order of magnitude lower average permeability at any depth than fluvial sandstones.

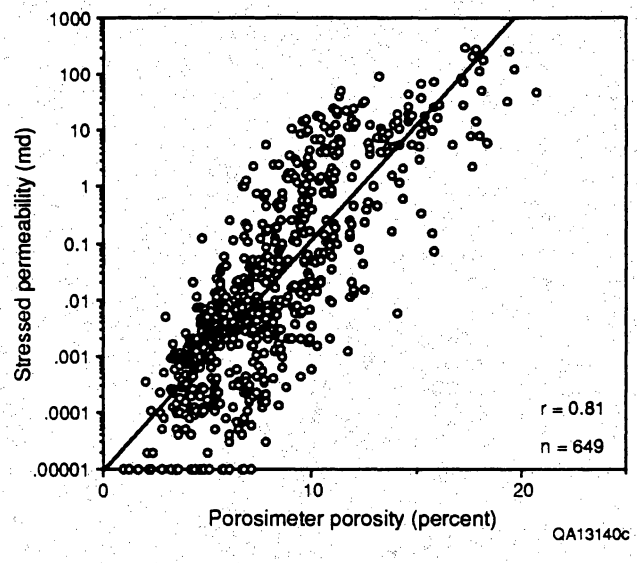

Figure 40. Plot of porosimeter porosity versus stressed permeability for 649 Travis Peak sandstones.

and permeability presented in figure 40 probably is artificial, caused by inclusion of invalid permeability measurements. Using data only from Travis Peak cooperative wells and SFE wells, Luffel and others (1989) calculated a correlation coefficient of 0.89 for the linear regression between porosity and log stressed permeability in Travis Peak sandstones.

Although porosity is the primary control on permeability in Travis Peak sandstones, other variables such as sorting also affect permeability. Some parameters influence permeability indirectly, by occluding porosity. The relationships between permeability and various textural and mineralogic parameters in clean sandstones were quantified from the petrographic data base (table 2). Statistically significant correlation exists between permeability and volume of quartz cement, volume of total cement, primary porosity, secondary porosity, total thin-section porosity, microporosity, minus-cement porosity, sorting, and porosimeter porosity (table 2). All of these factors contribute to the wide range of permeability values at any given depth.

Primary and secondary porosity are both significantly correlated with permeability (0.67 and 0.47, respectively), but primary porosity has a higher value of r^2, the coefficient of determination, and thus explains more of the permeability variation. Therefore, although primary porosity is less abundant than secondary porosity in Travis Peak sandstones, it is evidently more important in determining permeability. Primary pores may be better interconnected than are secondary pores, resulting in a greater contribution to permeability. Although microporosity cannot be measured directly, it can be estimated as the difference between porosimeter measured porosity and total thin-section porosity. The correlation coefficient between microporosity and log stressed permeability is 0.42 (table 2), indicating that microporosity is less important than either primary or secondary porosity in controlling permeability. Some of the scatter in the relationship between porosimeter porosity and permeability (fig. 40) is due to the fact that a porosimeter measures all porosity and cannot distinguish between a sample whose porosity consists mostly of primary pores and a sample whose porosity is mainly secondary pores or micropores.

Table 2. Linear regression correlation coefficients between log stressed permeability and various textural and mineralogic parameters in 66 clean Travis Peak sandstones.

Parameter	Correlation Coefficient
Quartz cement (%)	r = -0.40[1]
Dolomite cement (%)	r = -0.18
Ankerite cement (%)	r = -0.21
Total carbonate cement (%)	r = -0.23
Illite cement (%)	r = -0.06
Chlorite cement (%)	r = -0.06
Reservoir bitumen (%)	r = +0.16
Total cement (%)	r = -0.51[1]
Primary porosity (%)	r = +0.67[1]
Secondary porosity (%)	r = +0.47[1]
Microporosity (%)	r = +0.42[1,2]
Total thin-section porosity (%)	r = +0.66[1]
Minus-cement porosity (%)	r = -0.38[1]
Grain size (phi)	r = -0.18[3]
Sorting (phi)	r = -0.56[1,3]
Log porosimeter porosity (%)	r = +0.89[1]
Log unstressed permeability (md)	r = +0.99[1]

[1]Significant at the 99% confidence level.

[2]Sample size is 59; samples with thin-section porosity>porosimeter porosity were eliminated.

[3]Grain size in phi accounts for negative r values.

Quartz cement is the only authigenic mineral that by itself has a significant effect on permeability, but total cement volume explains a greater amount of the variation in permeability than does quartz cement alone (table 2). Permeability decreases with increasing volume of ankerite, dolomite, and total carbonate cement, but the relationships are significant only at the 90 percent confidence level. Permeability has no trend with volume of authigenic illite or chlorite cement.

Permeability in clean sandstones increases with better sorting but has no significant relation to grain size (table 2). Among all sandstones, permeability generally decreases with increasing matrix content. The relationship between permeability and matrix is not linear, however, because low permeability also occurs in sandstones that have low volumes of matrix but that have large volumes of authigenic cement.

Permeability varies significantly among samples taken from different sedimentary structures (table 3). The highest average permeability occurs in samples from high-energy sedimentary structures such as crossbedding and planar to slightly inclined laminae. Samples from sedimentary structures with poor sorting, such as ripple cross lamination with clay drapes, or heavily bioturbated sandstones, have lower average permeability. Even among clean sandstones, samples of ripple-cross-laminated sandstones have low permeability. At least part of the variation in average permeability among samples from different sedimentary structures may be due to differences in grain size. Clean ripple-cross-laminated sandstones have an average grain size of 0.118 mm, compared to an average of 0.165 mm in crossbedded sandstones. Assuming equal sorting, the coarser grained sandstones would be expected to have higher permeability at the time of deposition than would the finer grained ones (Beard and Weyl, 1973). Although the sandstones have undergone a complex sequence of diagenetic modifications since they were deposited, some of the original permeability differences due to grain size variations may have persisted.

As a result of the combined influence of all these different factors, permeability in Travis Peak sandstones typically ranges over four orders of magnitude within a single sandstone bed

Table 3. Distribution of average porosity and permeability by sedimentary structure.

	ø (%)	Stressed k (md)	Unstressed k (md)	Grain size (mm)
All Sandstones				
Crossbedding	9.2 (78)	0.196 (50)	0.527 (74)	0.166
Clean ripples	8.3 (46)	0.009 (21)	0.073 (44)	0.105
Planar laminations	9.1 (63)	0.097 (32)	0.317 (62)	0.139
Bioturbated	8.9 (53)	0.012 (38)	0.047 (51)	0.100
Massive	10.2 (12)	0.030 (4)	1.382 (11)	0.158
Contorted bedding	6.7 (11)	0.002 (7)	0.025 (11)	0.120
Ripples with thick clay drapes	7.3 (20)	0.003 (15)	0.023 (19)	0.090
Clean Sandstones				
Crossbedding	9.1 (61)	0.197 (39)	0.526 (58)	0.165
Clean ripples	7.1 (19)	0.005 (11)	0.039 (19)	0.118
Planar laminations	8.2 (41)	0.052 (19)	0.289 (41)	0.139
Bioturbated	9.1 (13)	0.199 (10)	0.245 (13)	0.144
Massive	9.2 (8)	0.057 (3)	1.249 (8)	0.174
Contorted bedding	8.7 (3)	0.017 (2)	0.031 (3)	0.131
Ripples with thick clay drapes	10.3 (4)	—	0.058 (3)	0.102

(fig. 41). In general, however, deeper sandstones have lower average porosity and permeability. A typical fluvial sandstone at 7,400 ft has average porosity of 10.1 percent and average stressed permeability of 0.91 md (fig. 41). A comparable fluvial sandstone from 9,950 ft has average porosity of only 5.0 percent and average stressed permeability of 0.007 md (fig. 41). Similarly, a paralic sandstone from 5,950 ft has average porosity of 16.2 percent and average unstressed permeability of 103.3 md, but a comparable paralic sandstone from 8,215 ft has an average porosity of 8.4 percent and average unstressed permeability of 0.25 md (fig. 41).

Controls on Porosity and Permeability

If no petrographic information were available from these samples, the loss of porosity and permeability with depth in Travis Peak sandstones probably would be attributed simply to increased compaction. However, based on information derived from viewing these sandstones in thin section, compaction is not the explanation. Instead, the decline in porosity and permeability with burial depth in the Travis Peak probably is the result of the following combination of diagenetic and physical modifications: (1) increasing cementation, particularly by quartz, with depth, (2) decreasing secondary porosity with depth, and (3) increasing overburden pressure with depth that closes narrow pore throats but does not significantly change grain packing. Porosity is affected mainly by (1) and (2), but permeability is a function of all three factors.

Compaction—The trends of decreasing porosity and permeability with depth are not interpreted to be the result of greater compaction in the deeper sandstones. Minus-cement porosity has no trend with increasing depth (Dutton and Diggs, in press) but exhibits a wide range at all depths around a central value of about 26 percent. The explanation for the lack of a trend with depth is that compaction took place mainly within the first several thousand feet of burial, prior to significant cementation by quartz (Dutton and Land, 1988). Once the phase of extensive quartz precipitation occurred at burial depths of 3,000 to 5,000 ft (914 to 1,524 m),

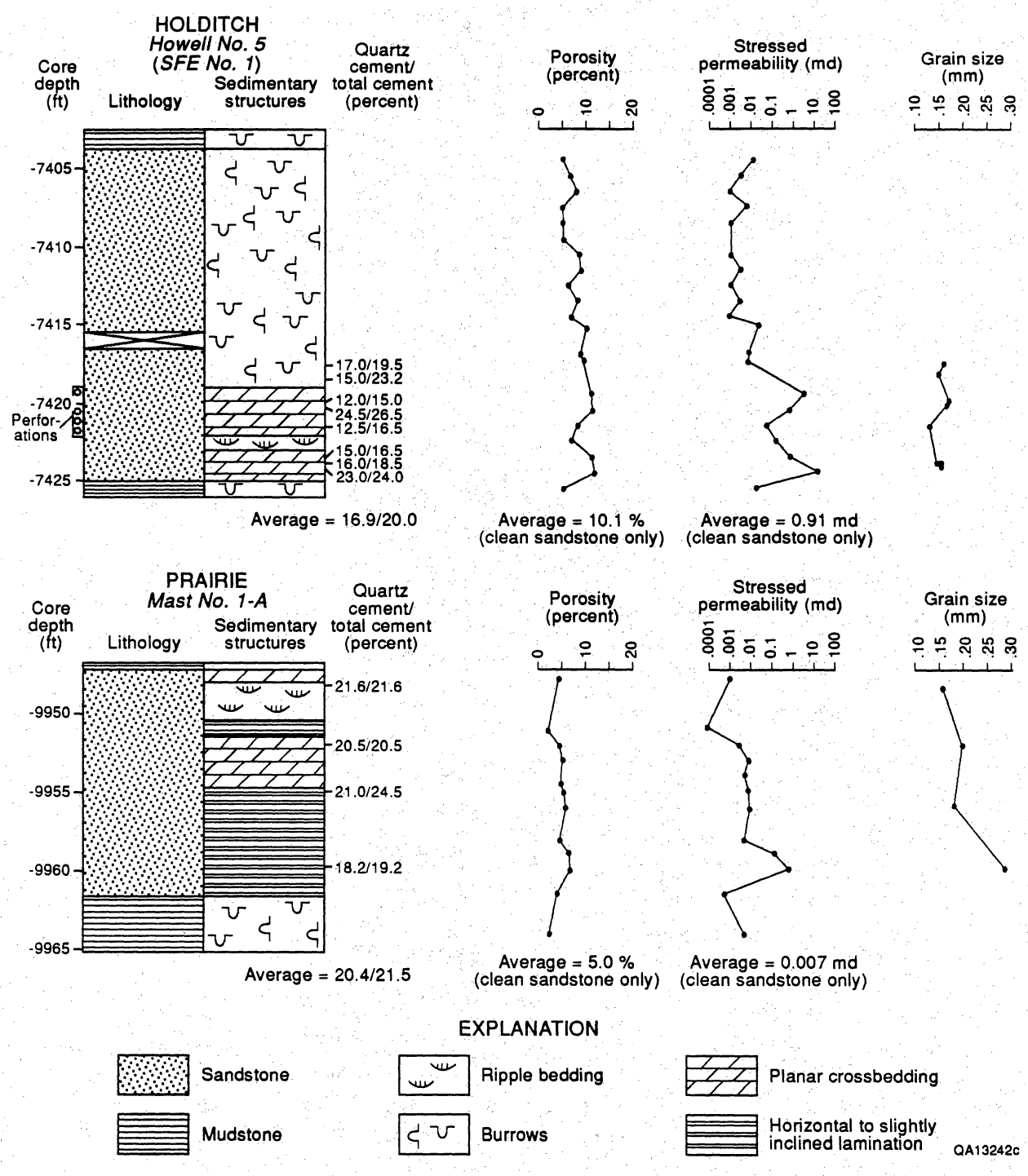

Figure 41. Comparison of sandstones from similar depositional environments at different present burial depths. (a) Fluvial channel sandstones at 7,400 ft in the Holditch Howell No. 5 well have significantly higher average porosity and permeability than do comparable fluvial deposits in the Prairie Mast No. 1-A well at 9,950 ft. (b) Paralic sandstones at 5,950 ft in the Mobil Cargill No. 14 well have higher porosity and permeability than do paralic sandstones at 8,200 ft in the ARCO Phillips No. 1 well.

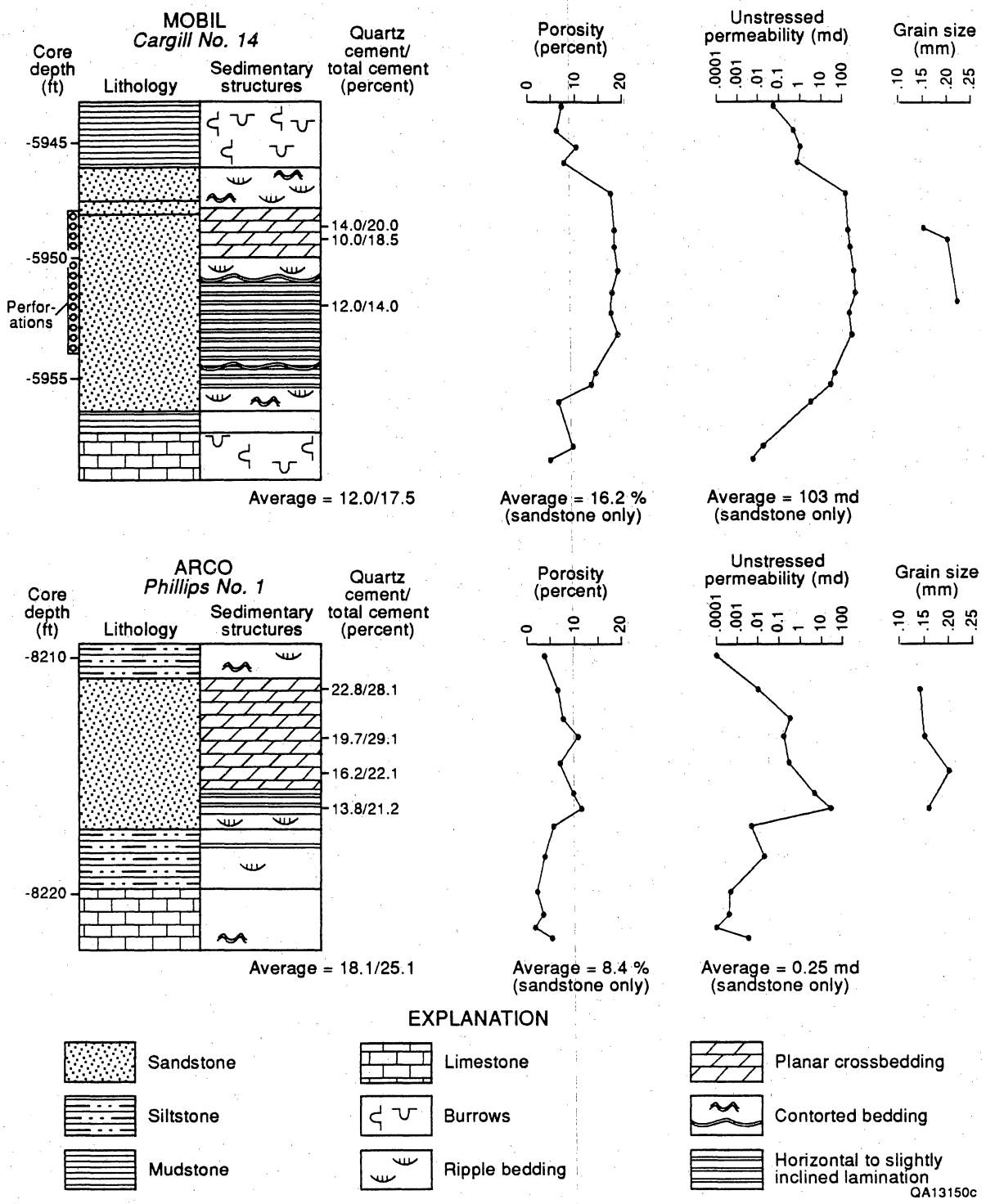

Figure 41 (cont.)

further mechanical compaction by grain rearrangement was largely ended. Continued burial of some sandstones to a total depth of 6,000 ft (1,829 m) compared to burial of others to as much as 10,000 ft (3,048 m) did not cause a difference in compaction. Thus, porosity cannot be predicted simply as a function of mechanical compaction.

Cement—Permeability decreases significantly in clean sandstones with increasing total volume of authigenic cement (fig. 42) and quartz cement (fig. 43). Increasing cement decreases permeability by occluding porosity, particularly primary intergranular porosity. The relationship between quartz and permeability is not as strong as between total cement and permeability because some samples with low volumes of quartz cement nevertheless have very low permeability as a result of abundant ankerite and dolomite cement. Because total cement increases with depth (fig. 44), permeability decreases, and the main reason for the increase in total cement with depth is the increase in quartz cement (fig. 30). None of the other authigenic cements in the Travis Peak has a significant trend with depth except for illite, which decreases with depth.

The increase in quartz cement with present burial depth is the result of the following two phases of quartz cementation in the Travis Peak (Dutton and Diggs, in press): (1) an early episode of quartz cementation by meteoric water that resulted in relatively uniform distribution of quartz within the formation, and (2) a later episode related to the development of stylolites that preferentially added quartz cement in the deepest sandstones. Stylolites are most abundant in sandstones deeper than 8,000 ft (2,438 m). Interestingly, 8,000 ft (2,438 m) seems to mark a boundary between two populations in parameters such as porosity in clean sandstones (fig. 35) and permeability (figs. 37 and 38).

Secondary Porosity—A second reason for the observed decrease in porosity and permeability with depth is the fact that fewer secondary pores were generated in deep Travis Peak fluvial sandstones than in shallow ones (fig. 36). The average volume of secondary porosity in clean fluvial sandstones at 6,000 ft (1,829 m) is 4.7 percent, compared with an average of 1.6 percent at 10,000 ft (3,048 m) (fig. 36). One explanation for this difference in

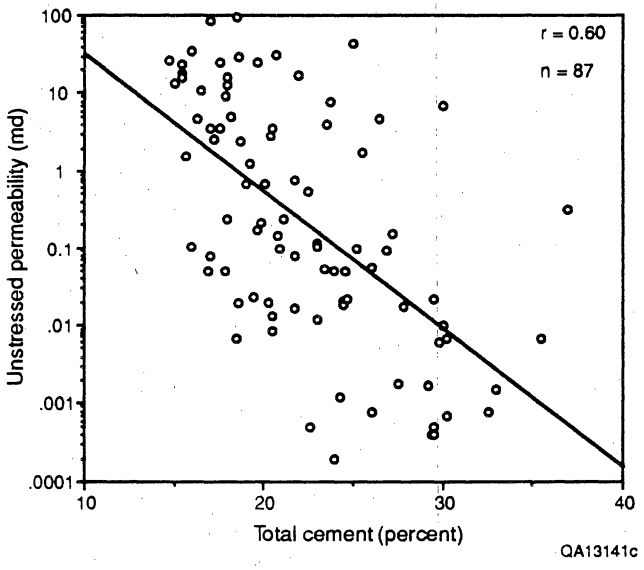

Figure 42. Inverse relationship between total cement volume and unstressed permeability in clean sandstones. Volume of authigenic cement is a major control on permeability in Travis Peak sandstone.

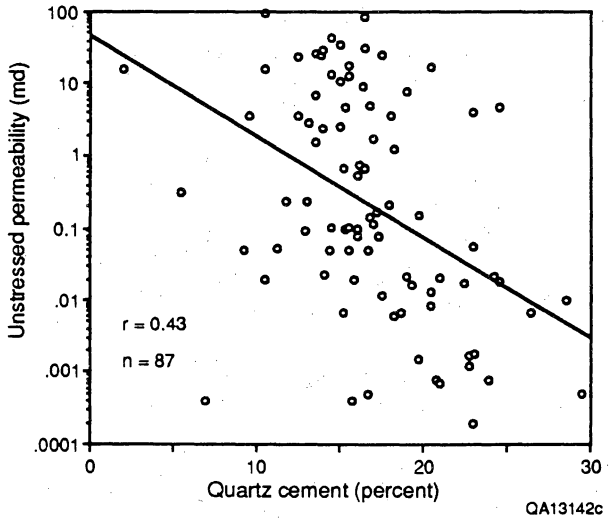

Figure 43. Inverse relationship between quartz cement volume and unstressed permeability in clean sandstones.

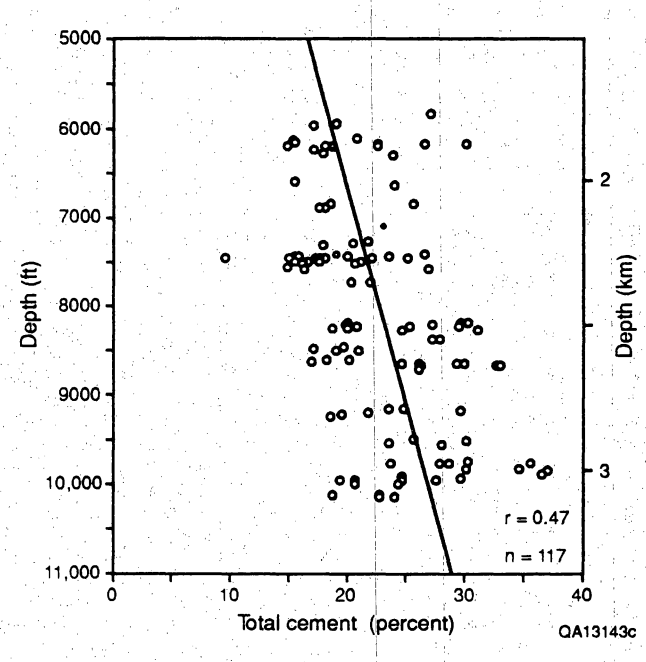

Figure 44. Total cement volume in clean sandstones as a function of present burial depth. Total cement volume increases significantly with depth.

secondary porosity with depth is an original difference in grain size and feldspar content with depth. As relative sea level rose during deposition of the Travis Peak, younger sandstones in the study area were deposited in progressively more distal parts of the fluvial facies tract and thus have finer grain size. The change in feldspar content probably is a result of the changing grain size. Odom and others (1976) found that detrital feldspar is most abundant in the <0.125 mm size fraction of quartz-rich sandstones. Thus, as progressively finer grained sandstones were deposited in the study area throughout Travis Peak time, the detrital feldspar content increased.

An estimate of the original volume of feldspar in each sandstone sample can be calculated by adding the present feldspar volume to the volume of secondary porosity, because most secondary pores formed by feldspar dissolution. The results indicate that the average feldspar content in fluvial sandstones at 6,000 ft (1,829 m) was 8.1 percent at the time of deposition, compared with 3.1 percent at 10,000 ft (3,048 m). The hypothesis that original feldspar content was related to sand grain size is supported by the statistically significant correlation that exists between grain size and restored feldspar content in clean fluvial sandstones ($r = 0.36$, $n = 132$, significant at the 99 percent confidence level). Of the original feldspar, 58 percent has dissolved at 6,000 ft (1,829 m), compared with 52 percent of the original feldspar at 10,000 ft (3,048 m). Thus, apparently about half of all the feldspar in the Travis Peak dissolved and formed secondary pores. Because the shallowest sandstones started with the greatest volume of feldspar, they generated the most secondary porosity.

The trend in secondary porosity with depth only occurs in fluvial sandstones. Paralic sandstones probably do not show a similar trend because they do not vary in grain size or original feldspar content with depth. Paralic sandstones at all depths in the Travis Peak represent the same approximate position in a facies tract, and thus did not change systematically in grain size through time.

Overburden Pressure—A third factor involved in the decrease in permeability with depth is the greater overburden pressure at 6,000 ft (1,829 m) compared to 10,000 ft (3,048 m). The

increased overburden apparently has little effect on porosity, but it probably has a greater effect on permeability (Jones and Owens, 1980). In these well-cemented, low-permeability sandstones, all that remains of many primary pores are narrow slots between quartz overgrowths that connect larger secondary pores (Soeder and Chowdiah, 1988). Increasing overburden probably further narrows or closes these slot-shaped pores and thus has a major effect on permeability, without significantly changing porosity (Jones and Owens, 1980; Soeder and Chowdiah, 1988). Evidence for the importance of overburden pressure on permeability is provided by the difference in permeability measured under ambient conditions compared to restored net overburden pressure. At high permeability values, both measures of permeability are similar, but as permeability decreases, the difference between the two increases. At stressed permeability values of 0.00001 md, the difference is an order of magnitude, so unstressed permeability is measured as 0.0001 md. The difference in porosity measured under stressed and unstressed conditions is generally uniform over the range of porosity in the Travis Peak ($r = 0.99$) (Luffel and others, 1989). Porosity measured under ambient conditions averages 0.3 porosity units less than porosity measured under net overburden conditions. Evidently the closing of narrow pore throats, which has an important influence on permeability, has little impact on total porosity.

Depositional Environment—At all depths in the Travis Peak Formation, paralic sandstones have an order of magnitude lower permeability than do fluvial sandstones (fig. 39). Two mains reasons probably explain the permeability differences. First, paralic sandstones are finer grained and thus would have had lower permeability at the time of deposition than the coarser grained fluvial sandstones (Beard and Weyl, 1973). Second, paralic sandstones had significantly greater volumes of authigenic cement precipitate in them during burial diagenesis than did fluvial sandstones, 22.7 percent versus 29.4 percent. Paralic and fluvial sandstones contain similar volumes of quartz cement, but because paralic sandstones have more authigenic dolomite, ankerite, illite, chlorite, and reservoir bitumen, they contain an average of 7 percent more total cement. Thus, the already lower permeability in paralic sandstones would have

decreased more during burial than permeability in fluvial sandstones because of the occlusion of more porosity by cement.

Conclusions

Porosity and permeability decrease significantly with depth in the Travis Peak Formation in East Texas. However, these trends are not simply functions of greater compaction with depth. Instead, original grain size and composition differences in the sandstones, combined with diagenetic modifications during burial diagenesis, have resulted in the present distribution of porosity and permeability in the formation. Permeability in the Travis Peak Formation is a function of porosity and overburden pressure. Porosity, in turn, is determined by original sediment sorting, volume of primary porosity occluded by authigenic cement, and amount of secondary porosity generated by feldspar dissolution.

Precise prediction of sandstone permeability at any given depth is impossible because permeability within one sandstone bed commonly ranges over four orders of magnitude. However, average permeability decreases with depth, so the range of expected permeability values can be estimated.

NATURAL FRACTURES

Core- and log-based studies of fractures in nine wells in East Texas documented fracture type, attitude, abundance, shape, microstructure, and fracture-fill mineralogy and microstructure (Laubach, 1989a; Dutton and others, in press). Results of this study are applicable to evaluation of Travis Peak reservoirs and to deformation of massive sandstone during shallow burial and lithification. Cores were oriented by standard techniques (Nelson and others, 1987) and results generally have an uncertainty of less than 15° within a given well. Natural and drilling-induced fractures were distinguished on the basis of the criteria described by Kulander and others (1979). For petrographic studies of microfractures, samples were cut from core containing macrofractures (veins) and from oriented core that lacked veins. Microfracture attitude was measured on the universal stage from 20 sets of 3 orthogonal thin sections from 1 well, Holditch Howell No. 5. For other wells with oriented core, microfracture attitude at a given depth was determined from single thin sections.

Fracture Abundance

Fractures are widespread in the Travis Peak Formation, particularly in highly indurated, deeply buried parts of the formation in northern Nacogdoches County. They were observed at a range of depths in core or with borehole-imaging logs (Formation Microscanner, borehole televiewer; Laubach and others, 1988) throughout the geographic area of the study and in all stratigraphic subdivisions of the Travis Peak Formation. The variability and local high density of fracture development is illustrated by two cores from the Holditch SFE No. 2 well in northern Nacogdoches County. Only a few short fractures are present the core from the shallow interval (fig. 45) but numerous fractures occur in the core from the deeper interval of this well (fig. 46). Significant fracture development is not restricted to deeper parts of the formation, however.

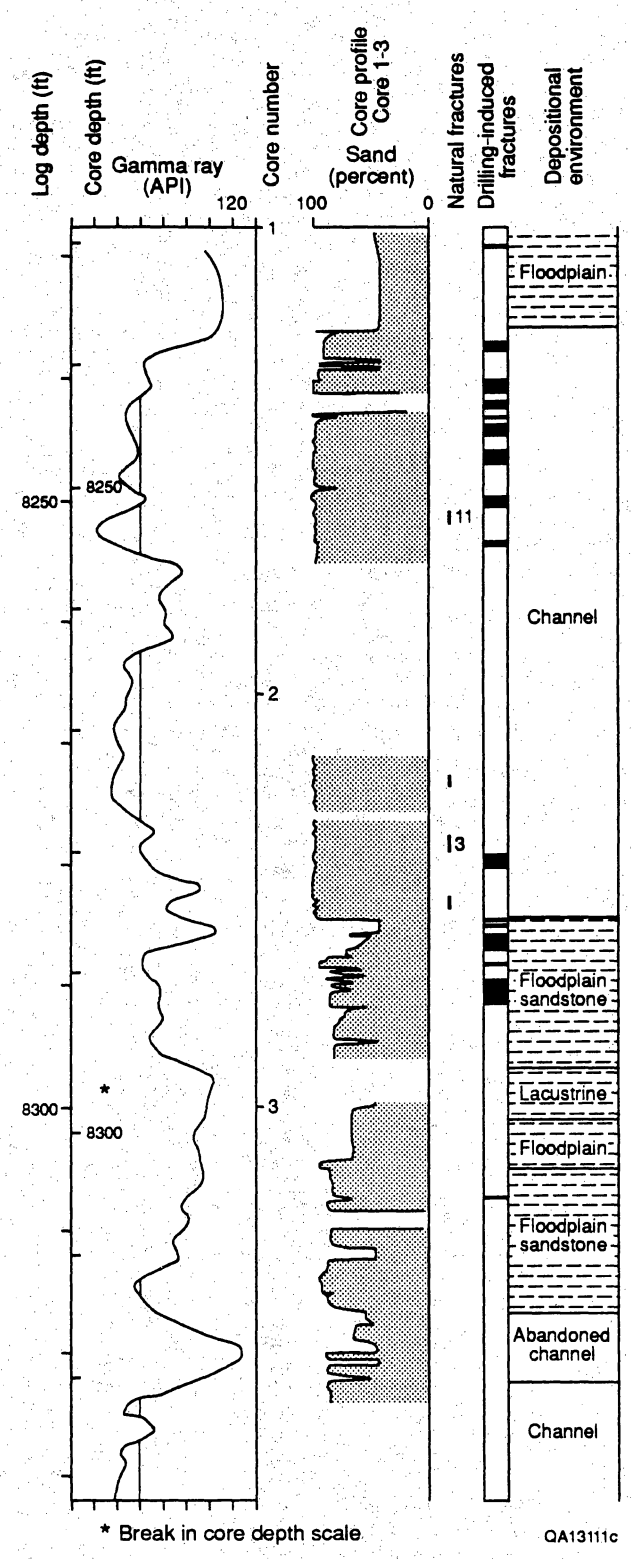

Figure 45. Core gamma ray log, core profile, fracture distribution, and environmental interpretation for core 1-3, Holditch SFE No. 2 well. Note that few natural fractures occur in this interval.

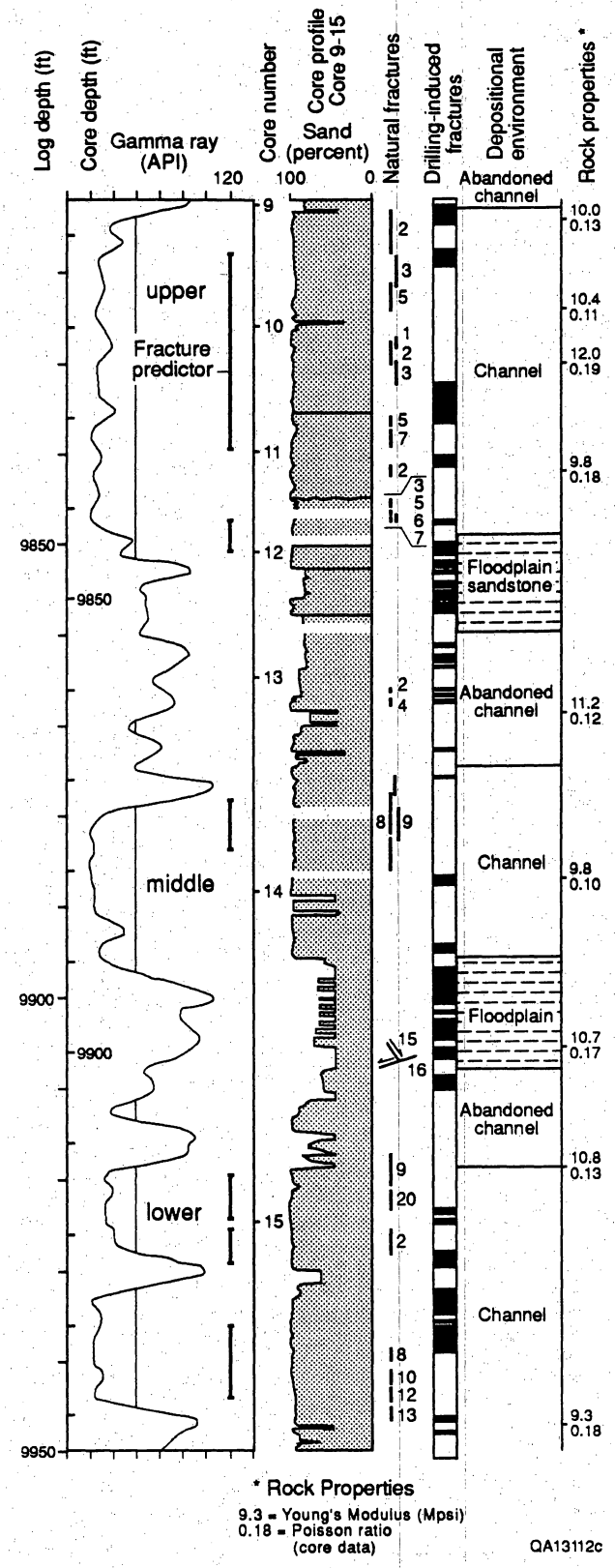

Figure 46. Core gamma ray log, core profile, fracture distribution, and environmental interpretation for core 9-15, Holditch SFE No. 2 well. Static rock property measurements from core plugs in this interval are also indicated. This core interval illustrates numerous fractures in lower Travis Peak Formation.

Fractures as much as seven feet tall from approximately 6,200 ft (3,047 m) in the Arkla Scott No. 5 well in Waskom field are among the longest recovered in this study (Laubach, 1989a, p. 5).

Fracture abundance is difficult to quantify with vertical core in the Travis Peak because fracture dip is subparallel to the core axis, and fracture spacing is generally greater than the four-inch (10-cm) diameter of the core, implying a fracture spacing of greater than four inches (10 cm). One measure of abundance is fracture number, defined as the total length of fractures in a cored interval normalized to the thickness of cored rock. It appears, on the basis of fracture number, that natural extension fractures in sandstone are more abundant in the lower Travis Peak than in the upper (Laubach, 1989a). Fracture abundance could be greater in fold hinges and adjacent to faults, but only slightly greater fracture abundance was documented in the hinge of a small fold in Waskom field and none of the study wells were in close proximity to faults (Laubach and others, 1987). The most highly fractured rocks encountered in this study, with fracture spacing in core of as little as approximately one inch (2 to 3 cm), occur in North Appleby field in areas of homoclinal dip distant from any fold.

Fracture Attitudes

Fractures in Travis Peak sandstone typically are nearly vertical and strike east-northeast to east, with a range of strikes from 028° to 130° and a mean strike of 083° (fig. 47). Considerable fluctuation in fracture strike is evident from well to well, within a given well, and within any depth interval in a single well. Part of this fluctuation may result from errors in core orientation. No abutting or crosscutting fractures were observed, and there is little evidence for multiple fracture sets. Subvertical drilling-induced fractures and natural extension fractures have similar strikes, but observations of fractures in continuous core intervals show that natural and drilling-induced fractures are not precisely parallel. For example, in one continuous core from Prairie Producing Mast No. A-1, the average angle between natural and induced fractures is 22°.

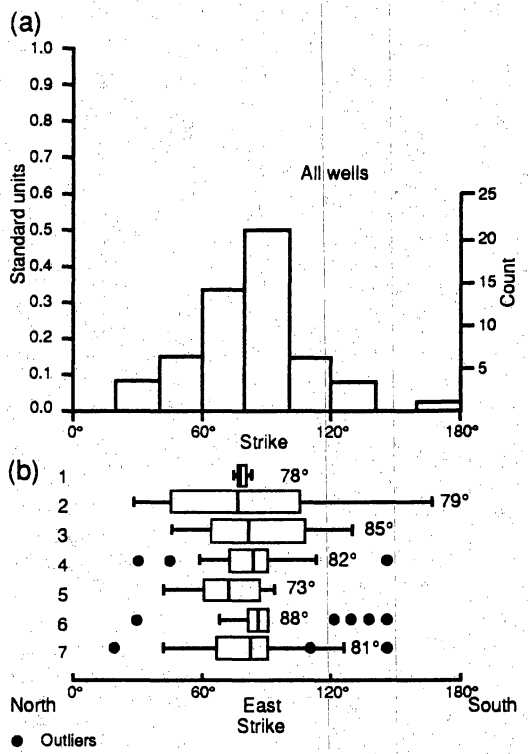

(c)

Well	Mean Strike	Min.	Max.	Std. Dev.	No. of Fractures
1 *SFE No.3* *	78°	74°	83°	4.6	3
2 *SFE No. 1*	79°	27°	167°	44.8	10
3 *C.W. Sam Hughes No. 1*	85°	46°	130°	30.2	6
4 *SFE No. 2* - all	82°	28°	121°	19.2	34
5 *SFE No. 2* - upper	73°	42°	94°	16.2	13
6 *SFE No. 2* - lower	88°	28°	121°	19.1	21
7 All wells**	81°	27°	167°	26.0	54

*Only fractures oriented with paleomagnetic method are included
**Includes one fracture from *Prarie Mast No. 1-A* well

QA13121c

Figure 47. Strikes of natural fractures in Travis Peak sandstones. (a) Histogram showing data from all wells in the study. (b) Box plots of data from the indicated wells and intervals within wells. The center half of the data (from the first to the third quartile) is represented by the rectangle (box) with the median indicated by a bar. The horizontal lines right and left of the box extend to values that represent 1.5 times the spread from the median to the corresponding edge of the box. Points plotted separately are outliers.

Strikes of natural and drilling-induced fractures in the same core locally deviate by as much as 85°, although the difference is commonly 5° or less. Mean angle between natural and drilling-induced fractures is 17°, and the mean angle in individual wells is between 10° and 20° (Laubach and Monson, 1988).

Fracture Morphology and Dimensions

Natural fractures in the Travis Peak Formation can be divided into two major types: (1) mineralized, subvertical, dilational fractures produced by net extensional strain perpendicular to fracture strike and (2) gently dipping shear fractures. Extension fractures occur predominantly in sandstone, whereas shear fractures are primarily in shale and silty mudstone. Travis Peak extension fractures are veins that commonly are filled or partly filled with authigenic minerals such as quartz and carbonate minerals (calcite or ankerite/dolomite). These fractures have been interpreted to result from a combination of extensional tectonic strains and hydraulic pressurization in the diagenetic environment (Laubach, 1988a, 1989a). Shear fractures in Travis Peak mudstone may result from processes such as compaction and soil formation in the shallow subsurface (Laubach, 1989a). Our study focused on the extension fractures in sandstone because they are more likely to have a direct effect on reservoir quality.

An important characteristic of many Travis Peak extension fractures is that they are partly or completely open when observed in core. Petrographic evidence of delicate fracture-lining and bridging minerals in fractures demonstrates that many were also open in the subsurface, including fractures from depths of as much as 9,934 ft (3,028 m). Open fractures are lens-shaped in cross section and have widths that range from microscopic (<0.05 mm) to 5 mm. Because the mineral fill in fractures is irregularly distributed, open pore networks or channelways within fractures are curved to anastomosing and have rough walls. Open fractures were sampled from both the upper and lower Travis Peak, but the widest fractures are from the

lower Travis Peak in the Holditch SFE 2 well. These fractures are also the shortest and least continuous.

The only fracture length dimension of vertical fractures that can be measured in vertical Travis Peak core is fracture height; the important fracture characteristics of length (in plan view) and interconnectivity could not be measured. A spectrum of fracture heights is present at any given depth in the Travis Peak, the tallest fractures being as much as 8 ft (2.5 m) high. Tall fractures are composed of coplanar segments, ranging in length from inches to tens of inches, which are commonly arranged in relay and en echelon patterns. In cross section, segments are separated locally from adjacent segments by intact rock.

Most fractures do not extend completely across sandstone beds, even where the beds are apparently of homogeneous composition. Instead, they terminate within beds (e.g., figs. 45 and 46). Fractures that cross shale interbeds thicker than ~ 2 mm were not observed. Fractures show various styles of termination including simple tapering tips, blunt tips at lithologic interfaces, of zones of fracture splaying. Fractures that are truncated by stylolites are locally present in more deeply buried parts of the formation (Laubach, 1989a).

Characterization of Fractures with Borehole-Imaging Logs

Detection and characterization of fractures and stress direction indicators such as borehole breakouts in low-permeability reservoirs is an important goal of reservoir analysis. Two logging tools used for fracture and breakout detection are the borehole televiewer (BHTV)(Zemanek and others, 1970), an acoustic device that maps the smoothness of the borehole wall, and the Formation Microscanner (FMS*)(Bourke and others, 1989), a resistivity tool that produces a conductivity map of a portion of the borehole wall. We compared BHTV and FMS logs to core from three wells in the Travis Peak and one well that is in both the Travis Peak and Cotton Valley (Laubach and others, 1988). The Travis Peak provides a good test of fracture-imaging logs because natural fractures have complex geometry and variable mineral fill and because there

are borehole breakouts, drilling-induced fractures, and vertical sedimentary structures that must be distinguished from natural fractures for successful fracture analysis.

Vertical extension fractures in Travis Peak sandstone usually are visible on BHTV and FMS logs, but some fractures were missed by FMS pads on the two-pad version of the tool. Both BHTV and FMS give high-resolution images of fracture shape, but present commercial BHTV and FMS techniques do not give a quantitative measure of fracture aperture. Fracture orientation is readily obtained for inclined fractures from either BHTV or FMS logs, but the orientation of vertical fractures may be ambiguous on both logs. BHTV logs provide a clear view of breakout shapes and permit breakouts, washouts, and eroded fractures to be distinguished, enhancing the use of breakouts as stress indicators. These results show that BHTV and FMS logs are useful adjuncts to core-based fracture studies for evaluation of fractured reservoirs.

Contrasts and Similarities between Travis Peak and Cotton Valley Fractures

Vertical natural extension fractures and fracture zones from the Taylor Sandstone (Cotton Valley Group) from a single well, the Mobil Cargill No. 15 well in Waskom field, were sampled for comparison with fractures in the Travis Peak. The Taylor sandstone fractures are east-northeast-striking subvertical extension fractures confined to sandstone beds, as are the fractures in the Travis Peak in the Mobil Cargill No. 15 and adjacent wells. There are some differences in fracture style and mineral fill between fractures in the two units (Dutton and others, in press).

Fractures in the Taylor Sandstone are tall, narrow fractures with height/width ratios of 3,000 to 6,000. Short, wide, vug-like fractures, common in some deep Travis Peak core (e.g., the lower zone of Holditch SFE No. 2) were not observed. Fractures and interconnected fracture zones range in height from a few inches to over four feet (5 cm to over 1.2 m), which is similar to fracture heights in Travis Peak core from the nearby Arkla Scott No. 5 and Holditch Howell No. 5 wells, but dissimilar to fracture dimensions in northern Nacogdoches County wells in this

study. Taylor Sandstone fractures are arranged in more continuous vertical networks than is typical of most Travis Peak fractures. Vertical interconnection of fractures within the Taylor Sandstone is also suggested by fracture traces imaged with BHTV and FMS logs that are more continuous than those imaged in Travis Peak wells (Dutton and others, in press; Laubach and others, 1988). Despite apparently greater vertical connectivity within sandstone beds, fractures in Cotton Valley sandstone do not cross shale interbeds in the cores we studied.

The azimuth of 30 natural fractures in the upper Taylor Sandstone ranges from 005° to 175°, with a vector mean strike of 082°. Three natural fractures in the Taylor Sandstone that were oriented by paleomagnetic methods have strikes of 077°, 074°, and 083° (fig. 47). These results agree with strikes of fractures in the Travis Peak in Waskom field (Dutton and others, 1987).

Fractures in the Taylor Sandstone are filled or partly filled with calcite and quartz, with calcite the predominant fracture-filling mineral. Fracture-filling quartz is not as widespread as in the Travis Peak Formation, and quartz is rare in Cotton Valley fractures. Quartz precipitated before calcite. Calcite occurs as massive white crystals that variably fill fractures. The volume of fracture porosity filled by calcite varies considerably, in one example ranging from less than 10 percent to 100 percent within a single fracture. Fractures that macroscopically appear filled with calcite have considerable microporosity that locally is interconnected within the fracture.

Petrology of Travis Peak Fracture-Filling Minerals

Most extension fractures in Travis Peak sandstone are lined by quartz. Many fractures also contain ankerite/dolomite, calcite, clay minerals, and hydrocarbons. Minor amounts of anhydrite are locally present in a few fractures in Holditch SFE No. 2 core. The fine-grained clay minerals locally filling fractures are morphologically similar to diagenetic illite elsewhere in the Travis Peak. Fracture-filling and fracture-lining quartz occurs as faceted crystals and thin (50 to 100 μm) overgrowths in optical continuity with adjacent quartz grains. Ankerite occurs as

yellowish-white to yellowish-brown, blocky, rhombohedral crystals having diameters between 100 μm and 1 mm. Ankerite crystals are widely spaced (1 to 5 mm) on some fracture surfaces; less commonly, ankerite occurs as coalescent masses or completely fills fractures.

Crosscutting relations, where a younger phase grows across and covers a crystal face of an older mineral, establish the sequence in which fracture-filling minerals precipitated. Quartz precipitated first; it shows euhedral growth faces against both carbonate and clay minerals (fig. 48). Locally there is evidence for a second, minor episode of quartz precipitation following ankerite (Laubach, 1989a). Clay mineral precipitation postdates the main phase of quartz and ankerite precipitation. Feldspar exposed on fracture surfaces has a pitted or skeletal appearance that indicates partial dissolution, possibly following fracture opening and quartz precipitation.

Fracture-filling quartz in the upper Travis Peak contains planes of fluid inclusions that parallel fracture walls and commonly are symmetric about the centerline of the fracture (fig. 49). The alternation of inclusion planes and clear quartz is interpreted to represent an increment of quartz growth into a partly open fracture with subsequent reopening of the fracture preferentially along the fracture centerline. Quartz with such banded fluid-inclusion structure is developed discontinuously in fractures, and faceted crystals in fracture pore spaces indicate that fracture sealing was not complete. Euhedral crystals and locally fluid-inclusion-rich vein quartz have rims of fluid-inclusion-poor quartz. The boundary between these two types of quartz is planar to irregular. In contrast to quartz, ankerite shows no organized fluid-inclusion microstructure. Ankerite typically occurs as single crystals with euhedral to subhedral crystal faces. Internally, ankerite has sparse, thin twin lamellae and rare, narrow, intragranular fractures striking across, rather than parallel to, the main fractures.

Figure 48. Tracing from photomicrograph showing superposition of infilling mineral phases in Travis Peak fracture. Sample is from Holditch SFE No. 2 well.

Figure 49. Photomicrograph of fluid inclusions in Travis Peak quartz-filled fracture (vein).

Fluid Inclusion Microthermometry

Fluid inclusions in vein quartz record at least two fluids of contrasting salinity and temperature (figs. 50 and 51). The first generation, termed Type A, constitutes the planes of inclusions in banded patterns. SEM observations show that these planes are composed of layers of closely spaced, small (<0.25μm), equant *primary* inclusions interspersed with massive quartz layers containing planes of large (0.5 to 10 μm) inclusions with spherical or negative crystal shape. T_h data from these early inclusions suggest veins formed in the presence of warm (~125° to 140°C) brine (5 to 10 wt.% NaCl eq.)(Laubach and Boardman, 1989). These inclusions are interpreted to be synkinematic with respect to the opening of fractures. These early phase inclusions are locally surrounded by rims of fluid-inclusion-free quartz ("clear quartz rims"), which is locally in turn surrounded by postkinematic ankerite or calcite, and a small amount of late quartz. Inclusions in clear quartz rims occur as primary inclusions (Type C) and as secondary planes (Type B) that crosscut both early fluid-inclusion-bearing quartz and postkinematic quartz. Type B planes are subvertical, but they are not parallel or regularly spaced and they cut across planes defined by Type A inclusions. Type B inclusions are elongate to irregular with maximum length ranging from less than one to greater than 10 μm, and they commonly show evidence of necking. T_h for late inclusions ranges from 120 to 170°C, with a mean of 150°C. Mean salinity is 11 wt.% NaCl eq., but values range from 5 to >20 wt.% NaCl eq. The temperature range and variable salinity of late inclusions could have been caused by mixing of two fluids of different salinities during trapping (Laubach and Boardman, 1989). Primary carbonate inclusions have T_h of 157 to 178°C.

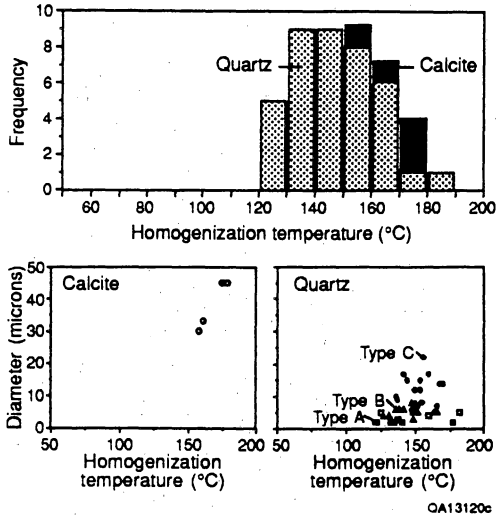

Figure 50. Homogenization temperatures from vein quartz and calcite. Samples are from Travis Peak veins, Holditch SFE No. 2 and Prairie Producing Mast No. 1-A wells.

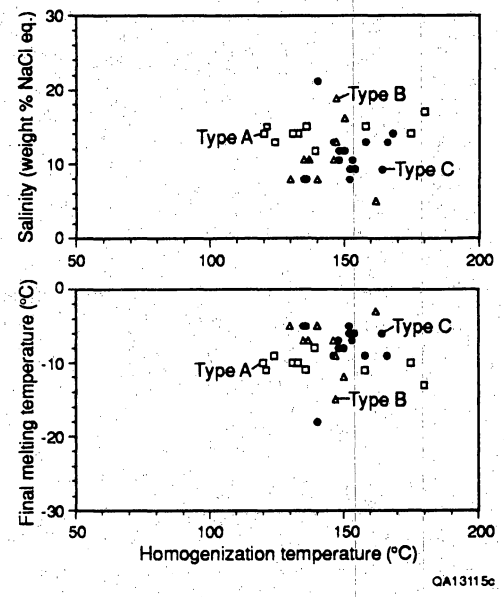

Figure 51. Homogenization temperature vs. salinity and final melting temperature. Samples are from Travis Peak quartz veins, Holditch SFE No. 2 and Prairie Producing Mast No. 1-A wells.

Relationship between Fracture Development and Diagenesis

Banded planes of Type A inclusions are interpreted to be crack-seal structures in fracture-filling quartz that indicate that quartz precipitated during episodic fracture opening (Laubach, 1988a). Transgranular microfractures (described below) in quartz cement, together with crack-seal structures, suggest fracture growth in highly indurated quartz-cemented rock. Postkinematic ankerite in some veins indicates that some fractures had ceased to widen prior to ankerite precipitation.

The paragenetic sequence of fracture-filling minerals is similar to that of authigenic cements in the Travis Peak Formation. For cements, the sequence consists of (1) quartz precipitation (main phase), (2) albitization and orthoclase dissolution, (3) illite and chlorite precipitation, (4) ankerite precipitation, and (5) minor quartz precipitation (Dutton and Land, 1988; Dutton and Diggs, in press). In veins, the main phase of quartz precipitation precedes the precipitation of vein illite and ankerite and partly dissolved orthoclase grains are visible on fracture surfaces; minor post-kinematic vein quartz precipitation followed vein ankerite precipitation. These relationships have been interpreted to indicate that quartz cement (main phase) and vein quartz (main phase) precipitation were broadly contemporaneous (Laubach, 1988a). However, the widespread occurrence of closed microfractures in pore-filling quartz suggests that fractures propagated during the late stages of or shortly after main phase quartz cementation.

The $\delta^{18}O$ stable isotope composition of vein quartz is also similar to the composition of quartz cement (Laubach and Boardman, 1989). Quartz cement values range between +20 ‰ (SMOW) at the top of the formation and +24 ‰ (SMOW) at the base (Dutton and Land, 1988). High-purity vein quartz samples from two wells fall between these two values (fig. 52). The isotopic composition of carbonate minerals in veins and cement is also similar.

Isotopic Composition of Vein Quartz

Depth (ft)	$\delta^{18}O$	Purity 1=most, 5=least	Fracture type/ generation	Cement generation
-9840.0	18.3	5	Vug (1)	2 and 3
-9871.7	21.8	2	Planar (2)	2
-9873.0	21.5	2	Planar (2)	2
-9873.0	22.9	1	Planar (2)	2
-10,108.0	22.3	1	Planar (2)	2

Isotopic Composition of Vein Carbonate

Well	Depth (ft)	Composition	$\delta^{18}O$	$\delta^{13}C$
SFE No. 2	-9527	Dolomite/ankerite	-11.25	-11.65
HH No. 5	-6242	Dolomite/ankerite	-10.13	-9.14
HH No. 5	-6303	Dolomite/ankerite	-11.33	-9.61
HH No. 5	-7471	Dolomite/ankerite	-10.45	-8.89

QA13118c

Figure 52. Isotopic composition of vein quartz and vein carbonate. Quartz compositions are from samples from various depths in the Holditch SFE No. 2 well. Fracture type refers to shape classification of fractures in the Travis Peak (Laubach and others, 1989a). SFE No. 2 = Holditch SFE No. 2; HH No. 5 = Holditch Howell No. 5.

Microfractures

Quartz-cemented quartz-arenites in the Travis Peak Formation contain microscopic (0.1 to 2 mm long) transgranular and intragranular fluid-inclusion planes, interpreted to be closed microfractures (Laubach, 1989b). Transgranular planes crosscut grains and quartz cement and therefore postdate deposition of the sandstone. In contrast, intragranular planes terminate within grains or at original detrital grain boundaries and do not cross quartz cement, and have a random orientation. They are probably inherited from a source rock of Travis Peak grains. Transgranular planes occur in closely spaced arrays directly adjacent to veins and as isolated planes in rock that lacks veins. Planes are 1 to 10 μm wide. Locally, dilation parallel to transgranular planes is indicated by quartz-filled discontinuities within disseminated impurities in detrital grains. Grain boundaries are not offset across the traces of transgranular planes.

Closed microfractures are composed of closely spaced, small (<10 μm) fluid inclusions that show shapes transitional between tubes and spheres. Locally, regions of tabular, plate-shaped pores or open microfractures grade laterally into fluid-inclusion planes composed of coplanar cylindrical or spherical inclusions. Fluid inclusions in the closed microfractures are composed of a single colorless, phase, possibly a brine. Fluid inclusions in both transgranular and intragranular planes are surrounded by quartz that is in optical continuity with host grains. Closed microfractures are generally subvertical.

Microfracture occurrence is highly dependent on rock type, with the greatest number occurring in quartz-cemented quartz-arenites. Point counts show as many as 10 to 15 planes per cm^3 in the most highly quartz cemented sandstone, but 0 to 4 fractures in a single thin section are more typical in less highly cemented sandstone. Microfractures are rare or are absent in rocks with clay matrix, abundant clay cement, or more than a few percent detrital feldspar or calcite cement. Coarser grained, poorly sorted rocks tend to contain more planes than do very fine grained, well-sorted rocks. Abundance of closed microfractures in Travis Peak samples that

do not contain macroscopic veins is much lower than that of some strongly deformed metasedimentary rocks where spacing of fluid inclusion planes may be 0.5 mm or less (Laubach, 1988b). Because of the preferred orientation of microfractures described below, the apparent abundance varies with thin section orientation. Microfractures and adjacent veins are generally subparallel where they occur in the same core (Laubach, 1989b).

In rocks that lack veins, microfractures also have a preferred orientation (fig. 53). Mean strikes of these isolated microfractures vary across the study area, but generally strike east-northeast. In the Holditch Howell No. 5 well the mean strike is 066±15° and in the Holditch SFE No. 2 well mean strike is 084±18°. Dispersion in microfracture strike is low within a given thin section, where planes are commonly subparallel, but between samples from different depths in the same well, fluctuation in mean microfracture strike is commonly as much as 30°. Strike of isolated microfractures ranges from 020 to 335°. The vector mean strike of all oriented isolated microfractures measured in this study is 075±21°.

Significance of Microfractures

Transgranular fluid-inclusion planes in the Travis Peak Formation are microfractures that evolved into fluid-inclusion planes in the diagenetic environment. Planes that are continuous across cement or several sedimentary grains must have formed *after* sandstone deposition, and cannot be inherited from source rocks that ultimately provided clastic grains for the Travis Peak. Lack of grain boundary offset indicates that they were extension fractures.

Isolated closed microfractures in the Travis Peak are paleostress direction indicators because they are derived from extensional microfractures and because they have a preferred orientation on the scale of a thin section. They also have a consistent orientation over a wide region. Microfracture attitude generally does not reflect stress concentrations between individual grains (i.e. Gallagher and others, 1974), probably because the pervasive quartz cement made the rock mechanically homogeneous. Instead, microfractures have a range of

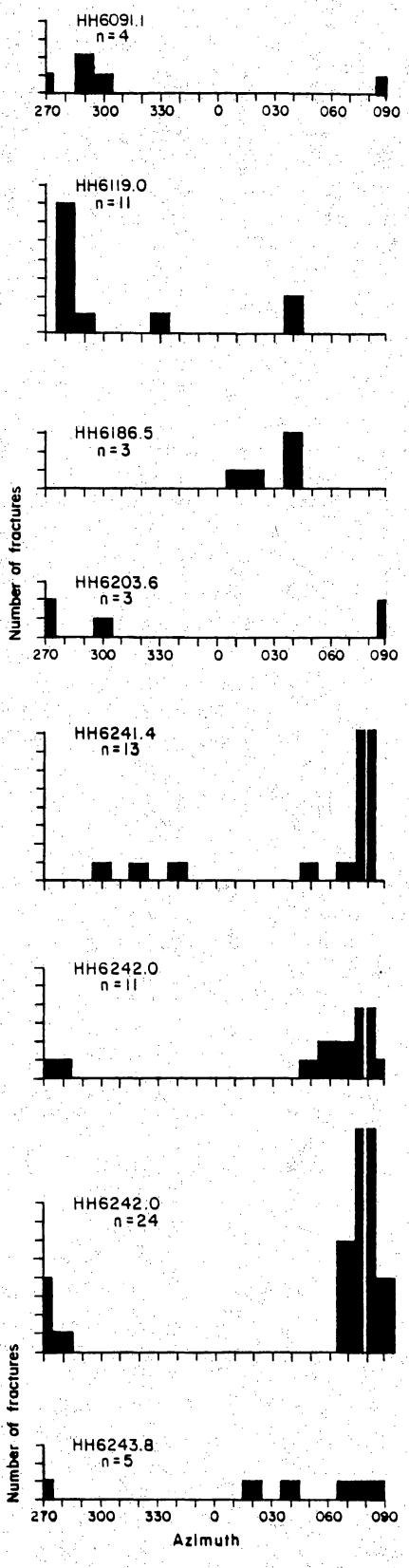

Figure 53. Preferred orientation of closed microfractures in a single well. Samples are from various depths in Holditch Howell No. 5 well. Histograms showing number of microfractures that strike in the indicated range. White bar in histogram indicates strike of macroscopic vein in core from that depth (Laubach, 1989b).

attitudes similar to those of veins. Isolated microfractures from a narrow depth range in a single well show fluctuation in strike that is comparable to the fluctuation in strike of macroscopic veins. Where veins and microfractures occur in the same samples, differences between them in strike are small. These results suggest that closed microfractures can be used to determine fracture attitudes in Travis Peak sandstone.

In sedimentary rocks deposited in passive margin basins during thermal subsidence, macroscopic veins are among the most reliable indicators of strain history (Hancock, 1985). Fracture orientations are difficult to obtain in subsurface studies of such rocks because of sparse fracture occurrence and failure of core orientation methods. In highly cemented, hard sandstones like those of the Travis Peak, the problem of obtaining oriented core is especially severe, and macrofractures may further interfere with core orientation procedures. In one Travis Peak well in this study, only one oriented macrofracture was obtained in over 425 ft (130 m) of core. Because core orientation methods are generally more successful in rock that lacks macrofractures (Nelson and others, 1987), the widespread occurrence in quartz-cemented sandstone of closed microfractures that have a preferred orientation can significantly augment analysis of subsurface fracture attitudes. In this study, analysis of closed microfractures approximately doubled the number of oriented fractures and provided information on fracture attitude in areas where no macroscopic veins were successfully oriented by conventional techniques.

In addition to providing needed data for tectonic analysis of regions with simple burial histories, information on fracture attitude has practical applications for structural analysis of many low permeability hydrocarbon reservoirs such as the Travis Peak Formation, where natural fracture orientation may significantly influence reservoir quality and reservoir stimulation engineering operations (Laubach, 1988c, 1989a). The close relationship between the occurrence of pervasive quartz cement and the formation of quartz veins and closed microfractures in the Travis Peak suggests that similar closed microfractures may be present in other sandstones where low permeability is the result of quartz cementation.

Interpretations of Fracture Origins

Most rocks near the earth's surface (depths less than 5 to 10 km) behave as brittle-elastic materials in response to natural stresses. Consequently, under the influence of extension, compression, flexure, uplift, cooling, and fluid migration, many rocks, and particularly those that have high stiffness and low tensile strength, contain networks of fractures of various types and sizes. Fractured Travis Peak sandstones typically have Young's modulus values of 9 to 10 Mpsi (for example, fig. 46) and low tensile strength, and generally are characterized by brittleness that make them susceptible to fracture development. The preferred orientation of extension fractures is normal to the regional south-southeast extension direction marked by Cretaceous and Tertiary normal faults, which suggests that tectonic strains play a role in fracture formation. Extension fractures could have formed perpendicular to the minimum confining stress, σ_3, when the combined effect of low values of σ_3 (resulting from a tectonic extension boundary condition), the low tensile strength of the rock, and high values of fluid pressure (P) were sufficient to cause fractures to propagate (Laubach, 1988a). High fluid pressures that may have facilitated fracturing are inferred from evidence for the injection of large volumes of quartz-precipitating fluids from outside of the study area. Such a process could help account for fracturing during burial in an of environment relative tectonic quiescence and for the association of fractures with evidence of fluid movement and crack-seal deformation (Laubach, 1988a, 1989c). For water temperatures of approximately 125°C (from Type A fluid inclusions in vein quartz), the $\delta^{18}O$ vein quartz composition of +21 to 22 ‰ (SMOW) is consistent with precipitation from a fluid with a $\delta^{18}O$ composition of + 2 ‰.

Applications to Reservoir Studies

Fractures in gas reservoir rocks such as the Travis Peak are potential channelways and reservoirs for hydrocarbons, and they may influence the success of production operations such as hydraulic fracture treatment (Laubach, 1989a). Preexisting fractures can dictate the direction of stimulation fracture growth and possibly also the style of fracture growth by preferentially opening during pressurization and by promoting fracture branching. An example of fracture branching localized by natural fractures is a hydraulic fracture that was created during an open-hole hydraulic stress test in a naturally fractured section of the Holditch SFE No. 2 well and subsequently recovered by overcoring (fig 54). The stress-test fracture shows multiple fracture strands arranged in a branching or anastomosing pattern. Such branching could lead to restrictions to fluid flow and, particularly if prevalent in the vicinity of the wellbore, high treatment pressures. Open natural fractures also need to be accounted for in fracture treatment design because they are possible avenues for enhanced leakoff.

Models for the formation of natural fractures in the Travis Peak were successfully used to predict fracture occurrence in Travis Peak experimental wells (Laubach and others, 1989b) and knowledge of fracture characteristics was used in design of hydraulic fracture treatment and other engineering operations in Travis Peak reservoirs in Waskom field and North Appleby field (Peterson, 1988; 1989; in press).

STRESS DIRECTIONS

Regional Stress Patterns

Recent movement on east-northeast-striking normal faults near the Mount Enterprise fault zone (Collins and others, 1980) indicates that mild regional extension is prevalent in this

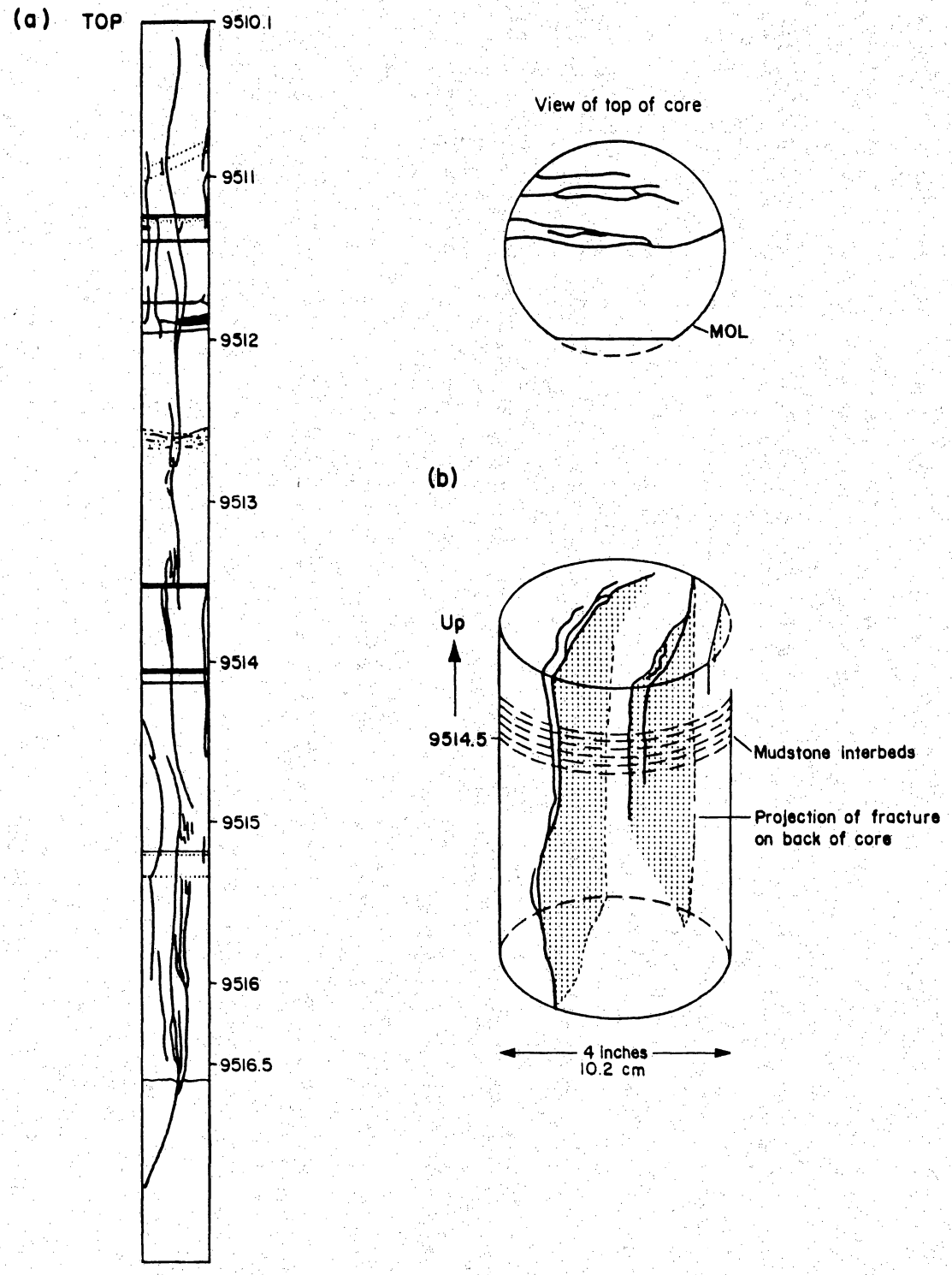

Figure 54. Sketch of a hydraulic fracture induced by open-hole stress test 2, Holditch SFE No. 2 well. (a) Overall sketch of the fractured interval showing multiple fracture strands. The fracture strands occur in very fine sandstone and occasionally in gradational to muddy sandstone, characterized by local thin beds of dark gray shale. (b) detail of part of the stress-test fracture set, showing three-dimensional relation of individual fracture planes. Inset shows a view of the top of the core in this interval. MOL indicates core reference orientation line (Laubach and others, 1989b).

part of East Texas. In the Travis Peak Formation, the greatest principal stress is vertical and reflects burial loading. Stress magnitudes were measured by hydraulic fracture methods (Whitehead and Robinson, 1989) and inferred from geophysical logging methods (Hunt, 1989). Discussion of these stress tests is beyond the scope of this paper; however, it has been suggested that lithologically controlled variations in stress magnitudes reflect the influence of Travis Peak diagenetic history (Laubach and others, 1989a). Our studies of stress directions in the Travis Peak Formation (Laubach and others, 1987; Baumgardner and Laubach, 1987; Laubach and Monson, 1988) and previous work (Gough and Bell, 1982) suggest that the modern least horizontal stress trends north-northwest, normal to regional fault strikes and the trend of the continental margin.

Stress Direction Indicators

Methods for determining horizontal stress directions that were used in this study include measurement of borehole breakout directions with caliper logs and borehole televiewer logs (Gough and Bell, 1982), anelastic strain recovery (ASR)(Teufel, 1982), differential strain curve analysis (Ren and Rogiers, 1983), and monitoring of the propagation direction of fractures created in hydraulic fracture treatments (Sorrells and Mulcahy, 1986) (figs. 55 and 56). Information from logs and core was used to measure the strike of extension fractures created in front of the drill bit during coring and strikes of fractures created during stress tests (Laubach and Monson, 1988), and these structures also provide stress-direction information.

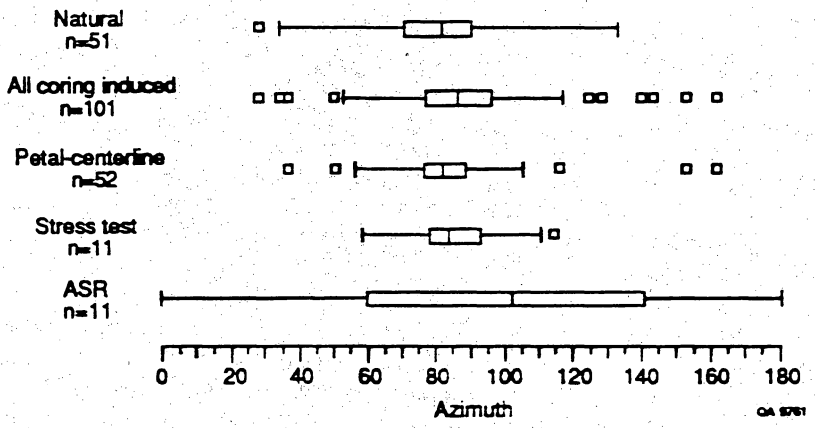

Figure 55. Box plots of stress-direction indicators in the Travis Peak Formation. The center half of the data (from the first to the third quartile) is represented by the rectangle (box) with the median indicated by a bar. The horizontal lines right and left of the box extend to values that represent 1.5 times the spread from the median to the corresponding edge of the box. Points plotted separately are outliers. Plots illustrate similarity of maximum horizontal stress directions derived from several indicators.

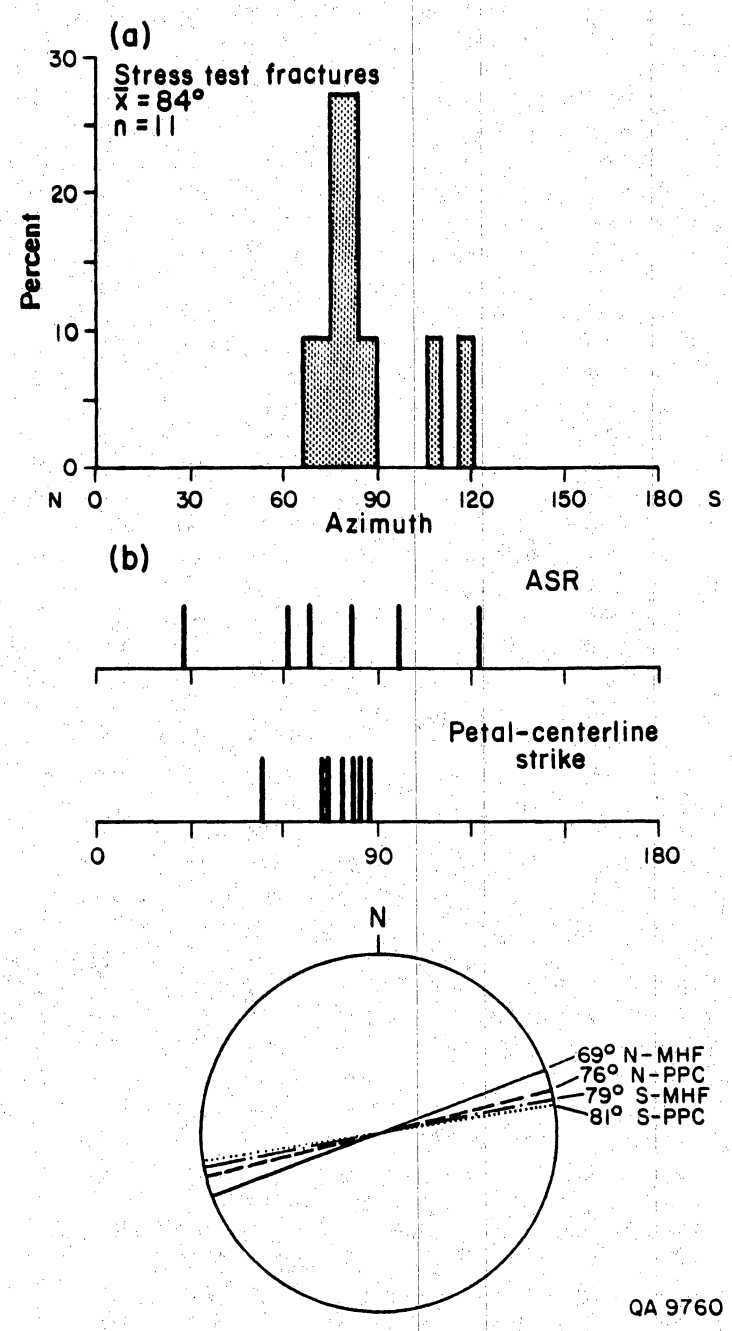

Figure 56. Stress direction indicators. (a) Histogram of fractures created in stress tests. (b) Trends of maximum horizontal strain from ASR experiments, Holditch Howell No. 5, from Owen and others (1988) and drilling-induced fractures in the same core interval (Laubach and Monson, 1988). Height of lines indicating fracture and ASR directions is arbitrary. (c) Stereographic projection of fractures created during hydraulic fracture treatment of Holditch Howell No. 5 (northern area) (N-MHF) and Holditch SFE No. 2 (southern area)(S-MHF). Strikes were determined by seismic monitoring in offset wells (G. G. Sorrells, personal communication, 1987). Average strikes of petal-centerline fractures in the northern (N-PPC) and southern (S-PPC) areas are shown for comparison.

Borehole Breakouts

Summary

Stress-induced wellbore breakouts are a type of borehole elongation that indicates the direction of horizontal principal stresses in the Travis Peak Formation (figs. 57, 58 and 59) (Baumgardner and Laubach, 1987). Previous studies (Gough and Bell, 1982; Plumb and Hickman, 1985, and others) show that breakouts develop parallel to *minimum* horizontal stress. The breakout azimuth in the Travis Peak is 344° (Laubach and others, 1987), consistent with previously identified north-northwest breakout trends in East Texas (Gough and Bell, 1982). This breakout trend indicates an average azimuth of 074° for *maximum* horizontal stress. This azimuth is similar to the mean direction indicated by various methods, including the strike of artificially induced fractures (figs. 55 and 56).

Wellbore Elongation Measurement

Previous work by Plumb and Hickman (1985) on wellbore ellipticity distinguished between elongations caused by intersection of the wellbore with natural fractures, washouts, and those caused by spalling of the wellbore in a stress field with unequal horizontal stresses (breakouts) (fig. 58). Work by Gough and Bell (1982), Plumb and Hickman (1985), and Zoback and others (1985) shows that breakouts develop parallel to the minimum horizontal principal stress. Near-vertical extension fractures that form in response to the present stress regime will be perpendicular to the minimum horizontal principal stress, and if wellbores elongate (erode) along these fractures, the largest diameter will be aligned with the maximum horizontal principal stress, at right angles to breakouts. Wellbore erosion may also occur parallel to natural

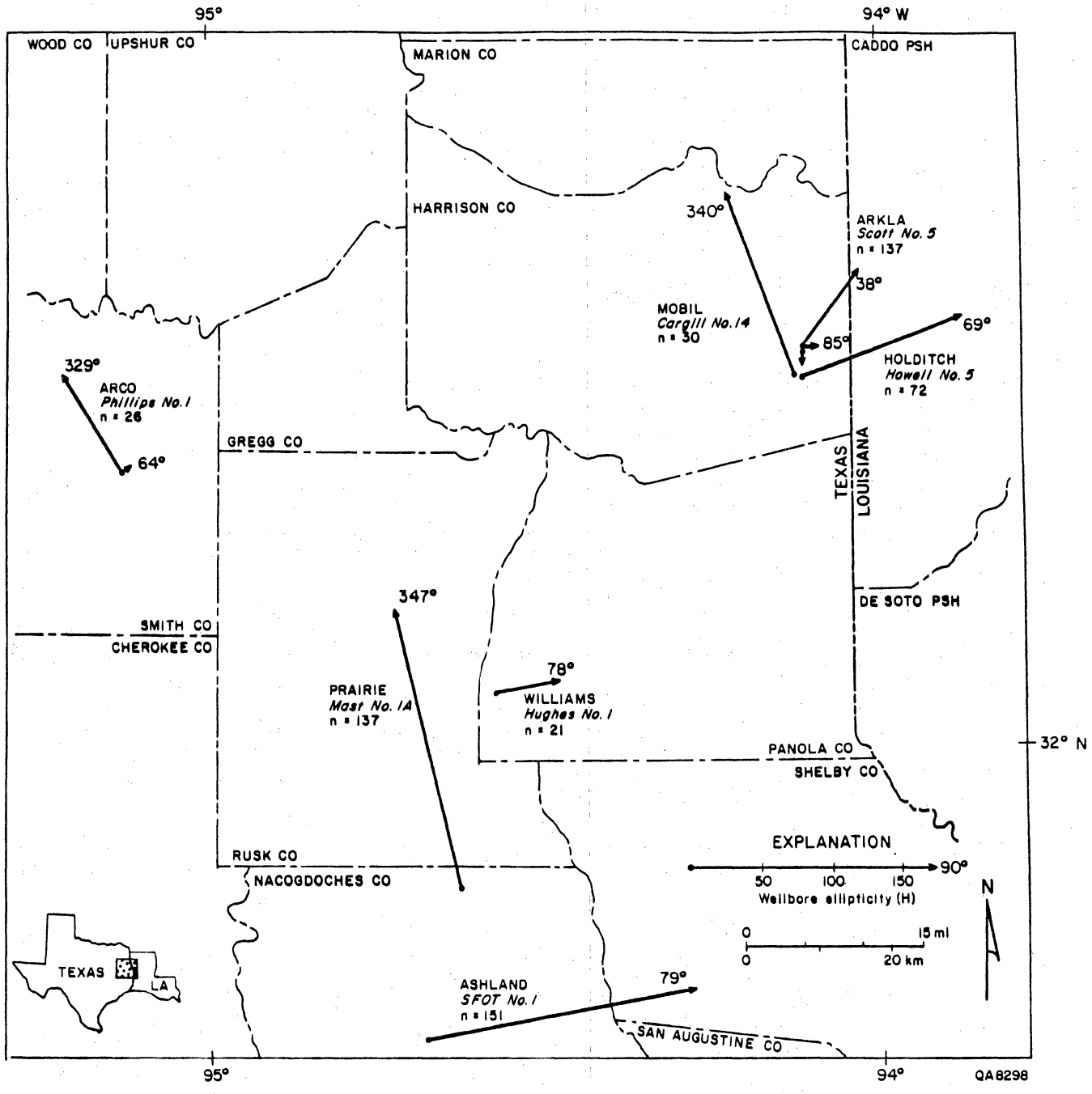

Figure 57. Map of seven wells with polar plots of H for wellbore ellipticity (Baumgardner and Meador, 1987). Distribution of wellbore ellipticity is strongly bimodal, with northwest- and northeast-trending peaks.

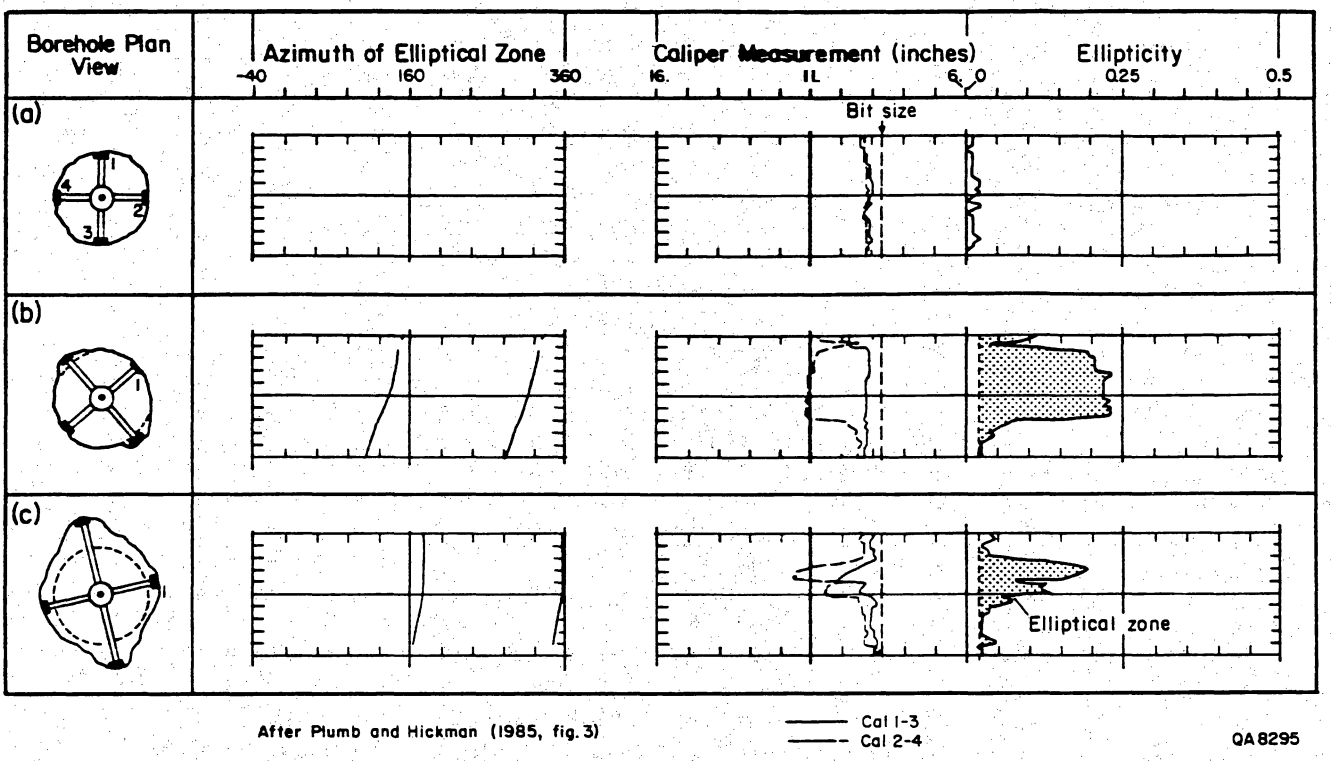

Figure 58. Plan views and sections of ellipticity logs for in-gauge borehole, borehole breakout, and washout. (a) Caliper readings for in-gauge hole are near bit size, hence no azimuth of elliptical zone is recorded. (b) Caliper 1-3 in breakout is 0.23. Caliper 2-4 marks the larger diameter. Azimuth of elliptical zone in upper 10 ft (3 m) of log section (b) is between 300 and 320 degrees. (c) Both calipers measure larger than bit size in washout. Caliper 2-4 marks the larger diameter. Maximum ellipticity is 0.19. Azimuth of elliptical zone in upper 10 ft (3 m) of log section (c) is 355 degrees. Major vertical divisions on log represent 10 ft (3 m).

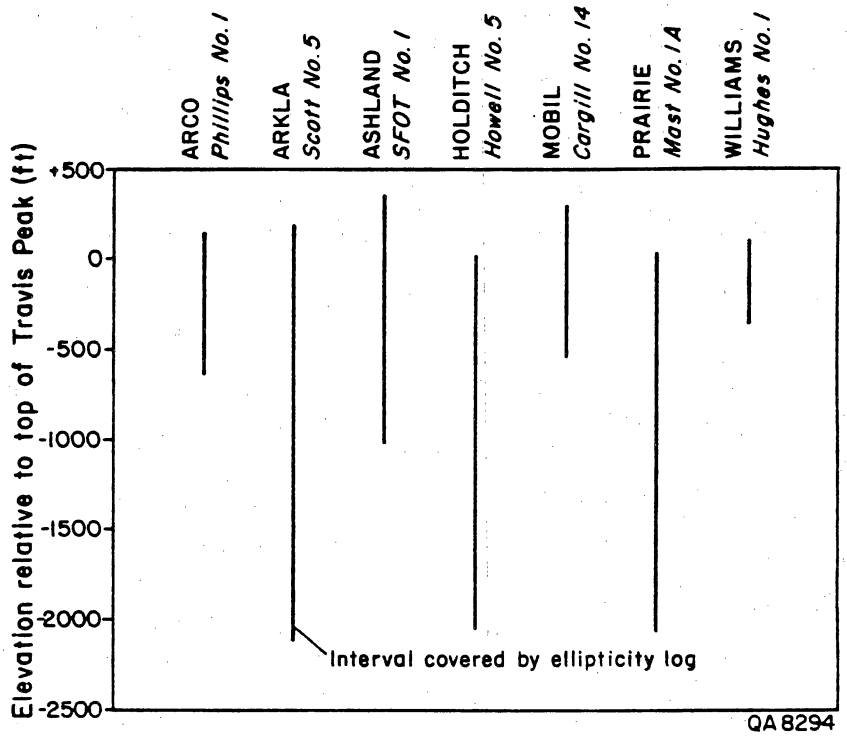

Figure 59. Plot of wells showing intervals in Travis Peak Formation covered by ellipticity logs in this study.

fractures that formed under a previous stress regime. Eroded or spalled extension fractures may have no significance for present stress orientations.

Seven wells in East Texas (figs. 57 and 59) were studied to determine the relationship of in situ stress, fracture patterns, and wellbore ellipticity. Zones of wellbore elongation were measured on ellipticity logs produced by ResTech, Inc. (fig. 58). Ellipticity is defined as follows (B. Ward, ResTech, personal communication, 1987):

ellipticity=|C1-C2|/bit size(1)

where: C1=reading from caliper 1-3 (inches)

C2=reading from caliper 2-4 (inches)

bit size=diameter of drill bit as recorded on well log (inches)

A total of 574 elliptical zones were detected (Baumgardner and Meador, 1987). Many of these elliptical zones are washouts in the classification of Plumb and Hickman (1985) because both calipers register borehole that is larger than bit size (fig. 58c). Nevertheless, these elliptical zones may be enlarged by stress-induced spalling or erosion of the wellbore along stress-related fractures.

Data from each well and from all wells combined were used to define directions of wellbore elongation. A consistent bimodal pattern of northeast- and northwest-trending ellipticity (fig. 57) indicates that the significant peaks of ellipticity for individual wells are not strongly affected by random processes. If all data from all wells are combined the resulting set contains two significant peaks that are exactly perpendicular: one at 344° and the other at 074°.

Interpretation of Wellbore Ellipticity

The significant values of wellbore ellipticity were arranged in two groups: northwest-oriented (from 329° to 347°) and northeast-oriented (from 38° to 85°)(directions are referred to

using the northern half of the compass: 270° to 0° to 090°). Most orientations of the significant vector sums of ellipticity from individual wells are subparallel either to the north-northwest-oriented minimum horizontal principal stress in the region or to east-northeast-trending fractures (Laubach, 1989a). These results suggest that subsurface stress controls wellbore ellipticity either directly through spalling of the wellbore (breakouts), or indirectly, through erosion of the borehole along vertical fractures (washouts).

Similar results have been reported for a large area surrounding the Waskom field. Gough and Bell (1982) concluded from borehole ellipticity trends that the area south of the Mexia-Talco Fault Zone has minimum principal stress that is horizontal and approximately perpendicular to the traces of normal faults. Brown and others (1980) measured the azimuths of wellbore elongations in 50 wells in the Schuler Formation at depths below about 9,200 ft (2,804 m). Mean elongation azimuth for all wells was 325°. Based on the orientations of vertical hydraulic fractures (east-west) (Strubhar and others, 1975) and recently active normal faults (northeast- southwest) in the area, Gough and Bell (1982) concluded that the northwest orientations of these elongation azimuths were approximately parallel to the least principal stress.

Northwest-trending wellbore elongations from wells in this study also show near-parallelism with (presumed) least principal stress. The parallelism between northwest-trending borehole elongations and minimum principal horizontal stress fits the model for stress-induced borehole breakouts (Gough and Bell, 1982; Plumb and Cox, 1987). It is reasonable to conclude that the northwest-oriented elliptical boreholes are a function of the regional stress regime and they indicate that hydraulic fractures would propagate perpendicular to them.

Analysis of BHTV logs shows that fractures in the borehole wall are significantly longer in the upper Travis Peak than in the lower part of the formation (Laubach, 1989a). If some wellbore elongations are caused by fractures, then they should have the same relationship with respect to depth. The ellipticity data were divided into two groups based on the previous determination of significant wellbore orientations and plotted against two measures of depth:

(1) depth below Kelly bushing (approximate ground surface), and (2) depth below top of the Travis Peak Formation. For the plot of ellipticity ratio and depth below Kelly bushing, no trend is apparent (fig. 60). However, for ellipticity data plotted relative to the top of the Travis Peak, a marked difference exists between the distribution of the northeast- and northwest-trending peaks (fig. 61).

Likewise, significant azimuths of wellbore elongation for the shallow and deep parts of the Travis Peak are quite different. For the part of the Travis Peak Formation that all wells penetrate (upper 370 ft [112 m]) the significant elongation azimuth is 077°. Conversely, for the lowest 580 ft (176 m) of the Travis Peak penetrated by three wells (Arkla Scott No. 5, Holditch Howell No. 5, and Prairie Mast No. 1A), the significant azimuth of elongations is 346°. These two azimuths are perpendicular (within the accuracy of these measurements).

Clearly, there is a marked difference in ellipticity orientation with respect to depth below the top of the Travis Peak, but not with respect to depth below present ground surface. The orientation of natural and drilling-induced fractures parallels the trend of borehole ellipticity in the upper Travis Peak; thus, it is possible that either pre-existing natural fractures, or drilling-induced fractures are controlling ellipticity in this part of the formation. In deeper parts of the formation, northwest-trending ellipticity probably is caused by spalling of the borehole (breakouts) in the regional stress regime. This hypothesis is consistent with observations of fracture length in the Holditch Howell No. 5 well. Fractures in the upper 460 ft (140 m) of Travis Peak are significantly longer than in the interval between 1,394 and 1,786 ft (425 and 544 m) below top of the formation.

To distinguish between the possible effects of depth and lithology on wellbore ellipticity, the orientation of elliptical zones was compared to lithology logs. Elliptical boreholes develop more often in shale than in sandstone. Almost half of all elliptical zones occur in shale, although shale comprises only 19 percent of the logged lengths of the boreholes. The orientation of elliptical zones is not affected by lithology.

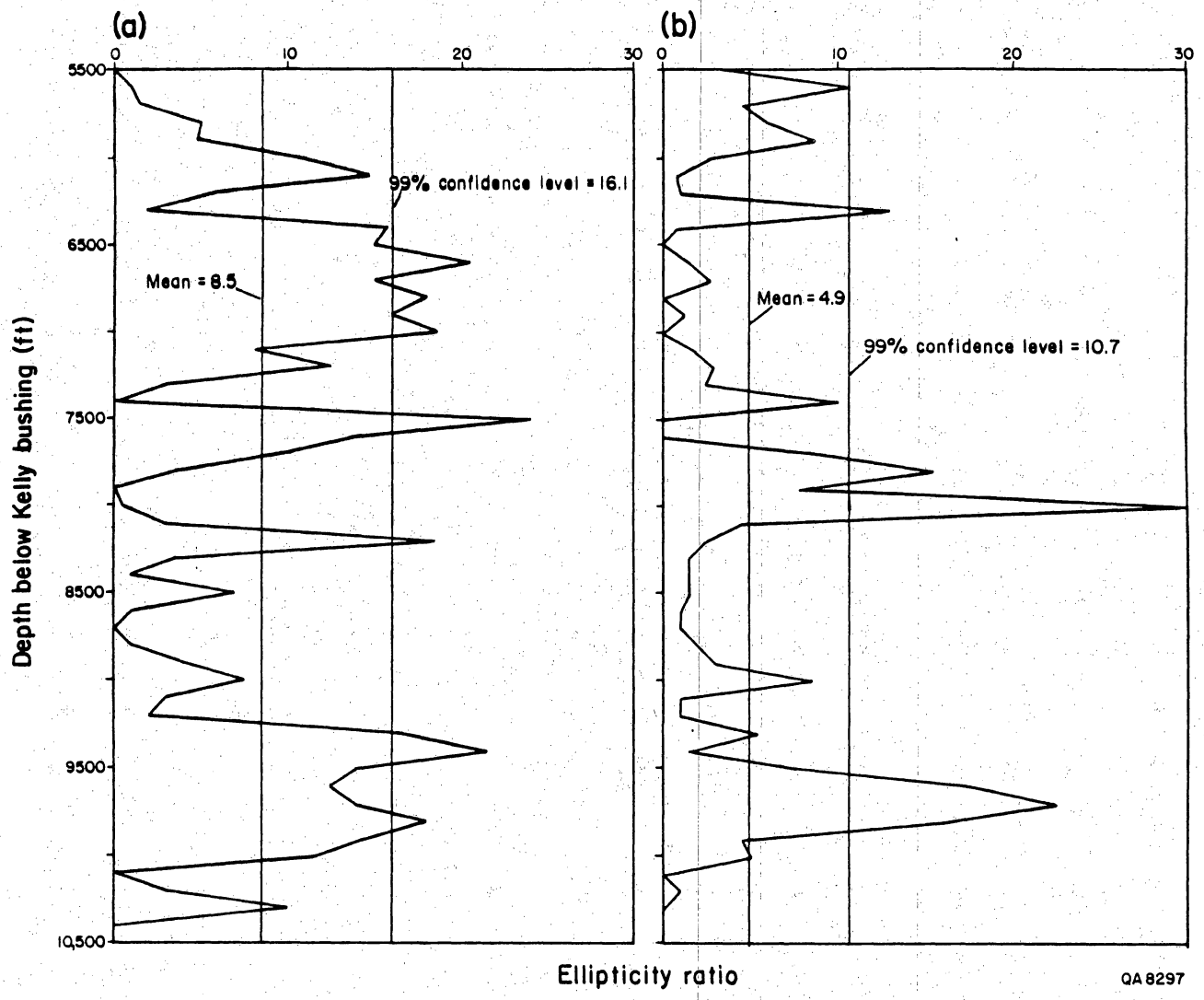

Figure 60. Plots of ellipticity ratio vs. depth below Kelly bushing (approximate ground surface). (a) Northeast peaks. (b) Northwest peaks. No clear distinction exists between the northeast and northwest peaks relative to depth below Kelly bushing.

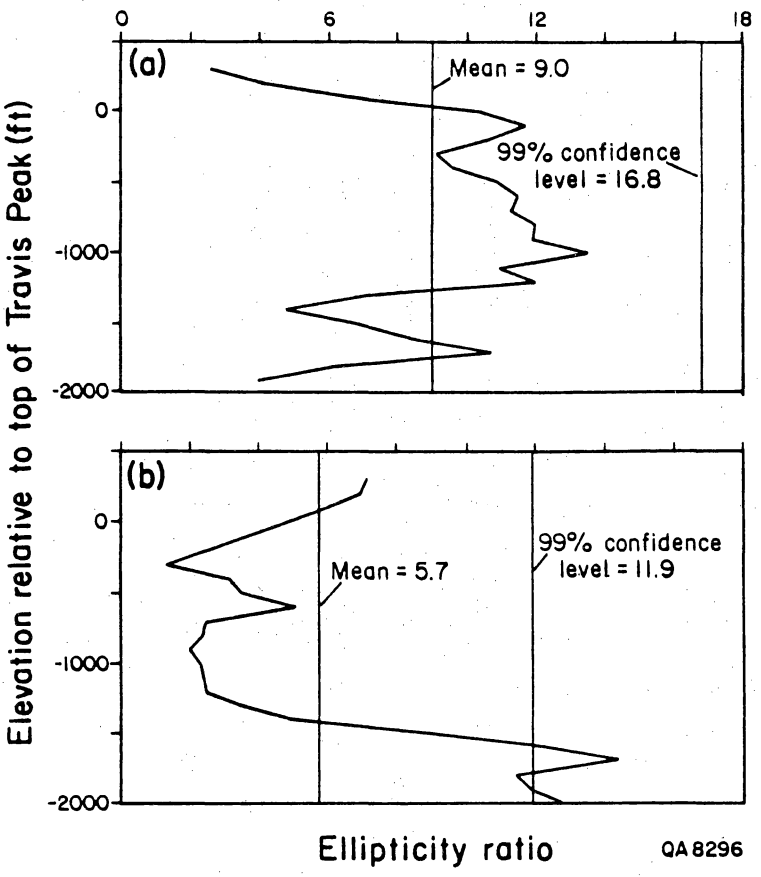

Figure 61. Plots of ellipticity ratio vs. elevation relative to top of the Travis Peak Formation. (a) Northeast peaks. (b) Northwest peaks. Ellipticities can be divided into two classes based on stratigraphic depth. Northeast peaks are concentrated above –1,300 ft (396 m). Northwest peaks are principally below –1,500 ft (457 m).

Ellipticity measurements were obtained within 10 ft (3 m) of nine of the ASR measurements reported in the study of Owen and others (1987). The range of orientations of elliptical zones (040° to 080°) is within the range covered by strain measurement orientations. Mean values for the overlapping zones are 093° for the strain measurements and 059° for the elliptical zones. These are not compellingly similar.

Owen and his coworkers (1987) identified four of their measurements as "most reliable data". The mean orientation value for three of these with corresponding ellipticity measurements is 069° (fig. 55). The mean direction of the three corresponding ellipticity measurements is 053°. That they are subparallel suggests that this ellipticity direction is indirectly related to the in situ stress, possibly by erosion along northeast-trending fractures. The mean direction of all four "most reliable" strain measurements is 077°. The significant azimuth of wellbore elongations in the upper 370 ft (112 m) of the Travis Peak (which covers most of the interval where strain measurements were made in the Holditch Howell No. 5 well) for all seven wells is 077°. Borehole televiewer observations show that this parallelism between strain recovery directions in one well and ellipticity measurements from a wide area is most likely the result of wellbore erosion along preexisting fractures at shallow depths in the formation.

Two directions of borehole elongation were observed with the BHTV log, and the marked contrast in the pattern of ellipticity suggests that the two directions have different causes. One type of elongation has the same orientation as fractures and is commonly associated with or localized along fracture traces. These elliptical zones appear to be caused by erosion of the borehole along preexisting fractures. The second type of elongation was observed at 030° to 090° to fractures and in unfractured zones. The plan view shapes of these elliptical zones suggests that they are true breakouts related to the regional stress field.

The similarities between orientations of peaks of wellbore ellipticity (344° and 074°) and (1) drilling-induced fractures (060° to 090°), (2) maximum strain recovery (most reliable data = 077°), and (3) minimum horizontal principal stress from hydraulic fracturing data (north-

northwest) (Gough and Bell, 1982) are quite strong. The significant azimuth for the 35 elongations that fit Plumb and Hickman's (1985) criteria for breakouts is 338°. This orientation is subparallel (as expected, based on Plumb and Hickman's [1985] work) to the north-northwest-oriented minimum horizontal principal stress in the northern Gulf coast region (Zoback and Zoback, 1980; Gough and Bell, 1982). These results suggest that the northwest-oriented wellbore elongations fit the criteria established by Plumb and Cox (1987) for stress-related ellipticity.

Strain Measurements on Core

Two techniques for determining stress directions from core are Anelastic Strain Recovery (ASR) and Differential Strain Curve Analysis (DSCA). ASR uses differential expansion (recovery) of core after its retrieval from the subsurface to infer directions of in situ stresses. The direction of maximum horizontal core recovery is interpreted to be the direction of maximum horizontal stress. This technique is most successful in homogeneous, unfractured rock (Teufel, 1982). The ASR results were obtained from 18 sandstone samples from Holditch Howell No. 5 (Owen and others, 1987) and from 3 samples from Prairie Producing Mast No. A-1 (Science Applications, 1985). DSCA is based on anisotropic contraction of core when hydrostatically loaded in the laboratory. Direction of maximum core contraction is inferred to be the direction of maximum horizontal stress (Ren and Rogiers, 1983). DSCA results were obtained from one mudstone sample in Holditch Howell No. 5 (Science Applications, 1985).

The maximum horizontal strain orientations calculated for samples from Holditch Howell No. 5 have a bimodal distribution. Anomalous strain recovery behavior of one group of five samples indicates that they contain lithologic heterogeneity or other influences that cause unreliable results. This group has an average azimuth of 117°. The six samples that had the best strain recovery response have an average maximum horizontal strain recovery azimuth of 077° (fig. 55). The DSCA result from Holditch Howell No. 5 also indicates an east-northeast azimuth

of maximum horizontal stress (90°±20°), although a single determination is not a reliable test of the method. ASR results from Prairie Producing Mast No. A-1 also suggest an east or northeast azimuth for maximum horizontal stress, and mean maximum horizontal stress for all ASR results from the two wells is 089°. The ASR results with the highest quality data from six samples in Holditch Howell No. 5 are not significantly different from the strike direction defined by drilling-induced fractures in the same core and the mean strike for the well (076°).

Massive Hydraulic Fracture Treatments

The strike of fractures created during hydraulic fracture treatment of three study wells, Holditch Howell No. 5, Holditch SFE No. 2, and Mobil Cargill No. 15, was measured by detection of associated microseismic activity during fracture treatment (Sorrells and Mulcahy, 1986; G. G. Sorrells, personal communication, 1987, 1989). This technique is considered to be one of the most reliable for detecting stimulation fracture orientation (Lacy, 1987; Sorrells and Mulcahy, 1986). The strike of the fracture created in Holditch Howell No. 5 is 069° and the strike of the fracture created in Holditch SFE No. 2 is 079° (fig. 56). These attitudes are close to the mean attitude of other stress-direction indicators in the two areas. However, despite the fact that the actual growth direction of the stimulation fracture is being monitored by this method, because the orientation of the fracture created in the massive hydraulic fracture treatment could be following the east-northeast strike of natural fractures rather than stress directions, this method may not provide a reliable *stress direction* estimate (Laubach, 1989a).

Fractures Created in Stress Tests

Fractures resulting from open-hole hydraulic fracture stress tests generally parallel the direction of maximum horizontal stress (Daneshy and others, 1986). Stress-test fractures were created under controlled conditions described by Whitehead and Robinson (1989) and later

were identified in core and on BHTV images (CER Corporation, 1987; Laubach and others, 1989b). The mean strike of 11 fractures created in stress tests in Holditch Howell No. 5 and Holditch SFE No. 2 wells is 084°, similar to other stress-direction indicators. Fractures created in stress tests are composed of single fracture planes or multiple anastomosing fracture strands (Laubach and others, 1989b). Where multiple strands occur, they are arranged in subparallel, en echelon sets (fig. 54).

Drilling-Induced Fractures

Extension fractures with distinctive geometry and surface structures are created during coring operations in many rocks (Pendexter and Rohn, 1954), and they are common in the Travis Peak Formation (Laubach, 1989a). These drilling-induced fractures should parallel maximum horizontal stress unless near-wellbore stress perturbations or mechanical anisotropy in the rock have a significant effect on fracture strike (Kulander and others, 1978; Lorenz and Finley, 1988). In the Travis Peak, they provide an accurate indication of stress direction (Laubach and Monson, 1988).

Drilling-induced fractures were distinguished from natural fractures based on criteria described by Kulander and others (1979). These criteria include (1) location of fracture origins near or within core, (2) characteristic fracture shapes, and (3) absence of mineralization. Fracture surface structures (plume structure and arrest lines) were used to identify fracture origins (Kulander and others, 1979). Our study focused on 101 oriented drilling-induced fractures from seven Travis Peak wells (figs. 55 and 56).

Drilling-induced petal and petal-centerline fractures have a distinctive geometry in core. They characteristically curve into the core in the downhole direction. Petal fractures are short, inclined fractures that are concave downward with dips measured at the edge of the core that range from 50° to subvertical. Petal-centerline fractures are single fractures that are composed of a short, smoothly curving concave downward petal segment that gradually merges in the

down-core direction with a planar centerline fracture segment that may bisect the core. The upper terminations of petal and petal-centerline fractures occur outside of the core, but the lower terminations generally occur within core, either at interbeds or in homogeneous rock. Commonly, core is not completely separated along petal-centerline fractures because fracture planes are composed of multiple strands rather than single fracture planes.

Several observations in Travis Peak core indicate that petal and petal-centerline fractures propagate in front of the core bit. The edges of petal-centerline fractures are commonly scored by the bit or are crosscut by grooves created by scribe knives located inside the core barrel assembly. Drilling-induced fractures in core can be correlated with fractures visible on BHTV logs. Lorenz and Finley (1987) interpreted such fractures to follow stress trajectories in front of the bit with strikes that reflect regional stress anisotropy.

Petal and petal-centerline fractures strike predominantly east-northeast throughout the study area in East Texas. The vector mean strike of 101 petal and petal-centerline fractures is 085°, with a range from 029° to 143°. Petal-centerline fractures have a mean strike of 081° and are strongly grouped between 070° and 090°. Within intact core, petal and petal-centerline fractures are parallel and have a strong preferred orientation. For example, 10 petal and petal-centerline fractures in 1 unoriented core from Holditch SFE No. 2 are precisely parallel.

Drilling-induced fractures from the northern and southern parts of the study area have similar strike. Mean strike of 14 petal and petal-centerline fractures in Holditch Howell No. 5, Mobil Cargill No. 14, and Clayton Williams Sam Hughes No. 1 wells (northern area) is 085°, which is identical to the mean strike of 73 petal and petal-centerline fractures in Prairie Producing Mast No. A-1 and Holditch SFE No. 2 (southern area). There are slight differences in the mean strike of petal-centerline fractures between the northern and southern areas, however. Petal-centerline strike is 076°±12° for the northern area and 081°±4° for the southern area.

Petal and petal-centerline strike fluctuates within individual wells. For example, the strike of eight petal-centerline fractures ranges between 055° and 090° in Clayton Williams Sam

Hughes No. 1 core, with a mean strike of 082°. Core results suggest that fluctuation in fracture strike within a well could be as much as 20°. A range of fracture strikes is also evident on BHTV and FMS logs (Laubach and others, 1988) where fracture orientations are known to within approximately 3°. BHTV results also indicate that fracture strike varies with depth. All of the fluctuation in strike cannot be accounted for by imprecise core orientation, since a range of fracture strikes is evident in some continuous sections of core and on BHTV logs.

Application to Reservoir Development

Knowledge of the strike of fractures created during hydraulic fracture treatment is important for fracture treatment design and reservoir development. Stimulation-fracture strike can be measured directly by a variety of techniques (Lacy, 1987), or fracture strike can be predicted from knowledge of maximum horizontal stress direction, which stimulation fractures tend to parallel. Efficient hydraulic fracture treatment of low-permeability reservoirs depends on reliable prediction of the stimulation fracture strike, which generally is parallel to the maximum horizontal stress.

The east-northeast trend of maximum horizontal stress inferred from the strike of borehole breakouts and drilling-induced fractures is similar to stress directions from core relaxation techniques (ASR) and hydraulic fractures created in stress tests and massive hydraulic fracture treatments, and is consistent with the east-northeast strike of recently active normal faults and open natural fractures in East Texas. These observations suggest that borehole breakouts and drilling-induced fractures are useful stress-direction indicators in this area.

CONCLUSIONS

The main goal of the geologic studies of the Tight Gas Sands program in East Texas was to document the geologic framework of the Travis Peak Formation. Insights gained from this multifaceted study increased the understanding of the geologic controls on the distribution and behavior of the Travis Peak tight gas reservoir. Within the Tight Gas Sands program, the geologic information supported the testing and application of new technologies for resource exploitation. Direct benefits of this research to gas producers are the collection and assimilation of information that could lead to improved gas recovery and lowered completion costs through better field-development and well-completion programs in the Travis Peak Formation and similar tight gas sandstones (Holditch and others, 1987).

In addition to reaching specific conclusions about the Travis Peak, this study also provides a methodology for future geologic studies of other low-permeability, gas-bearing sandstones. Stratigraphic, petrographic, and structural studies formed the three main areas of geologic investigation that were needed to characterize this tight gas sandstone. Major conclusions of the geologic studies of the Travis Peak are as follows:

Recent mapping and core description studies indicate that Travis Peak depositional systems in this region of the East Texas Basin include: (1) a braided- to meandering-fluvial system that forms the majority of the Travis Peak section; (2) deltaic deposits that are interbedded with and encase the distal portion of the fluvial section; (3) paralic deposits that overlie and interfinger with the deltaic and fluvial deposits near the top of the Travis Peak; and (4) shelf deposits that are present at the downdip extent of the Travis Peak. Shelf sediments interfinger with and onlap deltaic and paralic deposits, and the stratigraphy of the upper interbedded sandstone-mudstone interval implies retrogradational (onlapping) depositional conditions.

Stratigraphic correlation of channelbelt sandstones and interbedded mudstones provides a basis for identifying Travis Peak reservoirs and estimating their extent and geometry. Geometry and reservoir quality vary with respect to the original depositional processes that controlled sediment lithology, texture, and bedding, in addition to the degree of diagenesis. Sandstones at the top of the formation that were deposited in paralic and meandering-fluvial environments are thin and separated by mudstones. In most of the middle and lower portions of the Travis Peak, sandstones are dominantly braided-fluvial. In these sandstones, reservoir seals and internal barriers to fluid flow consist of burrowed, rooted, and diagenetically altered mudstones that originated in well-drained swamps and lakes adjacent to the channels, clay-clast conglomerates that line scoured channel bases, clay drapes, and abandoned-channel deposits. Best-quality reservoir sandstone exists in wide bands oriented parallel to depositional dip. Sandstone quality decreases at channel margins (levees), channel tops (abandoned channel deposits), and in interchannel areas where sediments are poorly sorted (siltstones and mudstones).

Petrographic studies indicate that the Travis Peak Formation contains mainly fine- to very fine grained sandstone, muddy sandstone, silty sandstone, and sandy mudstone. True claystones that could provide stress barriers to contain hydraulic fracture growth are rare. The sandstones are mineralogically mature, consisting of quartzarenites and subarkoses. Well-sorted sandstones had high porosity and permeability at the time of deposition, but their reservoir quality has been reduced by compaction and cementation. Cementation by quartz, dolomite, ankerite, illite, and chlorite and introduction of reservoir bitumen by deasphalting have reduced porosity to less than 8 percent and permeability to less than 0.1 md throughout most of the formation. Petrographic and SEM analyses supplied data on the mineral composition of reservoir and non-reservoir rocks that were used to calibrate well logs and identify zones of possible sensitivity to completion fluids.

Diagenetic studies indicate that structurally deeper Travis Peak sandstones are more intensely quartz cemented than are shallower sandstones. This variability in cementation

results in differences in mechanical properties, porosity, and permeability between upper and lower parts of the Travis Peak. Furthermore, differences in diagenetic history between fluvial and paralic sandstones have resulted in fluvial sandstones having an order of magnitude higher permeability than paralic sandstones at all depths. Because of the correspondence between extensive quartz cementation and fracture occurrence, abundant, open natural fractures should be expected in highly cemented sandstones. Natural fractures may contribute to production in lower Travis Peak sandstones that have very low matrix permeability.

One producing sandstone in the Travis Peak can cover several thousand acres, but maximum drainage areas are generally less than 80 acres (Holditch and others, 1988a). Hydraulic fracture half-lengths range from 100 to 200 ft (30 to 60 m) (Holditch and others, 1988b), well below the lateral dimensions of the sandstones. Due primarily to uniform stresses and a lack of vertical barriers to fracture growths, circular, east-west oriented fractures will form (Holditch, personal communication, 1988) that will vertically connect as many as six to eight stacked sandstones (CER Corporation and S. A. Holditch & Associates, 1988; Holditch and others, 1986; Holditch and others, 1988b). Predicting the propagation direction of hydraulically induced fractures is a key part of completion strategy, and geologic studies of core showed that borehole breakouts and drilling-induced fractures in core can be used as inexpensive and reliable methods of predicting horizontal stress directions and the direction of hydraulic fracture propagation. Hydraulic fractures propagate in directions subparallel to the east-northeast strike of the natural fracture; thus, hydraulically induced fractures may not intersect many natural fractures.

Among the effects that natural fractures can have on well treatments are increased leakoff, fracture branching, and curvature. Branching could cause high treatment pressures and detrimentally affect treatment results if not accounted for in treatment design. Geologic models indicate that natural fractures are not likely to be common in the upper Travis Peak sandstones and that special precautions for treating naturally fractured rock are not required in the upper zone, but in the lower Travis Peak, natural fractures are common and locally are extensively

developed. Such fractures may have caused high treatment pressures during hydraulic fracture treatment of the Holditch SFE No. 2 well by promoting the growth of multiple, branching fractures in the vicinity of the wellbore.

ACKNOWLEDGMENTS

This work was prepared for, and funded by, the Gas Research Institute under contract no. 5082-211-0708, Shirley P. Dutton, Principal Investigator.

The cooperation of the following companies and operators is gratefully acknowledged: Amoco Production Company (USA), ARCO Oil and Gas Company, Arkla Exploration Company, Ashland Exploration, Inc., Brasfield Oil and Gas Company, Delta Drilling Company, Henderson Clay Products, Inc., Marshall Exploration, Inc., Mobil Exploration & Producing U.S. Inc., Prairie Producing Company, Reynolds Drilling Company, Inc., Stallworth Oil and Gas, Inc., Sun Oil Company, and Clayton W. Williams, Jr.

The ideas and results presented here have evolved and benefited greatly from our interaction with other Tight Gas Sands Project contractors at CER Corporation, S. A. Holditch & Associates, Inc., ResTech, Inc., and Resources Engineering Systems, Inc. Research conclusions of numerous Bureau of Economic Geology scientists, particularly work by Robert J. Finley, Michael A. Fracasso, Karen L. Herrington, and Alva E. Saucier, were incorporated into this report. Karen L. Herrington performed SEM analysis and developed the freeze-drying technique used at the Bureau to preserve illite structure. Research assistants Sabine C. Boardman, Timothy N. Diggs, Bruce C. Gates, Peter H. Hennings, Thomas E. Hoak, Karen J. Meador, James K. Miller, Richard E. Paige, Alice W. Spencer, and John C. Wilson contributed to data gathering and synthesis. Core processing and handling was coordinated by Robert Sanchez, under the supervision of Allen Standen, Curator of the Bureau of Economic Geology Core Research Center. Core analyses were performed by Core Labs, NL ERCO, and Petrophysical Services, Inc. Eric R. Monson collaborated on fracture studies. Geochemical analyses were performed by DGSI, Inc.,

and Robertson Research, Inc. Lynton S. Land, Department of Geological Sciences, The University of Texas at Austin, ran the isotopic analyses.

Walter B. Ayers, Jr. reviewed the manuscript and made many valuable suggestions for improvement. Illustrations were prepared under the direction of Richard L. Dillon. Maris Strautmanis coordinated its production.

REFERENCES

Baumgardner, R. W., Jr., and Laubach, S. E., 1987, Wellbore ellipticity in East Texas: in situ stress or fracture-related spalling? (abs.): Eos, v. 68, no. 44, p. 1460.

Baumgardner, R. W., Jr., and Meador, K. J., 1987, Analysis of fracturing and wellbore elongation based on borehole televiewer, Formation Microscanner, and ellipticity logs: *in* Laubach, S. E., Baumgardner, R. W., Jr., and Meador, K. J., Analysis of natural fractures and borehole ellipticity, Travis Peak Formation, East Texas: The University of Texas at Austin, Bureau of Economic Geology topical report prepared for the Gas Research Institute under contract no. 5082-211-0708, p. 79–111.

Beard, D. C., and Weyl, P. K., 1973, Influence of texture on porosity and permeability of unconsolidated sand: Am. Assoc. Petroleum Geologists Bull., v. 57, p. 349–369.

Bebout, D. G., Budd, D. A., and Schatzinger, R. A., 1981, Depositional and diagenetic history of the Sligo and Hosston Formations (Lower Cretaceous) in South Texas: The University of Texas at Austin, Bureau of Economic Geology Report of Investigations No. 109, 70 p.

Bourke, L., Delfiner, P., Trouller, J. -C., Fett, T., Grace, M., Luthi, S., Serra, O., and Standen, E., 1989, Using Formation Microscanner* images: The Technical Review, v. 37, no. 1, p. 16–40.

Brown, R. O., Forgotson, J. M., and Forgotson, J. M., Jr., 1980, Predicting the orientation of hydraulically created fracture in the Cotton Valley Formation of east Texas: SPE Paper 9269, 55th Annual Fall Conference, p. 1–12.

Buffler, R. T., Watkins, J. S., Shaub, F. J., and Worzel, J. L., 1980, Structure and early geologic history of the deep central Gulf of Mexico, *in* Proceedings, Symposium on the origin of the Gulf of Mexico and the early opening of the central North Atlantic Ocean: Baton Rouge, Louisiana State University, School of Geoscience, p. 3–16.

Bushaw, D. J., 1968, Environmental synthesis of the East Texas Lower Cretaceous: Trans. Gulf Coast Assoc. of Geol. Soc., v. 18, p. 416–438.

CER Corporation, 1987, Observations and orientations of fractures induced through open-hole stress tests: contract report prepared for The Gas Research Institute, 16 p.

CER Corporation and S. A. Holditch & Associates (eds.), 1988, Advancements in Travis Peak Formation evaluation and hydraulic fracture technology, Staged Field Experiment No. 1, GRI Report 88-0077, 223 p.

Collins, E. W., Hobday, D. K., and Kreitler, C. W., 1980, Quaternary faulting in East Texas: The University of Texas at Austin, Bureau of Economic Geology Geological Circular 80-1, 20 p.

Cullom, M., Granata, W., Gayer, S., Heffner, R., Pike, S., Hermann, L., Meyertons, C., and Sigler, C., 1962, The basin frontiers and limits for exploration in the Cretaceous system of central Louisiana: Gulf Coast Association of Geological Societies Transactions, v. 12, p. 97–116.

Daneshy, A. A., Slusher, G. L., Chisholm, P. T., and Magee, D. A., 1986, In situ stress measurements during drilling: Journal of Petroleum Technology, v. 38, p. 891–898.

David K. Davies and Associates, Inc., 1985a, Fluid sensitivity evaluation, three Travis Peak sand zones, Ashland S.F.O.T. No. 1 well, Nacogdoches County, Texas: Kingwood, Texas, report prepared for Petrophysical Services, Inc., 52 p.

David K. Davies and Associates, Inc., 1985b, Fluid sensitivity evaluation, three Travis Peak sand zones, Prairie Producing Mast No. A-1 well, Nacogdoches County, Texas: Kingwood, Texas, report prepared for Petrophysical Services, Inc., 64 p.

Dutton, S. P., 1986, Diagenesis and burial history of the Lower Cretaceous Travis Peak Formation, East Texas: The University of Texas at Austin, Ph.D. dissertation, 165 p.

Dutton, S. P., 1987, Diagenesis and burial history of the Lower Cretaceous Travis Peak Formation, East Texas: The University of Texas at Austin, Bureau of Economic Geology Report of Investigations No. 164, 58 p.

Dutton, S. P., and Diggs, T. N., in press, History of quartz cementation in the Lower Cretaceous Travis Peak Formation, East Texas: Journal of Sedimentary Petrology.

Dutton, S. P., and Finley, R. J., 1988, Controls on reservoir quality in tight sandstones of the Travis Peak Formation, East Texas: SPE Formation Evaluation, v. 3, no. 1, p. 97–104.

Dutton, S. P., Finley, R. J., and Herrington, K. L., 1987, Organic geochemistry of the Lower Cretaceous Travis Peak Formation in East Texas: Gulf Coast Association of Geological Societies Transactions, p. 65–74.

Dutton, S. P., Fracasso, M. A., Laubach, S. E., Baumgardner, R. W., Jr., and Finley, R. J., 1988, Geologic analysis of the Travis Peak Formation, *in* CER Corporation and S. A. Holditch &

Associates (eds.): Advancements in Travis Peak Formation evaluation and hydraulic fracture technology, Staged Field Experiment No. 1, GRI Report 88-0077, p. 35–62.

Dutton, S. P., and Land, L. S., 1988, Cementation and burial history of a low-permeability quartzarenite, Lower Cretaceous Travis Peak Formation, East Texas: Geol. Soc. America Bull., v. 100, p. 1271–1282.

Dutton, S. P., Laubach, S. E., Tye, R. S., Herrington, K. L., and Diggs, T. N., in press, Geological analysis of the Travis Peak Formation and Cotton Valley Sandstone: *in* Peterson, R. E., ed., SFE No. 3 Comprehensive Well Report: CER Corporation and S. A. Holditch and Associates, Inc., prepared for Gas Research Institute.

Finley, R. J., 1984, Geology and engineering characteristics of selected low-permeability gas sandstones: A national survey: The University of Texas at Austin, Bureau of Economic Geology Report of Investigations No. 138, 220 p.

Finley, R. J., Dutton, S. P., Lin, Z. S., and Saucier, A. E., 1985, The Travis Peak (Hosston) Formation: geologic framework, core studies, and engineering field analysis: The University of Texas at Austin, Bureau of Economic Geology, contract report prepared for the Gas Research Institute under contract no. 5082-211-0708, 233 p.

Folk, R. L., 1974, Petrology of sedimentary rocks: Austin, Texas, Hemphill, 182 p.

Fracasso, M. A., Dutton, S. P., and Finley, R. J., 1988, Depositional systems and diagenesis of Travis Peak tight gas sandstone reservoirs, Sabine Uplift Area, Texas: SPE Formation Evaluation, v. 3, no. 1, p. 105–115.

Freeman, T. H., 1982, Bedform distributions, bedform dynamics, and preserved bedding types on a mesotidal sand ridge, Port Royal Sound, South Carolina: University of South Carolina, Master's thesis, 35 p.

Gallagher, J. J., Friedman, M., Handin, J., and Sowers, G. M., 1974, Experimental studies relating to microfracture in sandstone: Tectonophysics, v. 21, p. 203–247.

Galloway, W. E., Ewing, T. E., Garrett, C. M., Tyler, Noel, and Bebout, D. G., 1984, Atlas of major Texas oil reservoirs: The University of Texas at Austin, Bureau of Economic Geology Special Publication, 139 p.

Gough, D. I. and Bell, J. S., 1982, Stress orientations from borehole wall fractures with examples from Colorado, east Texas and northern Canada: Canadian Journal of Earth Sciences, v. 19, no. 7, p. 1358–1370.

Granata, W. H., Jr., 1963, Cretaceous stratigraphy and structural development of the Sabine Uplift area, Texas and Louisiana, *in* Herrmann, L. A., ed., Report on selected North Louisiana and South Arkansas oil and gas fields and regional geology: Shreveport Geological Society Reference Volume V, p. 50–95.

Greer, S. A., 1975, Estuaries of the Georgia coast, U.S.A.: sedimentology and biology. III. Sandbody geometry and sedimentary facies at the estuary-marine transition zone, Ossabaw Sound, Georgia: a stratigraphic model: Senckenbergiana Maritima, v. 7, p. 105–135.

Halbouty, M. T., and Halbouty, J. J., 1982, Relationships between East Texas Field region and Sabine Uplift in Texas: Am. Assoc. Petroleum Geologists Bull., v. 66, p. 1042–1054.

Hall, W. D., 1976, Hydrogeologic significance of depositional systems and facies in Lower Cretaceous sandstones, North-Central Texas: The University of Texas at Austin, Bureau of Economic Geology Geological Circular 76-1, 29 p.

Hancock, P. L., 1985, Brittle microtectonics: principles and practice. Journal of Structural Geology, v. 7, no. 3/4, p. 437–458.

Heald, M. T., 1956, Cementation of Simpson and St. Peter sandstones in parts of Oklahoma, Arkansas, and Missouri: Journal of Geology, v. 64, p. 16–30.

Holditch, S. A., Robinson, B. M., and Whitehead, W. S., 1986, Cooperative well report, Prairie Producing Company A. T. Mast 'A' No. 1, Nacogdoches County, Texas: S. A. Holditch & Associates, Inc., topical report prepared for the Gas Research Institute under contract no. 5083-211-0877, 76 p.

Holditch, S. A., Robinson, B. M., Whitehead, W. S., and Ely, J. W., 1987, The GRI Staged Field Experiment: Denver, Colorado, 1987 Society of Petroleum Engineers/Department of Energy Joint Symposium on Low Permeability Reservoirs, Proceedings, SPE/DOE Paper No. 16429, p. 409–427.

Holditch, S. A., Robinson, B. M., Whitehead, W. S., and Sullivan, R. B., 1988a, A comprehensive review of selected wells surrounding Staged Field Experiment No. 2, North Appleby field, Nacogdoches County, Texas: S. A. Holditch & Associates, Inc., topical report prepared for the Gas Research Institute under contract no. 5083-211-0877, 76 p.

Holditch, S. A., Robinson, B. M., and Whitehead, W. S.., 1988b, Post-fracture production and pressure transient analysis of SFE No. 1: S. A. Holditch & Associates, Inc., annual report prepared for the Gas Research Institute under contract no. 5083-211-0807, 56 p.

Howard, J. D., and Frey, R. W., 1973, Characteristic physical and biogenic sedimentary structures in Georgia estuaries: American Association of Petroleum Geologists Bulletin: v.57, no. 7, p. 1169–1184.

Howard, J. D., Frey, R. W., and Reineck, H.-E., 1973, Holocene sediments of the Georgia coastal area, *in* Frey, R. W., ed., The Neogene of the Georgia coast: University of Georgia, guidebook prepared for 8th Annual Georgia Geological Society field trip, 58 p.

Hunt, E., 1989, Development and application of stress profiles to fracture treatment design and analysis: Gas Research Institute, In Focus - Tight Gas Sands, v. 6, no. 1, p. 34–38.

Jackson, M. L. W., and Laubach, S. E., 1988, Cretaceous and Tertiary compressional tectonics as the cause of the Sabine Arch, East Texas and Northwest Louisiana: Trans. Gulf Coast Assoc. of Geol. Soc., v. 38, p. 245–256.

Jones, F. O., and Owens, W.W., 1980, A laboratory study of low-permeability gas sands: Journal of Petroleum Technology, v. 32, p. 1631–1640.

Kulander, B. R., Barton, C. C., and Dean, S. L., 1979, The application of fractography to core and outcrop fracture investigations: Morgantown Energy Technology Center, report prepared for U. S. Department of Energy, METC/SP 79/3, 174 p.

Lacy, L. L., 1987, Comparison of hydraulic-fracture orientation techniques: Journal of Petroleum Technology, v. 39, p. 66–76.

Laubach, S. E., Baumgardner, R. W., Jr., and Meador, K. J., 1987, Analysis of natural fractures and borehole ellipticity, Travis Peak Formation, East Texas: The University of Texas at Austin, Bureau of Economic Geology topical report prepared for the Gas Research Institute under contract no. 5082-211-0708, 128 p.

Laubach, S. E., 1988a, Subsurface fractures and their relationship to stress history in East Texas basin sandstone: Tectonophysics, v. 156, p. 37–49.

Laubach, S. E., 1988b, Fractures generated during folding of the Palmerton Sandstone, Eastern Pennsylvania: Journal of Geology, v. 96, no. 4, p. 495–504.

Laubach, S. E., 1988c, Significance of natural and coring-induced fractures in the Travis Peak Formation for reservoir stimulation: Transactions, Gulf Coast Association of Geological Societies, v. 38, p. 591.

Laubach, S. E., and Monson, E. R., 1988, Coring-induced fractures: Indicators of hydraulic fracture propagation direction in a naturally fractured reservoir: Proceedings, 1988 Society of Petroleum Engineers Annual Technical Conference, SPE Paper No. 18164, p. 587–596.

Laubach, S. E., Baumgardner, R. W., Jr., Monson, E. R., and Meador, K. A., 1988, Fracture detection in low-permeability reservoir sandstone: A comparison of BHTV and FMS logs to core: Proceedings, 1988 Society of Petroleum Engineers Annual Technical Conference, SPE Paper No. 18119, p. 129–139.

Laubach, S. E., 1989a, Fracture analysis of the Travis Peak Formation, western flank of the Sabine Arch, East Texas: The University of Texas at Austin, Bureau of Economic Geology Report of Investigation 185, 55 p.

Laubach, S. E., 1989b, Paleostress directions from the preferred orientation of closed microfractures (fluid-inclusion planes) in sandstone, East Texas basin, U.S.A.: Journal of Structural Geology, v. 11, no. 5, p. 603–611.

Laubach, S. E., 1989c, Origin of extension fractures in sandstone from a passive margin basin (abs.): Leeds, England, The University of Leeds, Deformation Mechanisms, Rheology and Tectonics, proceedings volume, unpaginated.

Laubach, S. E., and Boardman, S. C., 1989, Multiple generations of fluid inclusions in Cretaceous quartz veins from the Gulf of Mexico basin (abs.): Geological Society of America Abstracts with Programs, v. 21, no. 6, p. 64.

Laubach, S. E., Hoak, T. H., Dutton, S. P., and Diggs, T. N., 1989a, Coevolution of fracture pattern, rock mechanical properties, and diagenesis in a low-permeability gas reservoir sandstone, East Texas (abs.): Geological Society of America Abstracts with Programs, v. 21, no. 1, p. 16.

Laubach, S. E., and Jackson, M. L. W., in press, Origin of arches in the Gulf of Mexico basin: Geology, v. 18.

Laubach, S. E., Tye, R. S., Dutton, S. P., and Herrington, K., 1989b, Staged Field Experiment No. 2, Geological analysis of the Travis Peak Formation: *in* Peterson, R. E., ed., Application of advanced geologic, petrophysical, and engineering technology to evaluate and improve

gas recovery from low permeability reservoir sandstones: CER Corporation and S. A. Holditch and Associates, Inc., report no. GRI-89/0140 prepared for Gas Research Institute, p. 42–90.

Lorenz, J. C., and Finley, S. J., 1987, Significance of drilling and coring-induced fractures in Mesaverde core, northwestern Colorado: Sandia National Laboratories Report, SAND 87-1111, 29 p.

Luffel, D. L, Howard, W. E., and Hunt, E. R., 1989, Relationships of permeability, porosity, and overburden stress derived from an extensive core analysis data base in the Travis Peak Formation: Proceedings, Society of Petroleum Engineers 1989 Joint Rocky Mountain Regional Meeting and Low-Permeability Reservoir Symposium, Denver, Colorado, SPE Paper No. 18964, p. 729–740.

McBride, M. W., Woodruff, C. M., Jr., and Craig, L. E., 1979, Facies distribution within the Hosston Formation, central Texas—implications to low temperature geothermal waters: Gulf Coast Association of Geological Societies Transactions, v. 29, p. 172–178.

McCants, C. Y., 1982, Evolution and stratigraphy of a tidal flat complex within a mesotidal estuary: University of South Carolina, Master's thesis, 127 p.

McFarlan, E., Jr., 1977, Lower Cretaceous sedimentary facies and sea-level changes, U. S. Gulf Coast, *in* Bebout, D. G., and Loucks, R. G., Cretaceous carbonates of Texas and Mexico—applications to subsurface exploration: The University of Texas at Austin, Bureau of Economic Geology Report of Investigations No. 89, p. 5–11.

McGowan, M. K., and Harris, D. W., 1984, Cotton Valley (Upper Jurassic) and Hosston (Lower Cretaceous) depositional systems and their influence on salt tectonics in the East Texas Basin: The University of Texas at Austin, Bureau of Economic Geology Geological Circular 84-5, 41 p.

Moore, C. H., 1983, The Upper Smackover of the Gulf rim: depositional systems, diagenesis, porosity evolution, and hydrocarbon production: Applied Carbonate Research Program, Louisiana State University, Technical Series Contribution 12, 41 p.

Nelson, R. A., Lenox, L. C., and Ward, B. J., 1987, Oriented core: Its use, error, and uncertainty: American Association of Petroleum Geologists Bulletin, v. 71, p. 357–368.

Odom, I. E., Doe, T. W., and Dott, R. H., Jr., 1976, Nature of feldspar-grain size relations in some quartz-rich sandstones: Journal of Sedimentary Petrology, v. 46, no. 4, p. 862–870.

Owen, L. B., Toronto, T. W., and Sinha, K. P., 1987, Strain recovery measurements, Howell No. 5 well: Terra Tek Research, final report submitted to CER Corporation, 34 p.

Pallatt, N., Wilson, J., and McHardy, B., 1984, The relationship between permeability and the morphology of diagenetic illite in reservoir rocks: Journal of Petroleum Technology, p. 2225–2227.

Pendexter, C., and Rohn, R. E., 1954, Fractures induced during drilling: Journal of Petroleum Technology, v. 6, p. 15 and 49.

Peterson, R. (ed.), 1988, Advancements in Travis Peak Formation evaluation and hydraulic fracture technology, Staged Field Experiment No. 1, GRI Report 88-0077, 223 p.

Peterson, R. (ed.), 1989, Application of advanced geologic, petrophysical, and engineering technology to evaluate and improve gas recovery from low permeability reservoir sandstones (Volume 1): CER Corporation and S. A. Holditch and Associates, Inc., report no. GRI-89/0140 prepared for Gas Research Institute, 178 p.

Peterson, R. (ed.), in press, Application of advanced geologic, petrophysical, and engineering technology to evaluate and improve gas recovery from low permeability reservoir sandstones (Volume 2): CER Corporation and S. A. Holditch and Associates, Inc., report no. GRI-89/0140 prepared for Gas Research Institute.

Phipps, S. P., 1988, Deep rifts as sources for alkaline intraplate magmatism in eastern North America: Nature, v. 334, p. 27–31.

Plumb, R. A. and Cox, J. W., 1987, Stress directions in eastern North American determined to 4.5 km from borehole elongation measurements: Journal of Geophysical Research, v. 92, no. B6, p. 4805–4816.

Plumb, R. A. and Hickman, S. H., 1985, Stress-induced borehole elongation: a comparison between the four-arm dipmeter and the borehole televiewer in the Auburn geothermal well: Journal of Geophysical Research, v. 90, no. B7, p. 5513–5521.

Reineck, H.-E., and Singh, I. B., 1986, Depositional sedimentary environments: Berlin, Springer-Verlag, 551 p.

Ren, N.-K., and Rogiers, J.-C., 1983, Differential strain curve analysis, a new method for determining the pre-existing in-situ stress state from rock core measurements: Proceedings of the 5th International Congress on Rock Mechanics, p. 117–127.

ResTech, Inc., 1989, Development of petrophysical techniques for evaluating tight gas sands: Final technical report prepared for the Gas Research Institute under contract no. 5084-211-1062, 139 p.

Rogers, M. A., McAlary, J. D., and Bailey, N. J. L., 1974, Significance of reservoir bitumens to thermal-maturation studies, western Canada Basin: American Association of Petroleum Geologists Bulletin, v. 58, no. 9, p. 1806–1824.

Rosenfeld, M. A., 1949, Some aspects of porosity and cementation: Producers Monthly, v. 13, p. 39–42.

Royden, L., Sclater, J. G., and Von Herzen, R. P., 1980, Continental margin subsidence and heat flow: important parameters in formation of petroleum hydrocarbons: American Association of Petroleum Geologists Bulletin, v. 64, no. 2, p. 173–187.

Saucier, A. E., 1985, Geologic framework of the Travis Peak (Hosston) Formation of East Texas and North Louisiana, *in* Finley, R. J., Dutton, S. P., Lin, Z. S., and Saucier, A. E., The Travis Peak (Hosston) Formation: geologic framework, core studies, and engineering field analysis: The University of Texas at Austin, Bureau of Economic Geology, contract report prepared for the Gas Research Institute under contract no. 5082-211-0708, 233 p.

Saucier, A. E., Finley, R. J., and Dutton, S. P., 1985, The Travis Peak (Hosston) Formation of East Texas and North Louisiana: 1985 Society of Petroleum Engineers/Department of Energy Joint Symposium on Low Permeability Reservoirs, Denver, Colorado, Proceedings, SPE/DOE Paper No. 13850, p. 15–22.

Science Applications International Corporation, 1985, Stress determination from recovery strain measurements in tight gas sands - Mast #A-1, Nacogdoches County, Texas: Report Submitted to CER Corporation, 34 p.

Sorrells, G. G., and Mulcahy, C. C., 1986, Advances in the microseismic method of hydraulic fracture azimuth estimation: Gas Research Institute, In Focus - Tight Gas Sands, v. 3, p. 14-24.

Strubhar, M. K., Fitch, J. L., and Glenn, E. E., Jr., 1975, Multiple, vertical fractures from an inclined wellbore—a field experiment: Journal of Petroleum Technology, v. 27, p. 641–647.

Seni, S. J., 1983, Travis Peak Formation, East Texas, *in* Finley, R. J., and others, Geologic analysis of primary and secondary tight gas sand objectives, phase A—selective investigations of six stratigraphic units; phase B—initial studies: The University of Texas at Austin, Bureau of Economic Geology, topical report prepared for Gas Research Institute under contract no. 5082-211-0708, p. 175–188.

Soeder, D. J., and Chowdiah, P., 1988, Comparison of pore geometry in high and low permeability sandstones: Travis Peak Formation, East Texas: Proceedings, 1988 Society of Petroleum Engineers Symposium on Gas Technology, Dallas, Texas, SPE Paper No. 17729, p. 239–252.

Teufel, L. W., 1982, Prediction of hydraulic fracture azimuth from anelastic strain recovery measurements on recovered core: Proceedings, 23rd Symposium on Rock Mechanics: Issues in Rock Mechanics, R. E. Goodman and F. F. Hughs (eds.), SME/AIME, New York City, p. 29–33.

Tye, R. S., 1989, Stratigraphy and depositional systems of the Lower Cretaceous Travis Peak Formation East Texas Basin: The University of Texas at Austin, Bureau of Economic Geology, topical report prepared for the Gas Research Institute under contract no. 5082-211-0708, 80 p.

Tye, R. S., Laubach, S. E., Dutton, S. P., and Herrington, K. L., 1989a, The role of geology in characterizing low-permeability sandstones, North Appleby Field, East Texas Basin: Proceedings, Society of Petroleum Engineers 1989 Joint Rocky Mountain Regional Meeting and Low-Permeability Reservoir Symposium, Denver, Colorado, SPE Paper No. 18964, p. 355–365.

Tye, R. S., Diggs, T. N., Laubach, S. E., Herrington, K. L., and Dutton, S. P., 1989b, Preliminary geologic description, Mobil Cargill No. 15: The University of Texas at Austin, Bureau of Economic Geology, well report prepared for the Gas Research Institute under contract no. 5082-211-0708, 30 p.

Visser, M. J., 1980, Neap-spring cycles reflected in Holocene subtidal large-scale bedform deposits: A preliminary note: Geology, v. 8, p. 543–546.

Waal, J. A., Bil, K. J., Kantorowicz, J. D., Dicker, A. I. M., 1988, Petrophysical core analysis of sandstones containing delicate illite: The Log Analyst, v. 29, no. 5, p. 317–331.

Waples, D. W., 1980, Time and temperature in petroleum formation: application of Lopatin's method to petroleum exploration: American Association of Petroleum Geologists Bulletin, v. 64, no. 6, p. 916–926.

Whitehead, W. S., and Robinson, B. M., 1989, Development of in situ stress testing procedures and analysis: Gas Research Institute, In Focus - Tight Gas Sands, v. 6, no. 1, p. 29–34.

Zemanek, J. Glenn, E., Norton, L. J., and Caldwell, R. L., 1970, Formation evaluation by inspection with the borehole televiewer: Geophysics, v. 35, p. 254–269.

Zoback, M. D., Moos, D., Mastin, L., and Anderson, R. N., 1985, Well bore breakouts and in situ stress: Journal of Geophysical Research, v. 90, p. 5523–5530.

Zoback, M. L., and Zoback, M., 1980, State of stress in the coterminous United States: Journal of Geophysical Research, v. 85, p. 6113–6156.